A Surface Analytical Study of the Attachment of Bacteria to Metal Surfaces

A Thesis presented

by

Glenn Edward French

to

The Graduate School

in Partial Fulfillment of the Requirements

for the Degree of

Master of Science

in

Materials Science and Engineering

State University of New York at Stony Brook

May 1998

19990802 045
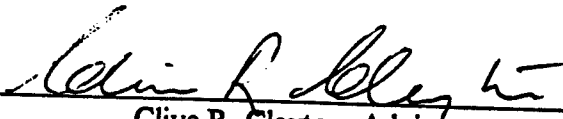
DTIC QUALITY INSPECTED 2

State University of New York

at Stony Brook

The Graduate School
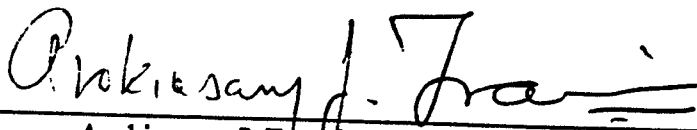
<u>Glenn Edward French</u>

We, the thesis committee for the above candidate for the
Master of Science degree,
hereby recommend acceptance of this thesis.

_____

Clive R. Clayton, Advisor
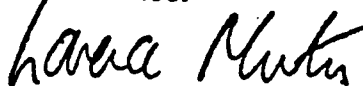Department of Materials Science and Engineering

_____

Gary P. Halada, Assistant Professor
Department of Materials Science and Engineering

_____

Arokiasamy J. Francis, Adjunct Professor
Department of Materials Science and Engineering

This thesis is accepted by the Graduate School

_____

The Graduate School

ii

Abstract of the Thesis

A Surface Analytical study of the Attachment of Bacteria to Metal Surfaces

by

Glenn Edward French

Master of Science

in

Materials Science and Engineering

State University of New York at Stony Brook

1998

The attachment of microbiologically produced organic acids and exopolymers to stainless steel was investigated. The organic acids investigated were lactic, oxalic and citric acid (a metabolic product of fungi) and an exopolymer extracted from the marine bacterium *Delaya marina*. Although organic acids tend to be weak acids and have a relatively low ionic conductivity they are environmentally common and the effects on corrosion of such acids are poorly understood. The reactivity and ubiquitous nature of lactic acid provides significant interest to the microbial corrosion field and the food industry. In a bacterial consortium, lactic acid is consumed by some bacteria and generated by others. Lactic acid is also common in the food industry, where its reactivity may cause

iii

health hazards by leaching of elements from the protective films of metals used in the food preparation, transport or storage.

For this inquiry the surface of 304 stainless steel was probed by performing electrochemical polarization in an aqueous 0.1M HCl solution. A modification of the 304 stainless steel passivation behavior in the 0.1M HCl was observed when the steel under went prior exposure to lactic acid prior to the potentiodynamic polarization. The steel surface was analyzed using x-ray photoelectron spectroscopy (XPS) to study the chemical composition of the passive film. It was determined that the mechanism by which the lactic, oxalic and citric acids alters the steel passivity was a combination of iron oxide dissolution and bonding of the organic acids to the surface. The dissolution was confirmed using Inductively Coupled Plasma - Atomic Emission Spectroscopy (ICP-AES).

Additionally the effect of citric acid on the corrosion of 304 stainless steel in the presence and absence of light was examined. The presence of light was found to accelerate the dissolution of the iron oxides and increase the amount of chromium hydroxides in the passive film. The C1s XPS spectra showed evidence of the presence of organic carboxylates bound to the surface.

Coupons of 304, Al6x stainless steels, aluminum alloy 2024-T3 and a high molybdenum stainless steel coating produced by Jet Vapor Deposition™ (JVD™) were exposed to *Desulfovibrio desulfuricans* in Postgate's growth media C for 5

days. Following exposure, the growth of the bacteria was examined by directly counting the cells to determine if the various concentrations of molybdenum in the alloys had any effect on the Sulfate Reducing Bacteria (SRB) growth rate. Additionally the inoculated and uninoculated Postgate growth media was analyzed by ICP-AES for Cu, Al, Mg, Fe, Ni, Cr and Mo to determine what if any alloy elements are dissolved or sequestered by the bacteria. The uninoculated growth media to which the AA2024 coupon was exposed contained aluminum, but the coupon in the SRB inoculated media did not. The Al6x coupons which were exposed to the growth media only showed dissolved molybdenum in the media, but not the coupons exposed to the SRB

Table of Contents

x

List of Tables

List of Figures

Acknowledgments

I would like to express my gratitude to the following people:

I Introduction

1.0 Microbiologically Influenced Corrosion (MIC)

There are various stages of microbial infestation and corrosion as illustrated in figure 1[1]. The first step is the conditioning film, which is the focus of this research. The second step is the reversible association where the extracellular polymers and proteins attach to the surface. Irreversible adhesion occurs when the microbial cells attach to the surface, then multiply. Other types of bacteria may join the colony to eventually form a biofilm. Finally sloughing (fragments breaking from the biofilm) can occur allowing rapid colonization of the pipe further down stream. It is the peripheral drag which slows the flow rate near the walls of the pipe which allows microbial infestation to occur.

The extracellular polymer or exopolymer performs the function of attaching the microbe to the substrate and acts as an ion sequestering mechanism either to prevent the microbes from being exposed to toxic ions or to capture a food source. The colony consists of many different types of microbes forming a microbial consortium where the microbes of one type may metabolize waste products, such as lactates, of other microbes and so on. Bacterial colonization correlates to sustained localized corrosion such as pitting rather than general corrosion, hence preventing or limiting repassivation.[2,3,4,5] In addition to aiding

1

metallic corrosion, fungi and bacteria have been observed to degrade polymers, polymeric composites and fiber reinforced composites.[6,7,8]

1.01 Organic Acids

The conditioning film consists of microbially produced acids and exopolymers. The organic acids studied consisted of lactic acid, oxalic acid and citric acid. Lactic acid was chosen for this research not only for the fact that it is consumed by Sulfate Reducing Bacteria (SRB) and is used in the Postgate's growth media C^9 (table 1), but also for the ubiquitous nature of lactic acid producing bacteria (table 2 lists the locations the bacteria have been found to exist). Lactic acid is a universal metabolite consumed by some types of bacteria and produced by others.[10] Lactic acid, as many organics, is known to react with itself, by hydrolysis of the carboxylic and hydroxyl groups of two separate molecules, to form other organic materials such as esters and ring structures.[11] Oxalic acid is produced by Lichens (symbiotic colonies of algae and fungi) which use oxalic acid to extract nutrients from stone and minerals by organic-metal complex formation. [12,13,14] The ability of the oxalic acid to remove metals from materials as stable as environmentally exposed stone surfaces makes this organic acid important. Citric acid is also a naturally occurring acid and produced by

2

fungi[15] as well as an important acid commonly used in the food industry. The bio-reactivity of iron-citrate complexes have been examined in depth indicating that ferrous and ferric iron will form complexes with citrate ions.[16,17]

Lactic, oxalic, and citric acids are single, binary, and ternary carboxylic acids, respectively. Therefore in addition to considering various microbial producers, the effect of the carboxylic acid functional group can also be assessed.

Although organic acids are ubiquitous and occasionally polymorphous there has been limited research performed on their effect on metallic corrosion. Some work has been done on the corrosion effects of acetic acid on copper[18] and stainless steels.[19] Current research focuses on the significance of the substrates by comparing the corrosion behavior of stainless steels prepared from metal powders in organic acids.[20] A study has been conducted by Farve and Landolt on the chelating ability of gallic acid, a naturally occurring organic acid for use as a possible corrosion inhibitor.[21] The chelation of the iron ions by gallic acid was found to involve both the hydroxyl and carboxyl groups. These are the same functional groups expected to play a role in metal ion chelation by citric and lactic acids. The structures of citric, oxalic and lactic acids showing these groups are illustrated in figure 2. Citric acid has also proven to be photo reactive.[22]

Therefore this parameter was also evaluated when exposing the steel samples to citric acid solutions.

1.02 XPS of MIC

Although microbiologically influenced corrosion (MIC) was first recognized more than 60 years ago[23] , research efforts have shown significant growth only in the last thirty years. The cost in 1978 to US industries from microbiological corrosion was estimated to be more than $16 billion.[24] Over the last 25 years surface analysis, in combination with electrochemical analysis, has played a major role in understanding of metallic corrosion.[25,26] This particularly complex form of corrosion, has not attracted much of the attention of applied surface scientists. This suggests that more surface analytical methods and practices should be suitably adapted to this form of corrosion.

There are various techniques to determine topography of microbiological samples without exposure to UHV. Two such techniques are the Environmental Scanning Electron Microscope (ESEM) and the biological Atomic Force Microscope (AFM). The ESEM can collect chemical information of a wet biofilm,[27] but no information on speciation . In addition, the surface sensitivity of ESEM is less than that of XPS. The biological AFM is useful for *in situ*

4

determination of topography[28] and the structure of large biomolecules.[29] In previous studies in this laboratory the suitability of X-ray Photoelectron Spectroscopy (XPS) to the study of biological species and their metabolic products was proven effective.[30,31] To ensure no cellular degradation occurs in the Ultra-High Vacuum (UHV) during XPS liquid nitrogen is used to cool the specimen for analysis. Figure 3 is a graph of elemental vapor pressures vs. temperature. As illustrated at $-50°$ C, volatile elements such as sulfur and carbon are extremely stable in pressures as low as 1×10^{-10} torr. Hence cooling the sample with liquid nitrogen ($-196°$ C ($77°$ K)) is more than sufficient for these studies.

The feasibility of XPS as an analysis technique for MIC has been proven by research previously done in this lab. A study of Uranium species bound to *clostridia sp.* cell walls was performed using both XPS under UHV and in air by X-ray Absorption Near Edge Spectroscopy (XANES). The spectra are reproduced in figure 4. Notice the excellent agreement of both the XPS at UHV and XANES at atmospheric pressure.[30] Additionally, the data showed agreement in determining that soluble uranyl-acetate exposed to bacteria in a growth medium was immobilized onto the cell walls as U^{4+}. While this example related to a bioremediation study, it serves to demonstrate that XPS has great potential for studies of microbiological corrosion. In a second study, the speciation of S

5

trapped in a biomass of *Desulfovibrio sp.* was determined using XPS. This was part of a larger study in which the bacteria was exposed to soluble forms of the elements expected to be slowly released from a passivated stainless steel such as type 317L.[31] The bacteria were grown in Postgate's medium C. Separate samples of bacteria were then inoculated with 0.2mM $FeCl_2$, Na_2MoO_4, $CrCl_3$ or $NiCl_2$. The molarity was chosen to represent the solution concentration expected at the alloy surface assuming a passive current density of $10\mu A$ cm^{-2}. The biomass was separated by centrifugation, dried and analyzed by XPS. According to the XPS results the metallic species were found to exist in several chemical states, including their sulfides, in all cases. However, more germane to this review is the detailed speciation of several sulfur states that were recorded and are reproduced in figure 5. The spectra shows the various stages of sulfur reduction according to the SRB reduction cycle illustrated in figure 6. The extent of the reduction process appears to be influenced by the nature of the metal added. This in turn was related to the release rates of several other metabolic products such as hydrogen sulfide, acetic and propionic acids which were reported.[32] The release of hydrogen sulfide and production of metal sulfides, sulfites and elemental sulfur are expected to increase very significantly the corrosiveness of the local environment.[33] It can be appreciated that correlating biofilms with corrosion events may be in practice

6

difficult if the chemical environment around the corrosion products is not adequately investigated.

To determine of the susceptibility of engineering alloys to microbiological corrosion, an accelerated test combining XPS analysis with electrochemical polarization analysis was developed.[34] The test first involved exposure of 304 and 317L stainless steel to fresh cultures of *desulfovibrio desulfuricans* followed by XPS analysis of the surface of the steel to determine the nature of subsequent chemical surface modification. The next stage involved electrochemical analysis in a test acid to evaluate the passivity and pitting characteristics of the stainless steel. Further XPS analysis was then performed on the steel samples following polarization at a potential selected from the polarization diagram in order to evaluate the nature of surface breakdown in the test acid. By combining this data, a model of surface chemical behavior could be determined that would provide a guide to alloy design for improved resistance to microbiological corrosion. Angular Resolved (AR) XPS was performed on the above specimens revealing significant sulfidation of Fe, Cr and Ni, with sulfides being present throughout the anodic film as indicated in figure 7.[34] The extent of the sulfidation was seen to vary considerably between samples. This analysis indicated that microbiological corrosion had taken place and had sulfidized the main passivating element Cr. This

7

would be expected to compromise the ability of the alloy to passivate. Unlike abiotic corrosion, microbiological corrosion appeared less consistent.

1.1 X-ray Photoelectron Spectroscopy

X-ray photoelectron spectroscopy (XPS) is a surface analysis technique originated by the Nobel laureate Dr. Kai Siegbahn based on Einstein's Nobel prize winning photoelectric theory. XPS provides chemical valance state information for species as low as 2% of a monolayer to approximately ten nanometers into the bulk depending on the mean free path of photoelectrons through the material. All elements are detectable by XPS with the exception of hydrogen, the sensitivity depends on the photo-emission cross section of the given element. Given elastic scattering conditions, the kinetic energy of the emitted electron (E_k) is equal to the incident X-ray energy (hv) minus the binding energy of the emitted electron (E_b) and the work function of the sample and the spectrometer (ϕ), as given in equation 1.

$$E_k = h\nu - E_b - \phi \qquad (1)$$

It is important to note that although core electrons are predominantly used for XPS analysis electrons are emitted from all the energy levels, allowing valance band spectroscopy or peaks from more than one orbital to be used for data confirmation. Figure 8 shows a schematic example of the photo-emission of a core electron from an atom. The ionized sample atom undergoes relaxation through filling of the core electron hole from a higher energy level. Then a hole in a higher energy level is filled by conduction of the electrons through the sample block from ground. If the sample is not a good conductor it will become positively charged and spectra will show a shift to a higher binding energy. This charge shifting can be corrected by subtracting the standard value adventitious carbon at 284.6 eV binding energy from the observed adventitious carbon position; the difference equals the sample charging. The emitted electrons are collected by the analyzer where the energies and relative counts are determined.

1.11 Instrumentation

There are two basic types of XPS electron energy analyzers, the cylindrical mirror analyzer (CMA) and the concentric hemispherical analyzers (CHA). The CMA is comprised of two concentric cylinders that are charged to allow only the passage of electrons of a selected energy. The emitted electrons follow two mirrored "S"

9

like paths through the concentric cylinders to the electron multiplier. The CHA uses two concentric hemispheres that are charged to allow the passage of only electrons of specific energies. A sample of the spectra collected by the analyzer is shown in figure 9, the vertical axis measures the counts of the electrons while the horizontal axis is the binding energy specific to each element as calculated in equation 1. Figure 9 shows a wide scan XPS spectra which gives information on all elements on the sample surface and little information regarding the speciation of each element: such information is derived from the narrow or higher resolution scans. The steps seen in figure 9 at the C 1s, O 1s and Fe 2p peaks can be used determine whether elements are present only in a thin film layer or throughout the bulk. Here bulk refers to relative to depths of several times the mean free path of the photoelectrons in the sample being analyzed. This is due to the fact that the background intensity is mostly comprised of scattered photoelectrons. Photoelectrons ejected from an element present in the bulk will be scattered as they exit the material. This energy loss will result in the step-like structures on the low kinetic energy (high binding energy) side of the peaks. From this we can see that the bulk of the sample surface layer is comprised of mostly Fe, Cr and O.

1.12 Spectral Features

Photoelectrons emitted from p, d and f orbitals generate spectral doublets, an example of which is shown in figure 10. This is called spin orbital splitting and is due to interactions between the total angular momentum of each electron (j) or j-j coupling. The distance between them is the energy difference between the separate spin orbitals (ΔE_j). The total electronic angular momentum (j) equals the sum of the orbital quantum number (l) and the spin quantum number (s) and therefore has two distinct values due to s equaling 1/2 and -1/2. The area ratio of each of these doublet peaks depends on the degeneracies (2j+1) and can be seen for various orbitals in table 3. Basically the degeneracies are the number of states with the same energies and can be found using the quantum number j.

Another group of spectral features often noted in XPS data are satellites. The three types of satellites are shake-up, shake-off and x-ray satellites. X-ray satellites are low intensity peaks that arise because the x-ray source is not totally monochromatic. In addition to the most intense $K\alpha_{1,2}$ lines there are also low intensity $K\alpha_3$, $K\alpha_4$ and $K\beta$ lines; these additional x-ray energies cause the satellites observed in figure 11. X-ray satellites appear on the lower binding energy side of the $K\alpha_{1,2}$ photoelectron peak because the $K\alpha_3$, $K\alpha_4$ and $K\beta$ x-rays are higher frequency and therefore higher energy x-rays.

11

Shake up satellites are due to the electrons in the atom being promoted to a higher unfilled energy level during emission of the photoelectron. The energy required to promote the electron is then not available to the photoelectron, therefore it appears that the atom has a higher binding energy generating a spectral peak on the high binding energy side of the primary peak. This sort of relaxation requires an unfilled outer orbital as illustrated in figure 12. For example Cu^+ with $3d^{10}$ (figure 13a)[35] does not produce shake up satellites while Cu^{2+} with $3d^9$ (figure 13b)[36] does.[37] The spectra can be used as a technique to differentiate between the two species as shown in figure 13.

Shake off satellites are similar to shake up satellites but result in ionization of the valance electrons, leaving two electron holes; one in the core level and the other in the valance level. Shake off satellites are rarely seen for solid state samples because they are lost in the inelastic tail. The shake off satellites have been identified in the inelastic tail of polymeric C 1s spectra, after double differentiation by Pireaux who used this technique to acquire information on the valance band structure of the polymers.[38]

The speciation of elements can be determined using the fact that chemical shifts occur between various atomic species. A chemical shift is the change in binding energy of core electrons for different valance states or different chemical

environments for the same element. For example in the case of NaCl vs Na metal, the Na ionized to Na^+ presents the core electrons with a higher effective nuclear charge, thus generating a Na 1s spectral shift to higher binding energy. Shifts can also occur for elements in the same valence state; an example of this effect can be seen for the organic molecule ethyltrifluoroacetate where the four different carbon atoms produce specific distinct chemical shifts. As seen in figure 14 the CF_3 group has the highest binding energy because of the high electron affinity of the F.[39] Second the carbon of the acetate group is shifted because it is bound to two oxygen molecules which influence the electronic screening of the C1s electron. Finally the close chemical shift of the carbon atoms bound to an oxygen atom is not fully differentiated from the methyl group.[39] Chemically, the binding energy (E_B) is roughly given by:

$$E_B = K Q + V + L - E_R \qquad (2)$$

Where K is an empirical constant, Q is the charge of the ion, L is the binding energy of a free neutral atom, V is the potential field generated by the surrounding atoms, and E_R is the relaxation energy of the remaining electrons (this is a negative value; hence it reduces the energy of the ion).

13

1.13 Angular Resolved XPS

The surface sensitivity of XPS is dependent on the photoelectron take-off angle (toa) or emission angle (ϕ). The technique of comparing spectra from different toa is called angular resolved x-ray photoelectron spectroscopy. Figure 15 shows that since photoelectrons are emitted radially from the surface and are collected from depths of approximately three times the mean free path of an emitted electron (λ) by changing the angle of the analyzer (ϕ) with respect to the sample surface various depths (d) can be probed:

$$d = 3\lambda \sin \phi \qquad (3)$$

It is important to remember that for single crystal surfaces, photo-electron diffraction may occur and cause false angular resolved XPS results. The topography of a surface is also important when dealing with angular resolved XPS data because if the surface topography is rough the low angle information is only collected from the peaks, and shadowing of the troughs occurs.

14

1.2 General Corrosion

There are two types of chemical reactions that define corrosion, oxidation and reduction. Oxidation is the loss of electrons from an element. In the corrosion model the places on the metal surface where oxidation occurs are called the anodic sites (The white areas in figure 16). The metal ions may become part of soluble complexes and go into solution, or they form a relatively insoluble protective layer on the metal which decreases dissolution of the metal. The electrons liberated from the reaction travel through the metal to the cathodic site (shaded areas on figure 16) where the reduction reaction occurs. Reduction is the decrease in charge of a chemical species by acquiring electrons, which in this case come from the metal surface. Figure 17 illustrates that both anodic and cathodic sites occur on a corroding surface. These two areas on the surface are the two halves of the reduction-oxidation (redox) reaction and the rate contributing step in the corrosion reaction governs the overall corrosion rate.

$$M + X = M^{+n} + X^{-n} \qquad \textbf{Reaction 1}$$

15

Figure 17 is a cross section diagram of corrosion occurring at an anodic site where the metal atoms (M) go into solution and the cathodic site where species in solution acquire electrons from the metal (reduction).

1.21 Activation Polarization

Activation polarization is used as an electrochemical analysis technique to assess the corrosion performance of a metallic sample. Figure 18 shows a modified Greene cell[40] similar to the one used for research. The working electrode is the specimen being analyzed. The counter or auxiliary electrode is used to supply current to the working electrode. It should be inert to the solution and therefore it is usually made of platinum. The salt bridge and luggin capillary are used to minimize the voltage drop or IR drop between the working electrode and the reference electrode. Polarization causes only one of the half cell reactions at a time to occur on the sample surface, while the opposite occurs on the platinum auxiliary electrode. The reference electrode senses the potential imposed on the working electrode. There are two common types of reference electrodes, the standard hydrogen electrode (SHE) and the saturated calomel electrode (SCE). Generally, reference cells are compared to the SHE by setting the SHE at zero volts. The reaction on the SHE is:
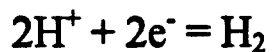
$$2H^+ + 2e^- = H_2 \qquad \textbf{Reaction 2}$$

The reaction that occurs at the surface of the SCE is:
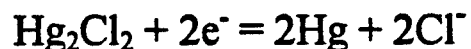
$$Hg_2Cl_2 + 2e^- = 2Hg + 2Cl^- \qquad \textbf{Reaction 3}$$

with a potential of 0.222 V vs. SHE.

The relationship between the potential, current density and the half cell reactions for a de-aerated situation are illustrated in figure 19[41]. The symbols β_a and β_c in figure 19 are the Tafel constants which represent the rate of the anodic oxidation and cathodic reduction reactions.[42] The over potential or applied potential (η) can be correlated to the current according to the Tafel equations. There are two Tafel equations; that for anodic oxidation:

$$\eta_a = \beta_a \log (i_a / i_o) \qquad (4)$$

and the Tafel equation for cathodic reduction:

$$\eta_c = \beta_c \log (i_c / i_o) \qquad\qquad (5)$$

where the subscripts a and c correspond to anodic and cathodic respectively. The subscript o stands for open circuit. Where these lines cross (see figure 19) is the corrosion current density (i_{corr}). The i_{corr} can be found experimentally from an active-passive polarization plot from extending the Tafel slopes until they cross. This is represented in figure 20 by the dashed lines. From figure 19 following the reaction:

$$M^{2+} + 2e^- = M \qquad\qquad \textbf{Reaction 4}$$

we can see that a surface oxide can be reduced if a negative potential of sufficient magnitude is applied for a sufficient time to the sample until the becomes constant. Specifically when the rate of current exchange between the metal surface and the and the solution is constant all the surface oxide has been reduced. This is called cathodic treatment and is used to reduce the surface to metal. The sample can then be potentiodynamically scanned producing a polarization plot similar to the one shown in figure 20, which shows a general potentiodynamic curve for a metal specimen. Comparing figure 19 to figure 20 we can see that the reaction occurring

18

in the cathodic region on figure 20 is a hydrogen evolution reaction (since the surface no longer possesses oxides which can be reduced) for a deaerated solution.

$$2H^+ + 2e^- = H_2$$ **Reaction 5**

For an aerated solution the dissolved oxygen can react with the hydrogen ions to give the reduction reaction shown in reaction 6.[43]

$$O_2 + 4 H^+ + 4 e^- = 2H_2O$$ **Reaction 6**

Similarly the active region can be seen to coincide with the metal dissolution reaction.

$$M = M^{n+} + ne^-$$ **Reaction 7**

The passive region (shown in figure 20) is where the metal ions form a protective or passive, relatively insoluble layer between the metal and the solution. The transpassive region of the active-passive polarization plot represents the same

metal dissolution reaction (reaction 7) of the active region. This is due to the high applied potential which causes the breakdown of the passive film.

1.22 Corrosion Rates

The corrosion rate of metals can be determined using Faraday's Law which correlates the mass dissolved (m) in grams to the current in amperes (I), time in seconds (t) and a correlation factor called the electrochemical equivalent in grams per coulomb (K).

$$m = K I t \tag{6}$$

The electrochemical equivalent (K) is equal to the atomic weight (w) divided by the number of equivalents or electrons in the reaction (n) and Faradays constant (F) 96500 Coulombs per equivalent.

$$K = w / n F \tag{7}$$

To acquire corrosion rate in grams per cm^2 per second (r) from the mass reacted divide the mass (m) by time (t) and the area (A). This produces equation 6:

$$r = m / t A = i a / n F \qquad (8)$$

where i (or i_{corr})is the current density (I / A), in amperes per cm^2. A more common way of presenting corrosion rates is depth per time or mils (0.001 in) per year (mpy). The mpy can be calculated by multiplying equation 6 by a proportionality constant and dividing by the density of the corroding metal (ρ).

$$r \ (mpy) = 0.129 \ a \ i / n \ \rho \qquad (9)$$

Polarization is the induction of either a cathodic or anodic reaction by an external source; for example, solution concentration or electrical activation. Activation polarization forces a specific half cell reaction to occur on the sample surface by selecting either a specific voltage or current.

21

II Experimental Methods and Procedures

There were three basic questions this research sought to answer:

(1) What effect if any do the organic acids have on the conditioning and corrosion of stainless steel and what is the effect of the surface conditioning and light on corrosion in citric acid solutions.

(2) What is the effect of exposure to the exopolymer of the marine bacterium *Deleya marina* on conditioning and corrosion.

(3) What are the effects of *Desulfovibrio desulfurcans* on the corrosion characteristics of both the heat treated and as polished stainless steel 304 and as polished aluminum alloy 2024-T3. Additionally Al6x stainless steel and a high molybdenum "stainless steel like" thin film, produced by Jet Vapor Deposition Process™ (JVD™), were exposed to both uninoculated Postgate C growth media and inoculated *desulfovibrio desulfurcans*. As with the 304 stainless steel and AA2024 coupons, cell counts and ICP-AES was performed the media after a 5 day exposure to these coupons, although for these samples no additional surface analysis was performed.

Lactic acid (see figure 2(c)) is an alhpa-hydroxy carboxylic acid, meaning it has both a hydroxyl (OH) functional group as alcohols do and the carboxyl (COOH) functional group of the carboxylic acids. Lactic acid was selected for its

ubiquitous presence in the bacterial community[10] and to help answer the question of what is the effect of the uninoculated media on the corrosion behavior of exposed samples.[16] Oxalic acid (see figure 2 (b)) is a di-carboxylic acid, meaning it has two carboxyl functional groups. It was selected for this research for it is known to play a role in the weathering of rocks and minerals by organic-metal complex formation.[21,22] Citric acid (see figure 2(a)) is a hydroxy-tri-carboxylic acid which simply put means it has a hydroxyl and three carboxyl functional groups. Citric acid can react with other citric acid molecules as lactic acid does to form derivatives such as esters.[44] Citric is a well know chelator of transition metals, forming various complexes.[14,15,45] Figure 21 is a flow diagram of the conditioning film research which includes the exopolymer and the citric photo-reactivity research. The concentration of 1 mM was selected because it was a concentration similar to that of other organics observed in environment.[46] The 5 minute exposure time was selected arbitrarily prior to the electrochemical analysis where an effect was observed; it was then decided for consistency to stay with the same time for all the various methods of analysis. The concentration of 0.1M was selected for the citric acid photo-reactivity research to be consistent with the research performed in the literature.[47]

Electrochemical analysis was selected to determine if the citric acid had an effect on the corrosion behavior of the samples through observing its active-passive polarization behavior. XPS was selected to determine what effect the organic acids had on the stainless steel surface; for example, to determine whether the organics were binding to the surface and/or how the passive film was changing if at all. Fourier Transform Infrared Microspectroscopic (FT-IRM) analysis was performed to confirm the results of the XPS, particularly relating to the binding of the organics to the surface. Inductively Coupled Plasma Atomic Emission Spectroscopy (ICP-AES) was added as a solution analysis technique to compliment the surface analysis, chosen specifically for its ability to detect elements at very low concentrations (ppb). Since the ICP-AES has no speciation capability, UV-Vis, was added, specifically to determine what iron complexes if any were in solution.

The exopolymer research consisted of observing the electrochemical behavior during potentiodynamic polarization of a stainless steel 304 coupon after exposure to the exopolymer. *Delaya marina* exopolymer was selected because it is a bacterium that generates large amounts of exopolymers. The exopolymer exposure took two forms; one in a static or unstirred solution and the other in a solution being magnetically stirred for the 5 min. exposure time. This was done to

24

determine any possible effects of water flow during exopolymer exposure. The protein containing exopolymer was used because it has been observed to bond to metal ions in solution[48] and the proteins were not believed to be foreign to the exopolymer.[32]

The SRB research followed a procedure previously developed in this lab. The choice of studying the unpolished "as heat treated" stainless steel 304 was to simulate the highly oxidized surface similar to that of a stainless steel weldment. The "as polished" stainless steel 304 was used as a self check with previous work done in the lab.[49] The choice of the aluminum alloy 2024-T3 was to extend the materials tested beyond austenitic stainless steels to other important structural alloys. AA 2024-T3 is an aluminum alloy commonly used in aircraft industry. Copper is a major alloying element in AA 2024-T3 used to improve the strength of the material by age hardening with precipitation of $CuAl_2$ in the slip planes and grain boundaries.[50]

2.1 Sample Preparation

Stainless steel 304 sheets Fe: 69.62, Cr: 19.27, Ni: 8.49, Mn 1.77, C: 0.053, Mo: 0.35, Si: 0.41, P: 0.031, and S: 0.008 wt % were cut in to coupons measuring 1.5 cm x 1 cm x 0.1 cm. These were sealed in a pre-evacuated ($3x10^{-3}$

25

torr) quartz tube and annealed at 1100°C for three hours followed by a water quench to prevent sensitization. The stainless steel 304 coupons were polished to a 1/4 micron diamond finish via the process shown in table 4. Following the polishing procedure the coupons were cleaned ultrasonically in isopropanol and distilled water.

The AA 2024-T3 samples, composition 4 wt. % copper and 1 wt. % magnesium and the remainder aluminum, were polished to the 600 grit SiC level.

The Al6x coupons, composing of 20 wt. % Cr, 23 wt. % Ni, 6.3 wt. % Mo and the balance Fe were polished to the 600 grit SiC while other coupons were unpolished, hence maintaining the "as heat treated oxide" layer. The JVD™ coupons consisted of Si wafers upon which the thin film (Cr 10 at.%, Ni 9 at.%, Mo 12 at.% balance Fe) was jet vapor deposited. No polishing was performed on the JVD™ coupons, which already possessed a mirror finish.

The coupons to be exposed to the SRB's were rinsed in ethanol to sterilize any bacteria on the surface then 18 MΩ deionized water to remove any of the ethanol, which is toxic to most bacteria.

2.2 Organic Acid Exposure

L(+)Lactic, oxalic and citric acids were prepared fresh for each experiment to ensure no bacterial contamination. 80, 90 and 175 mg / L respectively were added to distilled water to produce 1 mM solution of each of the acids. The steel coupons were immersed in the respective acid for 5 minutes then rinsed in distilled water to prevent the acid from accumulating on the surface simply through physical adsorption and drying.

2.21 Exopolymer Exposure

120 mg / L of *delaya marina* exopolymer was dissolved in distilled water. The steel coupons were immersed in the solution for 5 minutes then rinsed in distilled water to prevent the extra-cellular polymer from accumulating on the surface simply through physical adsorption and drying.

2.3 XPS Analysis

The XPS was performed using a modified VG Scientific ESCA 3 MK II spectrometer controlled by a VGX 900 computer-based data acquisition system. The vacuum was maintained below 4×10^{-9} torr while the sample was being analyzed. The system is equipped with a rotatable liquid nitrogen cooled sample

27

probe and turbo molecular pumped fast entry port. In all cases, the incident radiation was achromatic Al K-$\alpha_{1,2}$ with a source power of 400 watts providing a Full Width at Half Maximum (FWHM) of 1.35 eV for Au 4f$_{7/2}$. A hemispherical analyzer was used with entrance and exit slits width was set at 4 mm (0.16 in.). The analyzer energies were set at 100 eV and 1 eV steps for wide scans and 20 eV and 0.1 eV steps for narrow region scans. The spectra were obtained at several photoelectron takeoff angles, ranging from 20° to 90° with respect to the sample surface. Standard data for all peak parameters and sensitivity factors were developed from work performed in this laboratory. All fitting data is shown in table 5. The samples were transported into the XPS chamber in an Ar-purged glove bag. Charge shifting was corrected with the adventitious C 1s line at 284.6 eV as discussed in the XPS introduction. Nonlinear least-square curve fitting was performed. Parameters included the Gaussian / Lorentzian ratio, constant tail ratio, exponential tail slope, and constant/exponential tail mixing ratio. Background subtraction was performed using the Shirley method.[51]

2.4 Electrochemical Analysis of Organic Acids *and Delaya Marina* Exopolymer

The coupons were mounted on to Plexiglass™ holders measuring 2 cm x 1.5 cm x 0.5 cm using epoxy. The working electrode connection was made by physical contact to the back of the stainless steel 304 coupon with a copper wire as shown in figure 22.

The electrochemical analysis equipment used was a Gamry Corrosion Measurement System 100 (CMS 100). The experiments were conducted in a 1 L Greene cell (see figure 18) containing deaerated 0.1 M HCl . The counter electrodes were 1 mm diameter and 5 mm long platinum wires and the reference electrode was a saturated calomel electrode (SCE). The potentiodynamic scans were performed at 1 mV/sec from open circuit. No cathodic conditioning was applied.

This is an accelerated test which provides rapid surface information by using the electrolyte as a surface probe. For this purpose HCl was chosen because it does not form protective salts such as does sulfuric acid. The choice of this medium does not aim to simulate a naturally corrosive environment or one created in an industrial setting.

2.5 ICP-AES Analysis

The spectrometer used was a Varian Liberty 150 ICP-AES spectrometer which was interfaced with Varian Liberty ICP-AES 2.11 data acquisition and analysis system. Figure 23 is a schematic diagram of an ICP-AEC spectrometer similar to the one used for this research. The spectrometer was calibrated using 5 standard solutions ranging in concentration from 0 to 10 ppm of ions of the metals of interest. The metals that were scanned for were Fe, Cr, Ni and Mo for the stainless steel and JVD^{TM} coupons and Al, Mg, and Cu for the AA 2024 coupons. The 10 mls of inoculated and uninoculated SRB growth media was separated into 8 mls and 2 mls. The 8mls volume under went a 5:1 dilution, then was scanned for Al, Mg, Cu, Fe, Cr, and Ni. The 2 mls was diluted as a 2:1 ratio, and it was scanned for Mo.

2.6 FT-IRM Analysis

The FT-IRM was performed using a bright infrared source from a synchotron coupled with a Spectra-Tech, Inc. IRμs^{TM} scanning infrared microspectrometer. First spectra was collected for stainless steel coupons that were not exposed to the organic acid solutions, to acquire a background spectra which would include any carbonaceous contaminants that may be on

30

the surface. Secondly the organic acid exposed samples were scanned, and the previously collected background was removed and the data saved for peak position determination. A simplified diagram of the FT-IRM, including the scnchotron light source, is shown in figure 24.

2.7 Ultra-Violet Visible (UV-Vis) Analysis

The UV-Vis spectrophotometer used in this analysis a HP 8453 spectrophotometer. It is microprocessor controlled and the data collection software is HP 89532A UV-Visible ChemStation. The wavelength range was 190 to 1100 nm with 1 nm resolution. The integration time was 0.5 s, and the standard deviation was determined. The data was also collected and analyzed using the UV-Visible ChemStation software. A schematic of the UV-Vis Spectrophotometer optics are illustrated in figure 25.

100 mls of 1M concentrations of each of the organic acids (lactic, citric and oxalic) were added to separate 250 ml Erlenmeyer flasks. 5 g of Fe_3O_4 was added as a solid source of Fe^{3+} and Fe^{2+} ions. The solutions were filtered through 0.22 μm filters and analyzed in a quartz cuvette with a 1 x 1 cm^2 cross section.

2.8 Citric Acid Photo-Reactivity

Two stainless steel 304 coupons prepared as stated earlier, were immersed in 10 ml of a 0.1M citric acid solution, for 5 days. One sample was covered with an opaque beaker while the other was exposed to a 100 W incandescent light source, for the full 5 days. Following the exposure the samples were removed and rinsed in distilled water. Both samples were analyzed optically and with XPS.

2.9 SRB Preparation

The SRB research was performed following the flow chart in figure 26. The SRB were grown in a modified Postgate medium C^{52} the exact ingredients can be found in table 1. The modification of Postgates media included decreasing the amount of $FeSO_4$ by half, for the purpose of decreasing the amount of ferrous iron in solution so that the SRBs will seek out another Fe^{2+} source, specifically the stainless steel coupon. 10 mls of the media was dispensed into autoclaved 20 ml serum bottles, leaving the remainder of volume for gas production. *Desulfovibrio desulfurcans* (ATCC 7757) were selected for this research to be consistent with previous research performed in the lab.[34] Two coupons of both the stainless steel 304 and AA 2024-T3 were rinsed in

32

ethanol and water as above, then immersed in the media, one coupon per bottle. The bottles were then sealed and the media with one of each type of coupon was inoculated, the others were kept as controls. The bottles of inoculated media and the controls were both incubated for 5 days at 28° C. On the fifth day all the serum bottles were enclosed in an Ar purged glove bag where 0.5 ml samples of all the inoculated cultures and one control were extracted for cell counts. The remaining media was then filtered though 0.45 μm filters, stored and labeled for ICP-AES analysis. The coupons were rinsed in deaerated distilled water to remove the excess loosely bound biofilm. The coupons were then sealed in serum bottles for XPS analysis.

The stainless steel 304 samples were prepared according to ASTM standard G 48-76[53] for crevice corrosion, (see figure 27) prior to exposure to the SRB media. This was done since MIC is known to sustain localized corrosion.[2,3,4,5]

The microbiological growth was determined by direct enumeration of the cells according to a procedure developed by Kepner and Pratt.[54] The samples for cell counts were extracted from the serum bottles using a sterile pipette. 0.5 mls of the inoculated media and control media were separately added to 0.5 mls of formalin and sealed. The microbiological cells were

dispersed by adding 0.01 M Na₄PPi to each of the specimens. Next the cells were stained with a water fluorochrome solution (1.45 mls deionized 18 MΩ water filtered through 0.45 μm filters, 20μl of 10 μg/ml DAPI (4',6-diamidino-2-phenlindole)). The specimens were vacuum filtered, the filter membrane was then removed and direct cell counts were done from the membrane. The cell counts were performed by epifluorescence microscopy using a Zeiss Axioskop optical microscope at 1250x magnification.

III Results

3.0 Organic Acid Exposure Results

3.01 Electrochemical Analysis

All the polarization plots of the organic acid exposed stainless steel 304 coupons showed a higher current density at the primary passivation potential (Ep) as shown in figures 28, 29 and 30. It is also important to note that the pitting potential for the oxalic acid is lower than that of the stainless steel shown on figure 29. Although the citric acid exposed sample shown in figure 30 had the highest current density in the active region it also shows a higher more noble passive region than the unexposed stainless steel sample. From these results it was decided that XPS should be performed on a stainless steel coupon before and after exposure to ascertain how the organics were activating the metal.

3.02 XPS

Although the majority of coupons showed the following results, there were a minority that showed no significant change. This was later believed to be due to too low a concentration of the reactants and short exposure times. Comparing the iron spectra (figures 31,32,33,34,35,36) of the as polished stainless steel versus

35

iron spectra after organic acid exposure it is obvious that all samples show an increased iron metal peak. The Cr 2p spectra in figures 37, 38, 39, 40, 41 and 42 showed very little change from the organic acid exposure and certainly no change in the metal peak was observed. The O 1s spectra was then examined, figures 43, 44 and 45 shows that there is either an decrease in the amount of oxide on the surface or an increase in the amount of hydroxide adsorbed water. The nickel 2p spectra can be found in figures 46, 47, and 48 and although some samples show Ni and some do not the samples are self consistent. If there was Ni before exposure there was Ni after and also if the was no Ni before after is none after. Relating to the issue of the organic acids binding to the stainless steel surface the C 1s XPS spectra was examined and as shown in figures 49, 50, 51, 52, 53, and 54 there is little difference between the as polished samples and those exposed to the organic acids. It is also important to note that there were some samples that did show more carboxyl organic carbon but these samples were not consistent enough to report. Since the electrochemical data suggested the possibility of the acids being bound to the surface FT-IR was employed as an additional surface analysis technique, specifically for its sensitivity to organic bonds.

36

3.03 FT-IRM

The FT-IRM spectra shown in figure 55 is indicative of all the all the steel coupons analyzed independent of which acid to which it was exposed. From the literature a strong adsorption peak is expected between 1700 and 1725 cm^{-1} for the carbon oxygen double bond, and another characteristic peak at 1250 cm^{-1} for the carbon oxygen single bond.[55]

3.04 ICP-AES

Table 6 presents the results of ICP-AES analysis of the organic acid solutions after the exposures of the stainless steel 304 coupons. The only metal detected was iron; there was no chromium or nickel detected in any of the acid solutions. Table 6 also includes a sample of the deionized water used for the organic acid solutions, none of the metals were detected in the deionized water. From the amount of iron detected the acids range from oxalic being the most effective to citric being the least effective.

The ICP-AES of the SRB growth media only detected Al in solution (4.6 ppb / ml) from the AA 2024 exposed to the uninoculated growth media and Mo in solution from both the "as polished" (9.25 ppb/ml) and "as heat treated" (5.75 ppb/ml) uninoculated Al6x stainless steel coupons.

37

3.05 UV-Vis

Upon visible inspection all three of the acid solutions acquired a similar green tint. The position of the absorption peaks are presented for each of the organic acids in table 7.

3.1 Citric Acid Photo-Reactivity Results

After the 5 day exposure the citric acid solution that had been exposed to the incandescent light exhibited a lemony odor and there were only 3 mls of solution left in the beaker since the rest had evaporated. This is in contrast to the solution which was not exposed to the light where little to no evaporation was observed and the solution did not have an odor. This suggests that the odor was from a compound of higher vapor pressure at room temperature.

There are significant differences between the XPS data collected from the samples exposed in light and dark environments. The C 1s spectra (figures 56 and 57) for both the light and dark exposures show a distinct carboxylic acid group. The Fe $2p_{3/2}$ spectra toa $50°$ (figure 58) shows a significant difference in the iron oxide to iron metal ratio; the sample not exposed to the light shows a higher FeO and Fe_2O_3 than for the coupon exposed in the light. The Fe $2p_{3/2}$ spectra taken at a toa of $20°$ (figure 59) have a much higher signal to noise ratio making the fitting

unreliable. The toa 20° Fe $2p_{3/2}$ spectra seems to show a higher FeO and Fe_2O_3 to Fe metal spectra for the light exposed sample, basically the opposite of the toa 50° data. The Cr 2p spectra (figures 60 and 61) show higher $Cr(OH)_3$ to Cr_2O_3 from the light exposed coupon in comparison to the coupon not exposed to any light. The Ni $2p_{3/2}$ spectra (figures 62 and 63), as for all the spectra, is virtually the same for both the light and dark exposure coupons.

3.2   SRB Exposure Results

The "as heat treated" stainless steel 304 coupons showed visual evidence of microbial corrosion as round brown iron sulfide nodules, an example of which can be seen in Figure 64. The XPS found Fe, C, N, O and S as the predominant elements on the "as heat treated" steel surface. Figure 65 is a survey XPS scan of a 1000 eV wide region in which all the above elements can be seen. The high resolution XPS scan of the Fe 2p 3/2 can be found in figure 66; note that three out of the five Fe species found on the surface are sulfides.

The AA2024-3 sample exposed to the uninoculated SRB growth media showed visible signs of extreme corrosion, while the coupon exposed to the media containing bacteria did not. The coupon exposed to the SRB's did appear to have a biofilm adhering to the surface both samples can be seen in (figure 67). The XPS

spectra of the AA 2024-T3 showed the presence of Cu on the surface of the SRB exposed coupon and not the coupon exposed to the media only. This can be seen in figure 68, the Cu 2p $_{3/2}$ XPS spectra for both the SRB inoculated coupon and the coupon exposed to the media. The Mg 2s XPS spectra showed Mg on the surface for both samples, although the signal was stronger for the inoculated coupon (figure 69). Neither of the coupons provided a detectable S 2p spectra, as shown in figure 71. The Al 2p XPS spectra (figure 72) was present and strong in both coupons but the coupon in the uninoculated media had a shoulder on the lower binding energy side, indicative of Al metal.

The ICP-AES analysis of the uninoculated media and the SRB inoculated media was only able to detect Al in solution (4.6 ppb / ml) from the AA 2024 coupon which was exposed to the uninoculated growth media.

The data collected from the direct cell counts can be found in table 8. All of the inoculated solutions grew with no apparent inhibition or acceleration of the microbiological growth. The uninoculated control solution showed no cells ensuring that all precautions to sterilize the coupons was adequate.

40

IV Discussion

4.0 Organic Acid Exposure

4.01 Electrochemistry

The activation at Ep on the potentiodynamic polarization plot by the organic acids seem to alter the passive film in such a way to make the metal more soluble and/or less able to passivate. Since all the samples showed similar passive regions to the unexposed stainless steel, the surface activation by the organic acids seemed to vanish during the active passive-transition. This suggested that an organic species bound to the surface was dissolved from the surface during the high dissolution rates experienced at the critical current density.

4.02 XPS

The C 1s spectra (figures 49, 50, 51, 52, 53 and 54) did not show any major difference between the 304 stainless steel coupons that were exposed to the organic acids and the "as polished" 304 stainless steel coupons. This either means the organic species that were expected to be on the surface after the electrochemical polarization are not on the surface or the organic species are lost in the adventitious carbon spectra of the XPS.

41

The Fe $2p_{3/2}$ XPS spectra (figures 31, 32, 33, 34, 35 and 36) for the metal coupons which were exposed to the organic acids for 5 minutes prior to XPS analysis showed lower FeO and Fe_2O_3 to Fe metal ratio than for the unexposed metal coupons. This may be explained by to one of two mechanisms: one where the surface oxides and hydroxides are dissolved, thus reducing the attenuation length of the Fe $2p_{3/2}$ photoelectrons, or a second mechanism in which the metal in the surface oxide was reduced to the metallic state. The second mechanism is not thermodynamically possible, particularly in the acidic environment. To support the first mechanism, the O 1s spectra was analyzed for changes. Assuming the adsorbed water on the coupons to be constant, the O 1s spectra (figures 43, 44 and 45) shows a decrease in the surface oxides of the organic acid exposed coupons compared to the "as polished" coupons.

The Cr 2p XPS spectra (figures 37, 38, 39, 40, 41, and 42) of the "as polished" and coupons exposed to lactic, oxalic and citric acids showed no significant differences. This is of some concern since if the dissolution of the passive film allows more of the Fe metal photoelectrons to be detected, why would the same effect in the Cr spectra. This is probably due to a relatively stronger Cr metal signal.

The Ni 2p$_{3/2}$ XPS spectra (figures 46, 47 and 48) showed little to no change from the "as polished" to organic acid exposed. This was also surprising since as with the Fe, we would expect to see more of the Ni metal which is of highest concentration at the interface of the passive film and the metal substrate.

4.03 FT-IRM

The FT-IRM (figure 55) which shows no evidence of carboxyl groups on the coupons, confirms the XPS C 1s data which was also unable to distinguish carboxylic acids on the coupon surfaces. Therefore the electrochemical activity in figures 28, 29 and 30 is apparently due to the removal of the iron oxides, and not the presence of an organic acid bound to the surface of the 304 stainless steel coupons.

4.04 ICP-AES

The ICP-AES results (table 6) which detected Fe in solution but not Ni or Cr agree with the XPS data in which the iron oxides were observed to be dissolved. Even though the passive film can be as much as 30% Cr there was no Cr detected in the organic acid solutions suggesting an enrichment of Cr species on the 304 stainless steel surface.

4.05 UV-Vis

The greenish tint of the solutions is indicative of Fe^{2+} in a hydrated state such as $[Fe(H_2O)_6]^{n+}$. Therefore if the organic acids are complexing the Fe ions, the Fe^{2+} ion at least is in a highly hydrated state or not part of a complex at all. From table 7 the adsorbance peak of the oxalic acid at 961 nm is also related to a highly hydrated Fe^{3+} ion. Neither of the other acids had a peak in this position therefore there was no Fe^{3+} complex or the Fe^{3+} was much less hydrated. The later is unlikely since if there was no ability of the organic acids to dissolve the Fe^{3+} species the XPS would have more likely indicated large differences in the FeO and Fe_2O_3 species. The adsorption peaks at for the citric and lactic acids correspond to bonding using a pair of electrons from the hydroxyl groups which the oxalic acid does not have (see figure2).

4.1 Citric Acid Photo-Reactivity

The Fe $2p_{3/2}$ XPS spectra at toa 50° (figure 58) showed higher FeO and Fe_2O_3 to Fe metal ratio for the dark than for the light exposed coupon. Although it had a high signal to noise ratio the toa 20° spectra (figure 59) showed the opposite effect for the FeO and Fe_2O_3, which were higher for the light exposed coupon. This apparent paradox is most likely due to islanding of the oxides in

light exposed coupon. This theory is supported by the high signal to noise ratio of the 20° toa particularly for the light exposed coupon which shows the noisiest signal of the two coupons. The high signal to noise ratio at low toa's is usually due to surface roughness it is the surface roughness; that causes this oxides to appear higher for the light exposed coupon.

The Cr 2p XPS spectra collected at toa 50° (figure 60)and 20° (figure 61) both show a higher $Cr(OH)_3$ to Cr_2O_3 ratio for the stainless steel 304 coupon exposed to the citric acid in light compared to the coupons exposed in the dark. A low signal to noise ratio is also apparent for the toa 20 Cr 2p spectra.

In both cases the C1s XPS spectra (figures 56 and 57) carboxylic acid groups were found to be bound to the metal surface. We know that hydroxy-carboxylic acids such as citric acid are able to react with other citric acid molecules to form esters. Therefore it is possible that the change in open circuit potential that was observed by Scandelbury and Bastidas[22] was due to the esterification of the citric acid occurring on the steel surface and the activation of the Cr and Fe. The activation or the Cr can be seen in the increase in $Cr(OH)_3$ and the Fe activation caused dissolution of the Fe. It is important to recall that the work done by Scandelbury was performed for periods up to 27 days, so it is possible we are seeing the initiation of the effect he has reported. As determined by reviewing the

45

results from the 5 minute exposures and comparing those results to these, the reason for not detecting the acids on the metal surface can be either too short of an exposure of too low concentration of the organic acid, either of these leaving a lack of coverage of the organic acid on the steel surface.

4.2 SRB Exposure

Upon initial inspection the presence of Mg discovered by the XPS Mg 2s (figure 69) on coupon surfaces may be surprising since MgO, the likely form of corroded Mg, is soluble in water and would therefore dissolve into the solution. Recalling table 1 the source of the Mg becomes apparent; $MgSO_4$ is one of the Postgate medium C ingredients. The presence of the Al metal spectra in the Al 2p XPS spectra (figure 71) is due to the aggressive corrosion of the coupon from the uninoculated media which caused the coupon surface to become much rougher than it was prior to exposure. It is this roughness that also accounts for the lack of Cu, detected by the Cu $2p_{3/2}$ XPS spectra, (figure 68) on the uninoculated coupons surface. The uninoculated growth media may have even preferentially attacked the $CuAl_2$ rich regions, etching troughs and shielding any Cu that may still be present from detection at the take off angle of the analysis.

In the ICP-AES of the inoculated and uninoculated postgate growth

46

media C in which the stainless steel and JVD™ coupons were exposed, the only metal detected was Mo from the both the "as polished" and "as heat treated" Al6x coupons exposed to the uninoculated media. No Mo was detected for the JVD™ coupons even though they contain approximately twice the amount of Mo that the Al6x coupons do. This suggests there is a critical amount of Mo between that of the Al6x and the JVD™ samples which greatly enhances the corrosion characteristics of a material. The virtually iron free passive film of the JVD™ coupon [56] seems to prevent both SRB and organic acid attack of the surface.

Since we know molybdate inhibits the growth of SRB's, it is expected that table 8 would show differences corresponding to the content of Mo in the coupons exposed to the SRB's. The fact that there is no significant difference between the numbers of cells found in each of the SRB inoculated solutions suggests that the molybdate produced as a corrosion product of these stainless steels and "stainless steel like" coupons is not adequate to deplete the ADP pool of the SRB's.

The survey XPS scan (figure 65) of the "as heat treated' stainless steel 304 coupons which were exposed to the *desulfovibrio desulfuricans* inoculated media showed large amounts of Fe, O, S, N, and C on the coupons surface.

47

The Fe $2p_{3/2}$ XPS spectra detected various sulfidized iron species (figure 66). This agrees with the previous work performed done in this lab on "as polished" 304 stainless steel coupons.[49]

4.3 Exopolymer Exposure

On establishing that XPS can be a suitable technique for investigating cells and biomass, a study of the attachment of extracellular polymers to the molybdate anion was initiated.[57] There were three reasons for this interaction to be chosen. The first was that molybdate is often present in the outer portions of the passive film formed on Mo bearing stainless steels. Therefore it is relevant to any binding of the exopolymer to the steel. Secondly, molybdate is a powerful corrosion inhibitor which imparts pitting resistance to austenitic stainless steels and appears to control the level of hydration of the passive film.[58] Finally in a microbiological consortium, there is a need to understand the ability of molybdate to inhibit the growth of SRB's, as reported.[52] Any influence on the chemical state of Mo due to binding to the exopolymer may be expected to affect a change in the pitting resistance of the steel. In this study exopolymer was extracted from Delaya (pseudomonas) marina. Two samples were prepared: one containing extracellular proteins and the other free of proteins. Concentrations

from 0.01 and 0.05 M sodium molybdate were added. The details of this research

can be found in appendix 1. The molybdate was reduced to a pentavalent state

only in deaerated and proteinated exopolymer. This was first shown by XPS

spectra (figure 72a) and then confirmed by electron spin resonance.[57] These

experiments were repeated with molybdate that had been adsorbed onto 304

stainless steel (figure 72b) and subsequently immersed in a deaerated solution of

the exopolymer containing proteins, as shown in figure 72c. The initial molybdate

adsorption was not accompanied by any reduced form of molybdenum, whereas

both tetravalent and pentavalent forms of molybdenum resulted from the binding of

the exopolymer to the steel. A sulfur spectrum was observed for the exopolymer

containing protein but not for the deproteinated exopolymer. This indicated that

the source of the sulfur may be cysteine containing proteins. As shown in figure

73, cysteine contains an hydrophobic sulf-hydryl group (-SH) which on oxidation

with other cysteine residuals forms cystine, a disulfide head group (-S-S-) capable

of binding to metal. The literature suggests that intracellular proteins usually lack

disulfide bonds whereas extracellular proteins do not.[59] XPS analysis of the sulfur

and molybdenum showed an inverse relationship in their signal intensities. This

raises the possibility that pentavalent and/or tetravalent molybdenum may be bound

to a disulfide head group in one of the extracellular proteins, thus providing the

49

necessary attachment mechanism. This mechanism was later supported by *in situ* UV-Visible spectroscopy of an aqueous solution of cysteine doped with molybdate anions which yielded an absorbance peak characteristic of a Mo(V) - S complex.[60] Subsequent electrochemical analysis of the steel attached to the exopolymer in deaerated 0.1M HCl indicated that the amount of molybdate reduced by the exopolymer was insufficient to significantly reduce pitting resistance. This does suggest that cysteine-containing exopolymers may prevent molybdate inhibition of SRB growth.

V Conclusions

• The lactic, oxalic and citric acids activate stainless steel surfaces by dissolving iron oxides from the stainless steel 304 passive film. The iron in solution can then be used as a food source for microbial colonies.

• Citric acid has photo-corrosive characteristics and in high enough (0.1 M) concentration binds to stainless steel surfaces independent of the presence of light. Citric acid in the presence of light more actively dissolves the iron oxides, hydrates the chromium and possibly even reacts to form another organic molecule (an ester).

• In comparison to the uninoculated Postgate media C, which contains among other things lactate and citrate salts, the SRB inoculated media is less corrosive. This is due to the microbial production of a biofilm which acts as a barrier between the aggressive salts and aluminum surface.

• The presence of Mo in a stainless steel or "stainless steel like" coating has no effect on the short term growth rate of SRB's. however , a high Mo

stainless steel coating with a nearly Fe free passive film has been found to resist

SRB and organic acid attack of the surface.

VI Future Research

6.0 Organic Acid Exposure

The future research should focus on two most interesting questions remaining. One is the possible enrichment of the surface of Cr species. The fact that we do not see a Cr metal signal as we do Fe metal increase suggests that the surface may be enriched with Cr. The other is to pursue other engineering metals and alloys. For example there has been evidence from Lyberatos and Kobotiatis[61] that oxalate ions protect Al in Cl environments. Additionally the promising nature of the high Mo systems suggests interesting research possibilities.

6.01 Electrochemical Analysis

Due to the limited detailed information acquired from the electrochemical analysis the future of this type of research should consist of surveying various acids for possible attack of the as polished passive film. These experiments should include exposing the stainless steel coupons to other acids, organic acids and inorganic acids.

6.02 XPS Analysis

The ability of the XPS to detect species undetectable to the FT-IRM makes the XPS the suggested tool for determining if exposures of the organic acids to

other metals have an effect and what are the organics doing to the surface. This is the suggested tool to use when exposing the organic acids to pure metal constituents like Cr to determine what is the effect of the Cr.

6.03 FT-IRM

Since the FT-IRM had not even been able to detect the Citric acid on the surface on the surface of the light and dark citric acid samples the continuation of this as a viable analysis technique is based on the need for a grazing angle objective lens which can be used to acquire IR data with monolayer surface sensitivity. With such an objective or possibly higher solution concentrations this technique could be used to determine the existence and structure of chelated surface species.[62]

Standard solution FT-IR spectroscopy could be used to replace UV-Vis as the chelate or complex determining technique.

6.04 ICP-AES Analysis

This technique with its exceptional detection limits make it a useful complementary technique for the XPS analysis since it analyses the solution not the surface

VII References

1   Brian G. Shearer, Biofilm and the Dental Office, Journal of the American Dental Association, Vol. 127, Feb. 1996

2   M. J. Franklin, D. C. White, and H. S. Isaacs, Pitting Corrosion by Bacteria on Carbon Steel, Determined by the Scanning Vibrating Electrode Technique, Corrosion Science Vol. 32, No. 9, p952

3   R. C. Newman, W. P. Wong and A. Garner, A Mechanism of Microbial Pitting in Stainless Steel, Corrosion, Vol. 42, No 8, Aug 1986, p490

4   P. Angell, J.-S. Luo and D. C. White, Microbially Sustained Pitting Corrosion of 304 Stainless Steel in Anaerobic Seawater, Corrosion Science, Vol. 37, No. 7 p1096

5   X. Campaignolle and J.-L. Crolet, Method for Studying Stabilization of Localized Corrosion on Carbon Steel by Sulfate-Reducing Bacteria, Corrosion, June 1997 p 446

6   J. Gu, T.E. Ford, B. Mitton and R. Mitchell, Microbial Degradation of Polymeric Materials used as Insulation I Electronic Packaging Materials, NACE Corrosion 95 Proceedings Paper No. 202, p 4

7   P. Wagner, R. Ray, K. Hart and B. Little, Microbial Degradation of Stressed Fiber-Reinforced Polymeric Composites, Materials Performance, Feb 96, p 82

8   Ji-Dong Gu, Chun Lu, R. Mitchell, K. Thorp and A. Castro, Fungal Degradation of Fiber-Reinforced Composite Materials, Materials Performance, March/ 1997, p 37

9   J. R. Postgate, The Sulfate Reducing Bacteria, Cambridge University Press, Cambridge, UK, 96, 2nd ed., p 32, 1984

10   J. G. Carr, C. V. Cutting and G.C. Whitting, Lactic Acid Bacteria in Beverages and Food, Proceedings of a Symposium held at Long Ashton Research Station University of Bristol, p 370

56

11   Jørgen Ilum Nielsen and Stig Veibel, The reactivity of Lactic Acid and Some of its Simple Derivatives A Review, Acta Polytechnica Scandinavica, Chemistry Including Metallurgy Series No. 63, Copenhagen, 1967

12   D. Jones and M. J. Wilson, Chemical Activity of Lichens on Mineral Surfaces, International Biodeterioration, p 21, 1985

13   Eiju Yatsu, The nature of Weathering An Introduction, Sozosha, Tokyo, pp 318, 325, 1988

14   F. E. W. Eckhardt, Solubilization, Transport and Deposition of Mineral Cations by Microorganisms, The Chemistry of Weathering, J. I. Drever editor, D. Reidel Publishing Company, Boston, p 167, 1985

15   M. L. Guuerinot, E. J. Meidl, and O. Plessner, Citrate as a siderophore in *Bradyrhizobium japonicum*, Journal Bacteriology, 127, p 3298-3303

16   C. J. Dodge and A. J. Francis, Biotransformation of Binary and Ternary Citric Acid Complexes of Iron and Uranium, Environmental Science and Technology, Vol. 31, No. 11, p 3062, 1997

17   A. J. Francis and C. J. Dodge, Influence of Complex Structure on the Biodegradation of Iron-Citrate Complexes, Applied and Environmental Microbiology, Vol. 59, No. 1, p 112, 1993

18   S. -Z. Yao, J. -H. Chen, and L. -H. Nie, Bulk Wave Technique as a Real-Time Corrosion Probe in Low Conductivity Solution: *In-Situ* Corrosion Behavior of Copper in Acetic Acid, Corrosion, Vol. 53, No. 3, 1997, p 195

19   J. S. Qi and G. C. Lester, Corrosion of Stainless Steel During Acetate Production, Corrosion, Vol. 52, No. 7, p558, 1996

20   E. Otero, A. Pardo, M. V. Utrilla, F. J. Perez and C. Merino, the corrosion of AISI 304L and 316L Stainless Steels prepared by Powder Metallurgy in the Presence of Organic Acids, Corrosion Science, Vol. 39, No. 3, p 455, 1997

21   M. Farve and D. Landolt, The Influence of Gallic Acid on the Reduction of Rust on Painted Steel Surfaces, Corrosion Science, Vol. 34, No. 9, p 1481, 1993

22   J. M. Bastidas and J. D. Scantlebury, The Influence of Light on Corrosion Phenomena: the Behavior of Mild Steel in Citric Acid Solution, Corrosion Science, V.26, no. 5, 1986, p 341

23   C.A.H. von Wolzogen and L. S. van der Vlught, Water (The Hague) 18 (1934)p147

24   National Bureau of Standards (1978), Economic Effects of Metallic Corrosion in the United States, NBS special publication 511-1, N.B.S. Washington.

25   J. E. Castle in Application of Surface Analysis Methods to Environmental/Materials Interactions, Eds., D. R. Baer, C. R. Clayton and G. D. Davis, Electrochemical Society, Pennington, NJ (1991)p1.

26   Passivity of Austenitic Stainless Steels, Chapter VI, C. R. Clayton and I. Olefjord in Corrosion Mechanisms Eds., P. Marcus and J. Oudar, Marcel Dekker, New York (1995)

27   Patricia A. Wagner, Brenda J. Little, Richard I. Ray and Joanne Jones-Meehlan, Investigations of Microbiologically Influenced corrosion using Environmental Scanning Electron Microscope, Corrosion 92, NACE, Houston, TX, p 185/6 (1992)

28   I. Yu. Sokolov, M. Firtel and G. S. Henderson, *In situ* high-resolution atomic force microscope imaging of biological surfaces, Journal of Vacuum Science and Technology A 14(3), 1996, p 676

29   Helen G. Hansma, Atomic force microscopy of biomolecules, Journal of Vacuum Science and Technology B 14(2), 1996, p 1393

30   A. J. Francis, C. J. Dodge, G.. P. Halada and C. R. Clayton, XPS and XANES Studies of Uranium Reduction by *Chlostridium sp*. Environmental Science and Technology Vol. 28, 4, (1994), p 636

31   G. P. Halada, J. R. Kearns, C. R. Clayton, J.B. Gillow and A. J. Francis, The Application of XPS to the Study of M. I. C. Materials Performance, 31, (1992), p 48

32   C. R. Clayton, G. P. Halada, J. R. Kearns, J. B. Gillow and A .J. Francis, Spectroscopic Study of Sulfate Reducing Bacteria-Metal Ion Interactions Related to Microbiologically Influenced Corrosion, in Microbiologically Influenced Corrosion Testing ASTM STP 1232 Eds., Brenda Little and Jefferey R. Kearns ASTM Philadelphia (1994) p150

33   R. C. Newman, H. S. Isaacs and B. Alman Corrosion, 3, 8, (1980) p 261

34   G. C Chen, C. R. Clayton, R.A. Sadowski, J. R. Kearns, J. B. Gillow and A. J. Francis, Influence of Sulfate-Reducing Bacteria on the Passive Film formed on Austenitic Stainless Steel AISI 304, NACE Corrosion 95 Conference Paper # 217, Houston, Texas, (1995) 217/2

35   Richard P. Vasquez, CuCl by XPS, Surface Science Spectra, Vol. 2, No. 2, p141, 1993

36   Richard P. Vasquez, $CuCl_2$ by XPS, Surface Science Spectra, Vol. 2, No. 2, p163, 1993

37   D. Briggs, M. P. Seah Practical Surface Analysis Auger and X-ray Photoelectron Spectroscopy p 130 1984

38   J. J. Pireaux, R. Caudano and J. Verbist, C 1s Inelastics in Polymers, Journal of Electron Spectroscopy Vol. 5 p 269 1974

39   Stefan Hüfner, Photoelectron Spectroscopy Principals and Applications, 2nd Ed., Springer - Verlag Berlin Hidelberg p 32 1996

40   Denny A. Jones, Principals and Prevention of Corrosion, Macmillan Publishing Company, New York, p 101, 1992

41   Herbert. H. Ulig and R. Winston. Revie, Corrosion and Corrosion Control An Introduction to Corrosion Science and Engineering, Ed. 3rd, John Wiley and Sons, Inc., New York, p 49, 1985

42   Allen J. Bard and Larry R. Faukner, Electrochemical Methods
Fundamentals and Applications, John Wiley and Sons, Inc., New York, p 105,
1980

43   William D. Callister Jr., Materials Science and Engineering an
Introduction, 4th ed., John Wiley and Sons, Inc., New York, p 551, 1997

44   Morrison and Boyd, Organic Chemistry, 5th ed., Allyn and Bacon, Inc.,
Boston, p 872, 1987

45   A. J. Francis, Joshi-Tope, A. Geeta and C. Dodge, Biodegradation of
Nickel-Citrate and Modulation of Nickel Toxicity by Iron, Environmental Science
and Technology, Vol. 30, p 562, (Feb.) 1996

46   Jindrich Starek, Arnost Zukal and Jiri Rathousky, Comparison of the
Adsorption of Humic Acids from Aqueous Solutions on Active Carbon and
Activated Charcoal Cloths, Carbon, Vol. 32, No. 2, p 207, 1994

47   J. M. Bastidas and J. D. Scantlebury, The Influence of Light on Corrosion
Phenomena: the Behavior of Mild Steel in Citric Acid Solution, Corrosion
Science, V.26, no. 5, 1986, p 343

48   T. E. Ford, J.S. Maki, R. Mitchel, The Role of Metal-Binding
Exopolymers in Corrosion Proccsses, CORROSION/87, no. 380, Houston, TX:
NACE, 1987

49   G. Chen and C. R. Clayton, Influence of Sulfate-Reducing Bacteria on the
Passivity of Type 304 Austenitic Stainless Steel, Journal of the Electrochemical
Society, Vol. 144, No. 9, p 3141, 1997

50   Herbert. H. Ulig and R. Winston. Revie, Corrosion and Corrosion Control
An Introduction to Corrosion Science and Engineering, Ed. 3rd, John Wiley and
Sons, Inc., New York, p 352, 1985

51   D. A. Shirley, Physics Review, B5, 4709, 1972

52   J. R. Postgate The Sulfate Reducing Bacteria, 2nd Ed., Cambridge
University Press, Cambridge, UK, (1984), p 48

53	ASTM designation G 48-76, Standard Test Methods for Pitting and Crevice Corrosion Resistance of Stainless Steels and Related Alloys by the Use of Ferric Chlorine Solution, p 185, reapproved 1980

54	Raymond L. Kepner, JR. And James R. Pratt, Use of Fluorochromes for Direct Enumeration of Total Bacteria in Environmental Samples: Past and Present, Microbiological Reviews, Vol. 58, No. 4, p 612, 1994

55	Morrison and Boyd, Organic Chemistry, 5th ed., Allyn and Bacon, Inc., Boston, p 849-850, 1987

56	G. P. Halada, M. E. Monserrat, C. R. Clayton, S. V. Kagwade, J. Di, T. Tamagawa, A. R. Srivatsa, B. L. Halpern, A Study of the Passivation Mechanism in Highly Corrosion Resistant "Stainless Steel" Alloy Coatings Formed Using the JVD Process, Advances in Coatings Technologies for Surface Engineering, Editors: C. R. Clayton, J. K. Hirvonen and A. R. Srivatsa, The Minerals, Metals & Materials Society, TMS, PA 15086, (1996), p.353

57	G. Chen, S.V. Kagwade, G. French, T. E. Ford, R. Mitchell and C. R. Clayton, Metal Ion and Exopolymer Interaction: Surface Analytical Study, Corrosion, NACE, 52, 12, p 891, (1996)

58	Y. C. Lu, A. R. Brooks and C. R. Clayton, Bipolar Model of the Passivity of Stainless Steel: Part II Influence of Solution Borne Molybdate Ions, Corrosion Science, Vol. 29, No. 7, p 863 (1989)

59	L. Stryer, Biochemistry, 3rd ed., W. H. Freeman and Co., (1988), p 23

60	G. C. Chen, Ph.D. Thesis, State University of New York at Stony Brook, (1996), p 221

61	G. Lyberatos and L. Kobotiatis, Inhibition of Aluminum of 7075 Alloy Corrosion by the Concerted Action of Nitrate and Oxalate Salts, Corrosion, Vol. 47, No. 11, (1991) p 820

62	Kazuo Nakamoto, Chapter 4, Infrared Spectroscopy, Kazuo Nakamoto, and Paul J. McCarthy, S.J., Spectroscopy and Structure of Metal Chelate Compounds, John Wiley and Sons, Inc. New York, (1968), p 220

63   Curtis R. Hare, Chapter 2, Visible and Ultraviolet Spectroscopy, Kazuo Nakamoto, and Paul J. McCarthy, S.J., Spectroscopy and Structure of Metal Chelate Compounds, John Wiley and Sons, Inc. New York, (1968), p 73

Appendix I

Metal Ion and Exopolymer Interaction: A Surface Analytical Study [1]

G. Chen, S. V. Kagwade, G. E. French, T. E. Ford, R. Mitchell, and C. R. Clayton

Abstract

Various concentrations of molybdate (MoO_4^{2-}) were added to the protein-containing and deproteinated exopolymers of the marine bacterium *Deleya marina*. Interaction was investigated using x-ray photoelectron spectroscopy (XPS) and electron spin resonance (ESR). MoO_4^{2-} reduction was observed exclusively in the deaerated protein-containing exopolymer, resulting in the formation of a Mo^{5+} species. This species appeared susceptible to reoxidation in the presence of soluble oxygen. Only hexavalent molybdenum (Mo^{6+}) was seen in the aerated suspension. The reducing agents may have been the residual proteins that remained in the exopolymer without subsequent deproteination.

The influence of this reduction on corrosion resistance of Mo-bearing stainless steels (SS) was simulated with an austenitic type 304 SS (UNS S30400), whose surface was treated with MoO_4^{2-} before exposure to the exopolymer. In addition to formation of the Mo^{5+} species, a small amount of molybdenum dioxide (MoO_2) was detected, and hydration of the passive film increased. No evidence was found to indicate the

exopolymer attachment compromised corrosion resistance of the SS in deaerated 0. I M hydrochloric acid (HCI).

Introduction

As the importance of biofilms in microbiologically influenced corrosion (MIC) has become more understood, Interactions between bacterial exopolymers and metal substrata have received considerable interest from microbiologists and material scientists. [1-2] Exopolymers comprise the outermost extracellular polymeric envelope of many types of bacteria. They contribute a structural component to the biofilm, providing the basis for bacterial attachment to a substratum.[3-4] Exopolymers protect the bacteria and may influence uptake of ions and molecules into the microorganisms .[5-6] The binding ability of an exopolymer to a metal ion may be an important factor in adhesion of the biofilm to a metal substratum and

may determine its ability to attract and assimilate metal ions from the substratum and media.[7-8]

The objective of the present work was to study interaction of the exopolymer of a marine bacterium, *Deleya (Pseudomonas) marina*, with molybdate (MoO_4^{2-}) a group VI oxyanion.

Assimilation of trace metal ions by *D. marina* is of the order: Fe > Cd > Cu > Zn > Pb > Ni = Mn.[2,7] Interaction of metal ions with the crude exopolymer of this bacterium, as measured by their maximum binding abilities, varies in a different order: Mn > Cu > Ni > Fe. This interaction does not take place once the exopolymer is purified by deproteination. Therefore, the interaction is attributable to species that may be removed during deproteination, including functional amino groups and residual proteins.[2]

In the present work, x-ray photoelectron spectroscopy (XPS), electron spin resonance (ESR), and electrochemical methods were used to study interaction of the exopolymer with MoO_4^{2-}. XPS provides information about the electron-transfer process of the interaction through valence state analysis. The unique feature of ESR is its ability to identify unpaired electrons. ESR was used to characterize the products and confirm XPS observations of odd valence states. Concentrations of MoO_4^{2-}, from 0.01 M to 0.05 M, were added to protein-containing and deproteinated exopolymers to determine if reduction would occur.

Subsequently, an austenitic SS, type 304 SS (UNS S30400), was surface-treated with MoO_4^{2-}, exposed to the exopolymer, and characterized using XPS. Surface changes induced by the exopolymer were characterized by potentiodynamic polarization in deaerated 0.1M hydrochloric acid (HCl).

MoO_4^{2-} species were found to be present in the outer region of the passive film formed on Mo-bearing SS, where it is believed that MoO_4^{2-} is most effective in repelling the ingress of chloride ions (Cl^-), which are powerful producers of pitting corrosions. [9-11]

Experimental

Preparation of the Exopolymer

D. marina (ATCC 25374) was obtained from the American Type Culture Collection in Rockville, Maryland. The culture was maintained on slants of marine agar 2216 and stored at -20°C in glycerol. For exopolymer extraction, bacteria in batch cultures were grown to stationary phase (A_{660} = 2.7) in a defined minimal medium with glucose as the C source. Once the batch cultures reached stationary stage, they were centrifuged at 20,000 rpm for 20 min to separate cells from extracellular material. The supernatant was filtered through sterilized 0.2-μm filters and then concentrated in a stirred ultrafiltration cell with a nominal

molecular weight (MW) cutoff of 5,000. The concentrated supernatant was precipitated with three volumes of 95 vol% ethanol and stored at 4° C for 24 h. The precipitate was collected through centrifugation, dissolved in deionized water (18.2 MΩ), and dialyzed extensively with deionized water before lyophilization. The lyophilized solution product was considered crude exopolymer (protein-containing).

For subsequent deproteination, extraction was used to remove lipids, followed by extensive dialysis with deionized water. Deproteination was conducted several times with chloroform and isopropanol, followed by extensive dialysis. The deproteinated exopolymer then was lyophilized. Crude and deproteinated exopolymers were stored in a dessicator before experimentation. Chemical analysis of the exopolymer has been reported elsewhere.[2,12]

Addition of MoO_4^{2-} to the Exopolymer

Rehydration and sample preparation were performed in a nitrogen (N_2) - purged glove bag. Deionized water was deaerated by boiling and purging with ultra high-purity N_2 at least 20 min, cooled on ice, and placed in the glove bag. Exopolymer (1 mg [0.000035 oz]) was dissolved in 0.1 mL (0.003 oz) deaerated deionized water. Sodium molybdate (Na_2MoO_4) solution was deaerated,

transported into the glove bag, and pipetted into three aliquots of the exopolymer to give final concentrations of 0.01 M, 0.02 M, and 0.05 M MoO_4^{2-}. Aerated suspension was prepared without deaerating deionized water and the MoO_4^{2-} solution. Both suspension types were allowed to equilibrate for 4 h and then dropped onto a 1-cm^2 (0.16-in.1) piece of Si wafer that had been rinsed in 5% hydrofluoric acid (HF) solution to remove the surface oxide and then rinsed thoroughly in deionized water. As soon as a droplet started to dry, it was rinsed using deaerated deionized water to obtain a relatively thin exopolymeric film. The film was dried overnight in N_2 before XPS analysis. Ti (99.99%) coupons were polished to a 6-pm diamond finish, ultrasonically degreased in acetone, and rinsed in deionized water. These coupons were used in place o the Si wafer to investigate the influence, if any, of the substrata.

Processing of Type 304 SS Samples

Composition of the type 304 SS was (wt%): 69.62% Fe, 19.27% Cr, 8.49% Ni, 0.35% Mo, 1.77% Mn, 0.41% Si, 0.031% P, 0.008% S, and 0.053% C. Foils (1-mm [0.04-in.] thickness) were cut into 1-cm^2 coupons, annealed at 1,080°C for 1 h in an evacuated quartz tube, and quenched in water. The quenching-stabilized coupons were polished to a 6-gm diamond finish and

degreased ultrasonically in acetone. For XPS analysis, the coupons were surface treated with MoO_4^{2-} and exposed to the exopolymer directly. For electrochemical characterization, the coupons were mounted onto polymethyl methacrylate (PMMA) sample holders 2 cm by 1.5 cm by 0.5 cm (0.096 in.3) using epoxy resin before the MoO_4^{2-} treatment and exposure. Connection from the electrode to the potentiostat was made using a Cu wire placed between the sample and the PMMA block and passing through an 8-mm (0.32-in.) outer-diameter glass tube mounted on the PMAM block. Both sample types were placed in a N_2 filled glove box. Samples were rinsed thoroughly in deaerated deionized water and immersed in deaerated 0.1 M MoO_4^{-2} solution for 2 h. After the surface MoO_4^{2-} treatment, they were rinsed with deaerated deionized water and dried by blowing N_2 over the surface. A droplet of the exopolymer suspension was placed on each sample, and the samples were left in a sealed glass flask for 12 h. The samples then were processed for XPS and electrochemical characterization under two surface conditions, one being thoroughly rinsed with deaerated deionized water and the other unrinsed.

In addition to those samples, another type of sample was prepared by direct exposure to the protein-containing exopolymer for 5 min to study the effect of the adsorbed exopolymer on electrochemical behavior. The quenching-stabilized coupons were polished, rinsed, and mounted on the PMMA sample holders. They

were placed in the glove box, rinsed with deaerated deionized water, and immersed in the deaerated exopolymer suspension for 5 min, under two conditions: without disturbance and stirred mechanically to aid in adsorption.

XPS

A VG Scientific ESCA 3 Mark II XPS spectrometer was used for the analysis. The spectrometer was controlled using a VGX900 interface and data acquisition software. The samples were transported into the XPS chamber in an Ar-purged glove bag. The vacuum was maintained below 4×1^{-9} torr. To prevent outgassing, liquid N_2 cooling was provided. An Al K_α x-ray source (1,486.6 eV, 400 W) was used to provide a full width at half maximum (FWHM) of 1.35 eV for Au $4f_{7/2}$. The entrance and exit slit widths were set at 4 mm (0. 16 in.). Analyzer energies were set at 100 eV for wide-survey scans and 20 eV for region scans. Charge shifting was corrected with the adventitious C 1s line at 284.6 eV. Spectra were obtained at several photoelectron takeoff angles, ranging from 20' to 50' with respect to the sample surface. Nonlinear least-square curve fitting was performed. Parameters included the Gaussian/ Lorentzian ratio, constant tail ratio, exponential tail slope, and constant/exponential tail mixing ratio. Background subtraction was performed using the Shirley method.[13] Peak subtraction and secondary differentiation aided in peak identification.[14-16] Peak parameters used as standards

were obtained with the pure elements and compounds using the same spectrometer settings (Table 1).

ESR

An X-band Varian E- 12 ESR spectrometer was used. The microwave frequency was set at 9.51 GHz, and the magnetic field was scanned to find the resonant condition for the given species. The suspension containing 0.02 M MoO_4^{2-} was cooled with liquid N_2 to a temperature of 77° K during analysis. Suitable standards for Mo^{5+} were analyzed, yielding characteristic g values under the same conditions.[17-18]

Electrochemical Characterization

A Gamry CMS 100 potentiostat was used for electrochemical characterization. The experiment was conducted in the glove box at room temperature, using a 1-L Greene cell and a saturated calomel reference electrode (SCE). Counter electrodes were made of Pt wires 1-mm (0.039 in.) in diameter. The 0.1 M HCI solution was deaerated in the Greene cell at least 2 h before the working electrode was inserted. Potentiodynamic polarization started at a sweep rate of 1 mV/s from the open-circuit potential. Cathodic surface conditioning was not applied to avoid the influence of cathodic reactions on the surface. This test

simulated typical pitting conditions in a local area associated with a low pH and high Cl content.

Results and Discussion

XPS Analysis of the MoO42–Doped Exopolymers

The wide scan qualitatively revealed that the exopolymer consisted primarily of C, O, N, Ca, Si, and S. Ca, Si, and S signals were detectable only in the protein-containing exopolymer (Figure 1). The S signal indicated a possible disulfide bond, which is seen often in extracellular proteins,[19] whereas Si may have been a contaminant. The spectra showed a certain amount of charge shifting, compared to results of previous work where the surface charge was neutralized with an electron flood gun.[7] The binding energy (BE) difference between the C 1s in the present work and that with the electron flood gun was ~2.3 eV, equal to the BE difference of the other component peaks in the two investigations.[7]

Figures 2(a) and (b) show the Mo3d photoelectron spectra from the deaerated and aerated protein-containing exopolymers doped with 0.02 M MoO_4^{2-}. Reduction of MoO_4^{2-} to Mo^{5+}, took place only in the deaerated protein-containing exopolymer. The residual hexavalent Mo might have existed as Na_2MoO_4, and molybdenum trioxide (MoO_3) and/or molybdic acid ($H_2 MoO_4$). MoO_3 and H_2MoO_4 were fitted into one peak because their BE values were very close (Table

1). The absence of Mo^{5+} in the Mo3d spectra of the aerated sample indicated its susceptibility to oxidation when soluble O was present. Addition of MoO_4^{2-} substantially decreased the S signal, while the Mo signal also was reduced. This indicated interaction between MoO_4^{2-} and S species in the exopolymer. The fact that the Mo and S signals were reduced suggested formation of two possible products, a high-vapor pressure product that evaporated in the spectrometer chamber or a cluster of Mo and S compounds attenuating emission of the photoelectrons. The deaerated deproteinated exopolymer did not reveal this reduction effect when MoO_4^{2-} was provided. Spectroscopic features of the other major component peaks, such as C 1s, O 1s and N 1s, did not show obvious differences from those of the protein-containing exopolymer. Therefore, the major functional groups of the exopolymer most likely were not the reducing agents. It was postulated in previous work that the binding moieties to the metal ions probably were the functional amino groups and residual proteins from the biomass that remained in the crude exopolymer prior to subsequent deproteination processing.[2] Present results indicated this reduction more likely was caused by the residual proteins, and specifically, by the sulfide groups. Enzymatic interactions of S-containing proteins with Mo and their influence on microbial metabolism have been recognized.[21]

Reduction of MoO_4^{2-} resulted in a decrease in charging by 1.1 eV (Figures 2 [a] and [b]). From the charge shifting only, it was difficult to derive any information regarding molecular changes in the exopolymer induced by the reduction since no characteristic changes were seen in the spectra of C 1s, O 1s, and N 1s. The decreased charge shifting may have resulted from the decrease in the relative proportion of MoO_4^{-2}. A pure Na_2MoO_4 standard usually showed 4-eV charge shifting toward the high BE side because of its insulating nature.

The influence of MoO_4^{2-} concentration on the interaction was studied using the deaerated suspensions containing 0.01 M, 0.02 M, and 0.05 M MoO_4^{2-}. The most remarkable reduction was seen in 0.02 M MoO_4^{2-} in terms of the relative proportions of peak areas. An increase of MoO_4^{2-} concentration did not increase the degree of reduction, indicating the amount of the reducing agents was limited. The reduction process ended once the reducing agents were consumed.

ESR Analysis of the MoO_4^{2-} Doped Exopolymer

The reduction of MoO_4^{2-} in the deaerated protein-containing exopolymer was confirmed by ESR analysis (Figure 3). The corresponding g factor was 1.969, close to g values of Mo^{5+} found in Mo-containing enzymes.[22-23] In contrast, no MoO_4^{2-} reduction was found in the deproteinated exopolymer, which was consistent with XPS results.

To distinguish the role of the substratum in the reduction, similar studies were performed with the Ti coupons. Reduction of MoO_4^{2-} also occurred. There was no evidence to suggest the selected substrata played a role in the reduction process.

Exopolymer-Induced Reduction of MoO_4^{2-} on the Surface of Type 304 SS

The reduction effect of the exopolymer raised the issue of whether the corrosion resistance of Mo-bearing SS was compromised by attachment of the exopolymer, since externally bound MoO_4^{2-} salts are effective pitting inhibitors in Cl^- containing media. The interaction was investigated using the MoO_4^{2-} treated type 304 SS to simulate the surface condition of Mo-bearing SS, such as type 316 SS (UNS S31600), but without the interference of a constant source of Mo from the alloy. Samples were immersed in 0.1 M Na_2MoO_4 for 2 h, rinsed, and analyzed by XPS before and after exposure to the exopolymer.

MoO_4^{2-} surface treatment of type 304 SS resulted in formation of ferrous molybdate ($FeMoO_4$). The spectra of Mo 3d showed the existence of MoO_4^{2-} on the steel surface (Figure 4[a]). In contrast to the remarkable charge shifting in the Mo 3d spectra of the Na_2MoO_4, standard, the spectra revealed little charging and indicated close contact of the molybdate to the steel substratum. No Na signal was

detectable. The Fe2P$_{3/2}$ spectra revealed formation of FeMoO$_4$ associated with a significant decrease in relative proportions of ferrous oxide (FeO) and ferric oxyhydroxide (FeOOH) usually existing on the surface of a freshly polished coupon (Figure 5[a]).[24]

The Cr2p spectra essentially remained unchanged (Figure 6[a]), and Ni remained in its metallic form.[24] Relative proportions of the metal element on the surface are given in Table 2. There was a certain degree of depletion of Fe and enrichment of Cr, particularly in the outer region of the surface.

After the MoO$_4^{2-}$ treated surface was exposed to the deaerated protein-containing exopolymer, XPS analysis was performed, and the relative proportions of the surface metal elements were calculated (Table 2). The surface MoO$_4^{2-}$ was reduced by 50%, associated with a greater degree of surface depletion of Fe and enrichment of Cr. The Ni signal was no longer visible. Changes in the valence states of Mo3d, Fe2p$_{3/2}$ and Cr2p spectra are shown in Figures 4(b), 5(b), and 6(b), respectively. Reduction of MoO$_4^{2-}$ to Mo^{5+} took place to a greater extent in a few top mono-layers of the SS surface (Figure 4[b]). On comparing Figures 2 and 4(b), it was evident that these Mo3d spectra differed from those obtained from the suspension droplets by formation of MoO$_2$ on the surface. Formation of MoO$_2$ may have resulted from the interinfluence of the alloying elements, since the conversion of MoO$_4^{2-}$ to MoO$_2$ usually takes place under aerobic conditions.[9]

Consistency of the results may be seen from the $Fe2p_{3/2}$ spectra (Figure 5). The amount of $FeMoO_4$ was reduced greatly, showing little depth dependence. A dominant amount of Fe^{3+} existed in the outer layer, with a certain amount of FeO and FeOOH. The $Fe2p_{3/2}$ spectra from the sublayer consisted of a considerable amount of metallic Fe, Fe^{3+}, and oxyhydroxide, as well as a small quantity of Fe^{2+}. Finally, an increased proportion of chromium hydroxide $(Cr[OH]_3)$ appeared in the Cr2p spectra, particularly in the outer layer, indicating increased surface hydration (Figure 6).

Electrochemical Aspects

Potentiodynamic polarization was conducted in deaerated 0.1 M HCl to study the influence of MoO_4^{2-} treatment and subsequent exposure to the exopolymer on the passivation performance of type 304 SS. Evidence of surface modification by MoO_4^{2-} was revealed by a greater degree of anodic dissolution and a stable passivity at a higher overpotential (Figure 7). The influence of exopolymer was not considerable. The potentiodynamic polarization result was almost identical in the exopolymer-exposed and the unexposed steels. This did not mean that the surface would remain intact once a thick biofilm developed. The interaction of the exopolymer with MoO_4^{2-} indicated a potential mechanism for the bacterial attachment to the Mo-bearing steel substrata. In an environment where the

bacteria exist, depletion of surface Mo would reduce corrosion resistance of Mo-bearing SS.

The influence of the adsorbed exopolymer on the potentiodynamic behavior of type 304 SS in deaerated 0.1 M HCl is illustrated in Figure 8. Anodic dissolution was reduced, despite a lack of uniformity of the adsorbed layer of the exopolymer. However, a uniformly adsorbed layer, resulting from mechanical stirring, led to better surface stability, as indicated by the lower current density in the passive region.

CONCLUSIONS

❖ The protein-containing exopolymer of the bacterium *D. marina* had a reducing effect on MoO_4^{2-}, yielding products of Mo^{5+} under anaerobic conditions. The reduction could be induced by the S-containing residual proteins.

❖ This reduction also was seen on the surface of the MoO_4^{2-} treated austenitic type 304 SS and was associated with the formation of MoO_2.

❖ Exposure to the exopolymer resulted in the surface depletion of Fe and enrichment of Cr, rendering an increased hydration of Cr. However, evidence did not indicate that corrosion resistance of the SS was compromised by the exopolymer attachment.

Acknowledgments

TABLE 1
XPS Curve-Fitting Parameters

	Element		BE (eV)	1/2 FWHM (eV)	G/L	Exponential Slope	Tail Mix Ratio	Const. Tail Height
Fe	Fe2p$_{3/2}$	Fe	706.8	0.900	0.500	0.075	0.500	0.001
		FeO	709.0	1.100	0.500	20.0	0.500	0.001
		FeMoO$_4$	710.1	1.200	0.500	20.0	0.500	0.001
		Fe$_2$O$_3$	710.7	1.200	0.500	20.0	0.500	0.001
		Fe(OOH)γ	711.6	1.200	0.500	20.0	0.500	0.001
		Fe(OOH)α	712.6	1.200	0.500	20.0	0.500	0.001
Cr	Cr2p$_{3/2}$	Cr	574.1	0.700	0.650	0.050	0.500	0.001
		Cr$_2$O$_3$	576.3	1.200	0.500	20.0	0.500	0.001
		Cr(OH)$_3$	577.1	1.100	0.500	20.0	0.500	0.001
		CrO$_3$	578.3	0.700	0.500	20.0	0.500	0.001
Cr	Cr2p$_{1/2}$	Cr	583.3	1.000	0.650	0.060	0.500	0.001
		Cr$_2$O$_3$	586.0	1.300	0.500	20.0	0.500	0.001
		Cr(OH)$_3$	586.8	1.200	0.500	20.0	0.500	0.001
		CrO$_3$	587.5	0.900	0.500	20.0	0.500	0.001
Mo	Mo3d$_{5/2}$	Mo^{4+}	229.0	0.800	0.500	0.110	0.500	0.001
		Mo^{5+}	230.8	1.000	0.500	20.0	0.500	0.001
		Na$_2$MoO$_4$	231.9	0.800	0.500	20.0	0.500	0.001
		FeMoO$_4$	232.1	0.800	0.500	20.0	0.500	0.001
		MoO$_3$	232.5	0.800	0.500	20.0	0.500	0.001
		H$_2$MoO$_4$	232.7	0.800	0.500	20.0	0.500	0.001
Mo	Mo3d$_{3/2}$	Mo^{4+}	232.2	0.900	0.700	0.110	0.500	0.001
		Mo^{5+}	234.0	1.100	0.500	20.0	0.500	0.001
		Na$_2$MoO$_4$	235.1	0.900	0.500	20.0	0.500	0.001
		FeMoO$_4$	235.3	0.900	0.500	20.0	0.500	0.001
		MoO$_3$	232.8	0.900	0.500	20.0	0.500	0.001
		H$_2$MoO$_4$	232.9	0.900	0.500	20.0	0.500	0.001
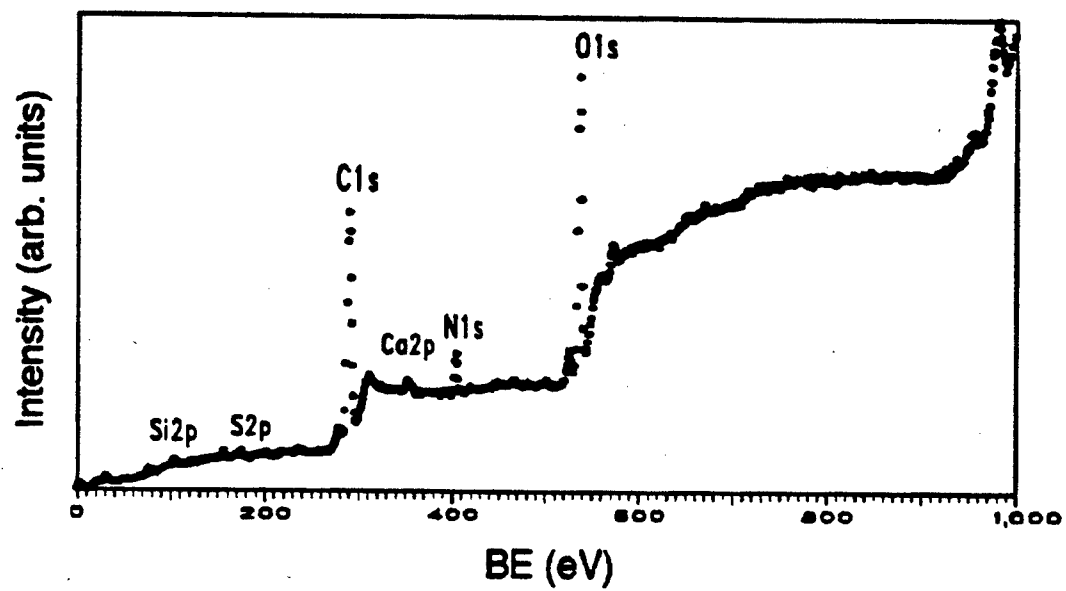
FIGURE 1. Composition of the protein-containing exopolymer of

D. marina shown in XPS wide scan.
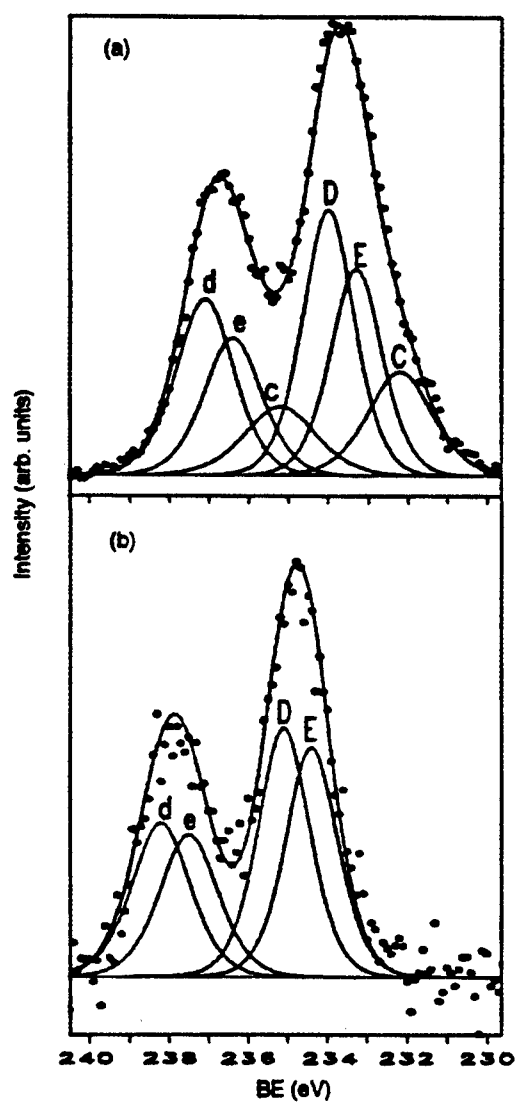
FIGURE 2. MoO_4^{2-} reduction induced by the deaerated protein-containing exopolymer of *D. marina* at takeoff angle of 25°: (a) deaerated suspension with 0.02 M MoO_4^{2-} and (b) aerate suspension with 0.02M MoO_4^{2-} (C, c: Mo^{5+},D, d: MoO_3 / H_2MoO_4;and E, e: MoO_4^{2-}).

g = 1.969

FIGURE 3. Mo^{5+}, shown in an ESR spectrum of the deaerated protein-containing exopolymer of *D. marina* with 0.02 M MoO_4^{2-} (field center: 3450. 0 Gauss [G]; scan width: 1,000 G; T = 77°K; and g = 1. 969).
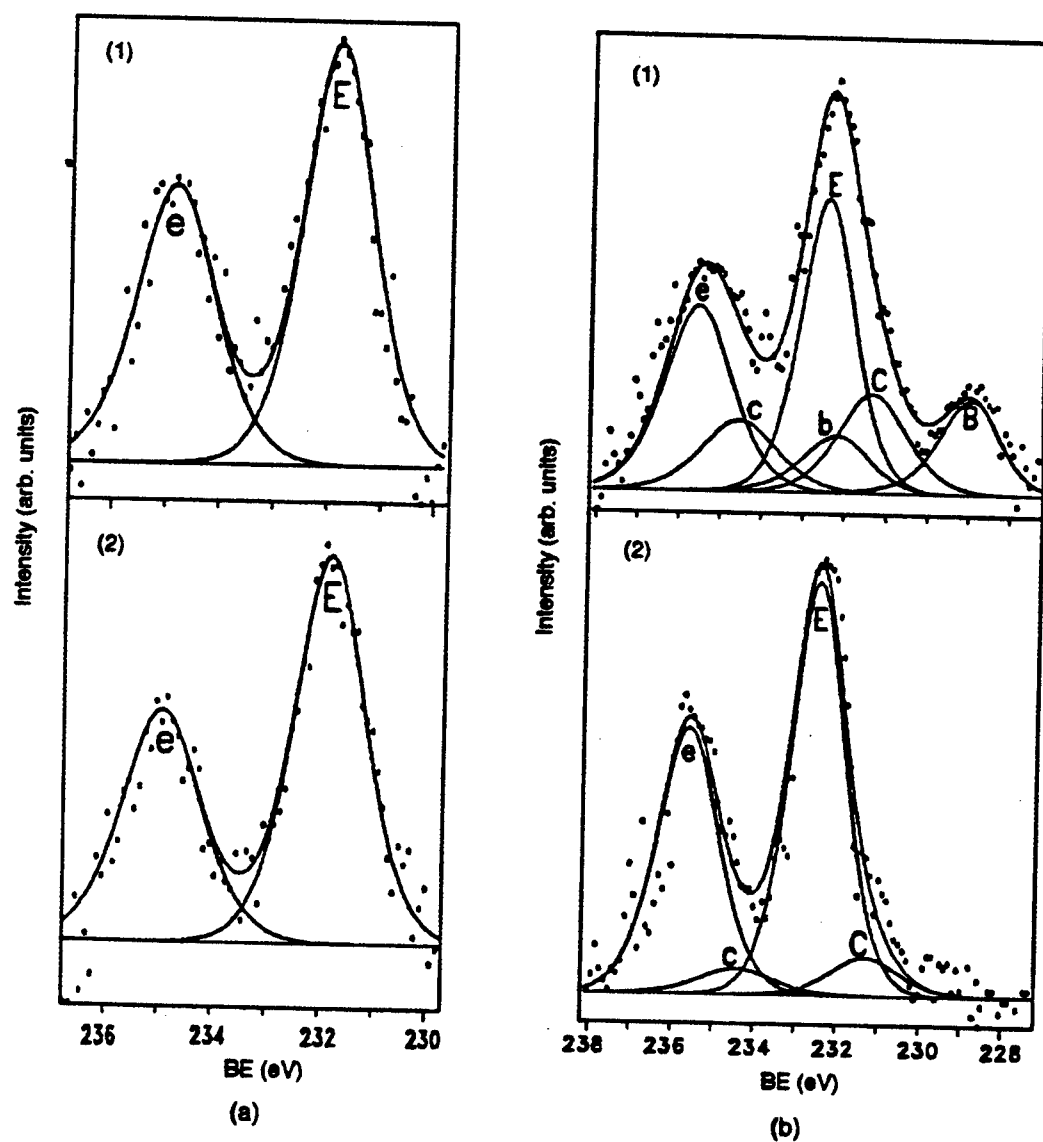
FIGURE 4. Influence of the deaerated protein-containing exopolymer of *D. marina* on Mo3d on the surface of type 304 SS (a) before exposure and (b) after exposure following MoO_4^{2-} treatment at: (1) takeoff angle of 20° and (2) takeoff angle of 50° (B, b: MoO_2; C, c: Mo^{5+}; and E, e: MoO_4^{2-}).
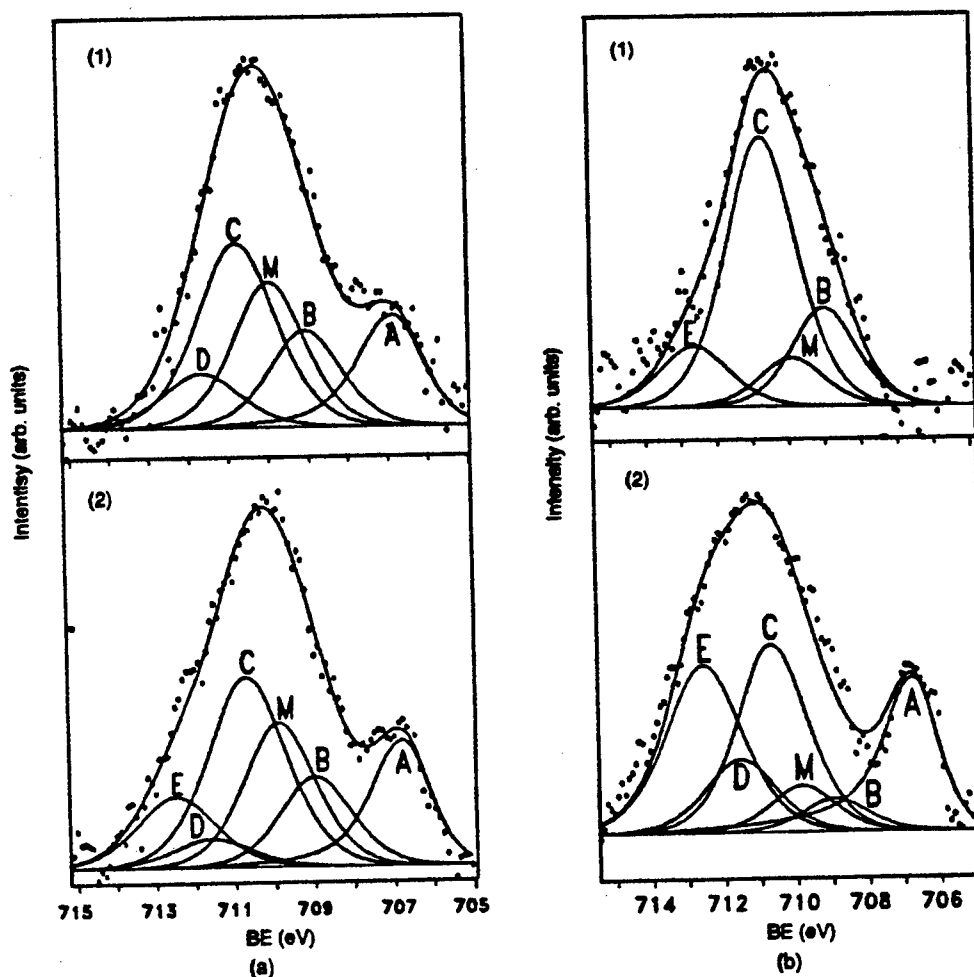
FIGURE 5. Influence of the deaerated protein-containing exopolymer of D. marina on the Fe2p on the surface of type 304 SS (a) before exposure and (b) after exposure following MoO_4^{2-} treatment: (1) takeoff angle of 20° and (2) takeoff angle of 50° (A: elemental Fe; B: ferrous oxide [FeO]; C: ferric oxide [Fe_2O_3]; D: ferric oxyhydroxide-α [Fe(OOH)$_\alpha$]; E: ferric oxyhydroxide-β [Fe(OOH)$_\beta$]; and M: ferrous molybdate [$FeMoO_4$])
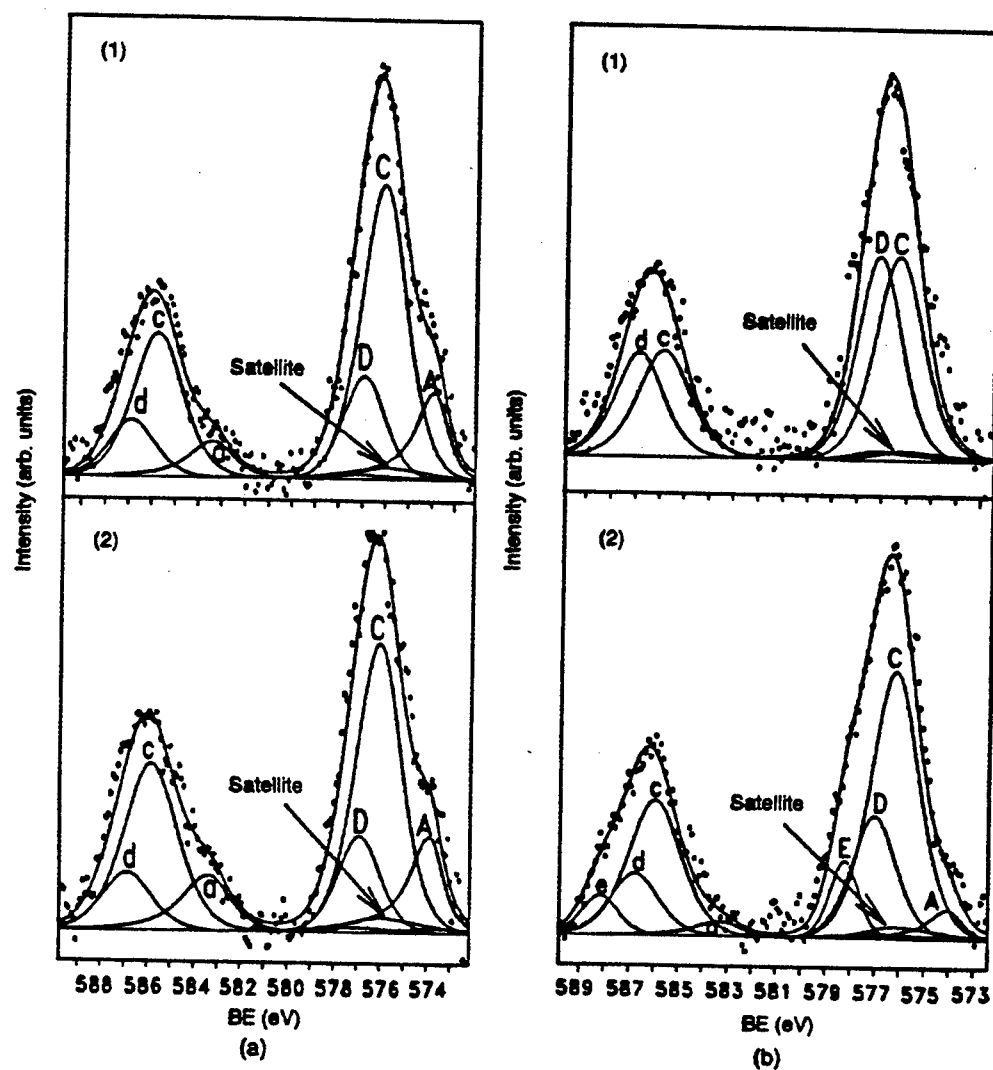
FIGURE 6. Influence of the deaerated protein-containing exopolymer of *D. marina* on Cr2p on the surface of type 304 SS (a) before exposure and (b) after exposure following MoO_4^{2-} treatment at: (1) takeoff angle of 20° and (2) takeoff angle of 50° (A, a: elemental Cr; C, c: chromic oxide $[Cr_2O_3]$; D, d: chromic hydroxide $[Cr(OH)_3]$; and E, e: chromium trioxide $[CrO_3]$).

TABLE 2
Relative Proportions of Alloy Elements
on the Surface of Type 304 SS After MoO_4^{2-} Treatment
and Subsequent Exposure to the Exopolymer of D. Marina

Treatment	Elements (at%)				Takeoff Angle
	Fe	Cr	Ni	Mo	
Polished to 6 μm	70%	28%	2%	—	20°
	72%	25%	3%	—	50°
MoO_4^{2-} treated	50%	35%	3%	12%	20°
	60%	27%	2%	11%	50°
MoO_4^{2-} treated and	46%	49%	—	5%	20°
exposed to D. marina	45%	50%	—	5%	50°

TABLE 2

Relative Proportions of Alloy Elements on the Surface of Type 304 SS After

MoO_4^{2-} Treatment and Subsequent Exposure to the Exopolymer of D. Marina.
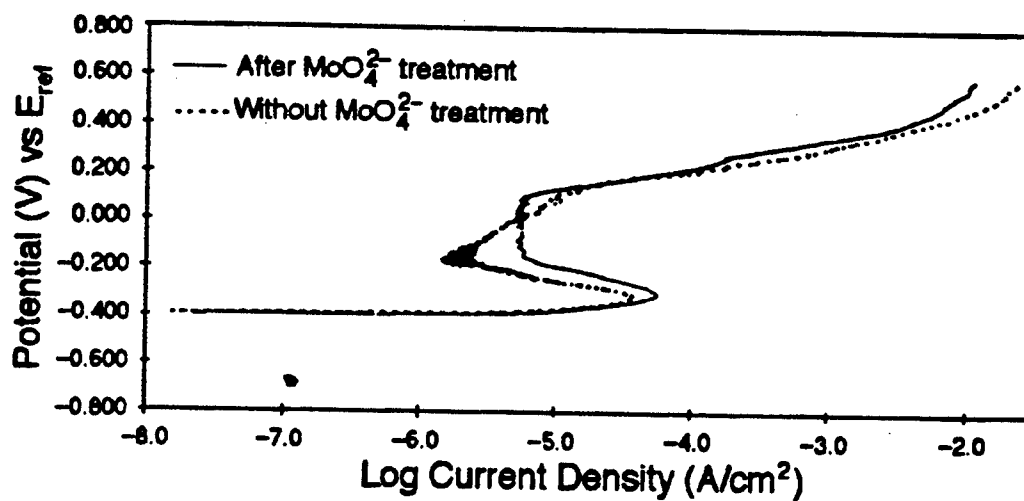
FIGURE 7. Effect of MoO_4^{2-} surface treatment on potentiodynamic polarization of type 304 SS in deaerated 0.1 M HCl ($E_{ref} = E_{SCE}$).
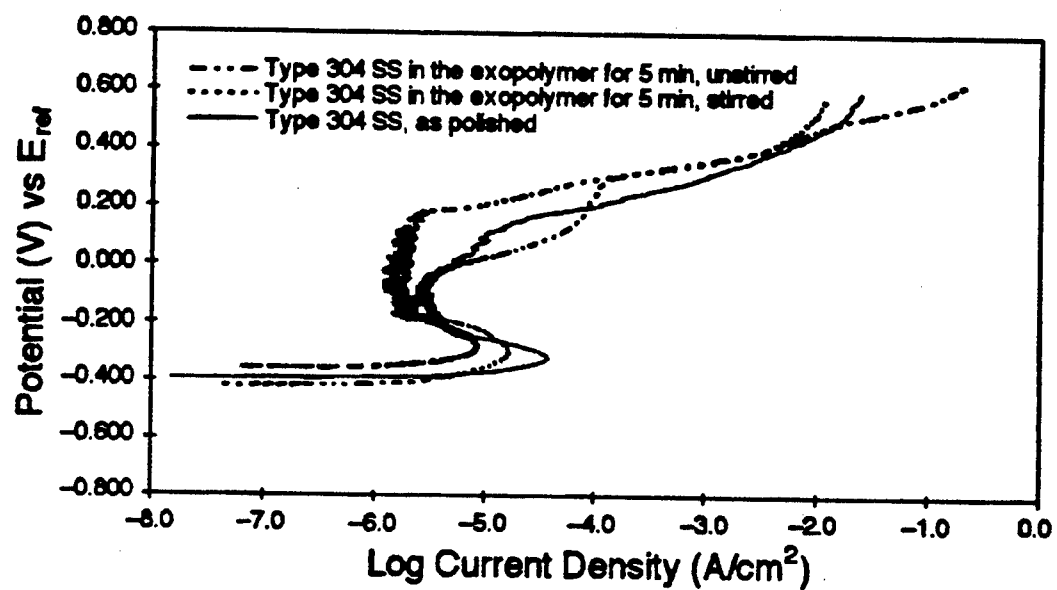
FIGURE 8. Potentiodymanic polarization diagrams of type 304 SS in deaerated 0.1 M HCl after5-min immersion in the deaerated protein-containing exopolymer of *D. marina* suspension.

References

1. W.G. Characklis, K.C. Marshall, eds., Biofilms (New York, NY: John Wiley and Sons, Inc., 1990), p. 635.

2. T.E. Ford, J.S. Maki, R. Mitchel, "The Role of Metal-Binding Exopolymers in Corrosion Processes," CORROSION/87, paper no. 380 (Houston, TX: NACE, 1987).

3. B.J. Little, P. Wagner, S.M. Gerchakov, M. Walch, R. Mitchel, Corrosion 42, 9 (1986): p. 533.

4. G.G. Geesey, M.W. Mittelman, "The Role of High-Affinity, MetalBinding Exopolymers of Adherent Bacteria in Microbial-Enhanced Corrosion," CORROSION/85, paper no. 297 (Houston, TX: NACE, 1985).

5. W.G. Characklis, K.C. Marshall, eds., Biofilms (New York, NY: John Wiley and Sons, 1990), p. 34 1.

6. J.S. Nickels, R.J. Bobbie, D.F. Lott, R.F. Martz, P.H. Benson, D.C. White, Appl. Environ. Microbiol. 41 (1981): p. 1,442.

7. T.E. Ford, J. Black, R. Mitchel, "Metal-Binding Exopolymer of Surface Bacteria," Amer. Soc. Microbiol. Annual Meeting, paper abstract no. I-77, Miami, Florida (Washington, DC: Amer. Soc. Microbiol., 1988).

8. G.G. Geesey, M.W. Mittelman, T. Iwaoka, P.R. Griffiths, MP 25, 2 (1986): p. 37.

9.   H.H. Uhlig, R.W. Revie, "Inhibitors and Passivators," in Corrosion and
      Corrosion Control, 3rd ed. (New York, NY: John Wiley and Sons, 1985),
      p. 263.

10.   Y.C. Lu, C.R. Clayton, A.B. Brooks, Corros. Sci. 29 (1989): p. 863.

11.   Y.C. Lu, C.R. Clayton, A.B. Brooks, Corros. Sci. 29 (1989): p. 881.

12.   T. Ford, E. Sacco, J. Black, T. Kelly, R. Goodacre, R.C.W. Berkeley, R.
      Mitchell, Appl. Environ. Microbiol. 57, 6 (1991): P. 1,595.

13.   D.A. Shirley, Phys. Rev. B 55 (1972): p. 4,709.

14.   A. Savitsky, M.J.E. Golay, Anal. Chem. 36 (1964): p. 1,627.

15.   A. Proctor, P.M.A. Sherwood, Anal. Chem. 54 (1982): p. 13.

16.   H.P. Yule, Anal. Chem. 38 (1966): p. 103.

17.   J.E. Wertz, J.R. Bolton, "Basic Principles of Electron Spin Resonance," in
      Electron Spin Resonance Elementary Theory and Practical Applications
      (New York, NY: Chapman and Hall, 1986), p. 17.

18.   R. Aasa, K.E. Falk, L.S.A. Reyes, Ark. Kemi. 25, 29 (1966): p. 309.

19.   L. Stryer, "Protein Structure and Function," in Biochemistry (New York,
      NY: W.H. Freeman and Co. 1988), p. 23.

20.   C.R. Clayton, Y.C. Lu, Surf. Interf. Anal. 14 (1989): p. 66.

21.   P. Kroneck, J.T. Spence, J. Inorg. Nucl. Chem. 35 (1973): p. 3,391.

22. B. Ghani, M. Takai, N.Z. Hisham, N. Mshimoto, A.K.M. Ismall, T. Tano, T. Sugio, Appl. Environ. Microbiol. 59, 4 (1993): p. 1. 176.

23. J.R. Pilbrow, "Biological Applications of Transition-ion EPR," in Transition Ion Election Paramagnetic Resonance (Oxford, England: Clarendon Press, 1990), p. 521.

24. G. Chen, C.R. Clayton, R.A. Sadowski, J.B. Gillow, A.J. Francis, "Influence of Sulfate-Reducing Bacteria on the Passive Film Formed on Austenitic Stainless Steel, AISI 304," COPROSION/ 95, paper no. 217 (Houston, TX: NACE, 1995).

Modified Postgates Medium C

Ingredients	Content (g/l)
KH_2PO_4	0.5
NH_4Cl	1.00
$CaCl_2·2H_2O$	0.06
$MgSO_4·7H_2O$	0.06
$FeSO_4·7H_2O$	0.002
Na_2SO_4	2.26
Na-citrate	0.30
Yeast extract	1.00
Lactic acid (80%)	3 ml
Deionized water (18.2 MΩ)	balance to 1000 ml

Table 1

Habitats or Substrates Where Lactic Acid producing Bacteria Have Been Isolated

Habitat or Substrate

Milk products

    Sour milk
    Butter
    Cheese
    Yogurt

Meat and meat products

    Fresh Meat
    Bacon
    Sausages
    Fermented sausages

Fermenting vegetables
    Cucumbers
    Olives
    Sauerkraut
    Silage

Fermented and unfermented
    beverages
    Beer wort and beer
    Whisky distilling mashes
    Grape must and wines

Apple juice and ciders
Sake'
Orange juice

Bread
    Leuconostoc in panary yeast
    Sour dough
    Pickles and sauces
    Tomato Ketchup
    Mayonnaise
    Pickled beetroot

Industrial situations
    Lactic acid manufacturer
    Dextran (blood plasma substitute manufacture)

Man and animals
    Mouth
    Alimentary tract
    Vagina
    Blood Stream
    Lungs

Table 2

Subshell	j values	Area Ratio
s	1/2	-
p	1/2, 3/2	1 : 2
d	3/2, 5/2	2 : 3
f	5/2, 7/2	3 : 4

Correlation table of subshells, j values and area ratios for spectra with spin orbital

splitting

Table 3

Polishing Procedure

Step	
1	240 grit SiC
2	600 grit SiC
3	0000 Emery paper
4	6 micron diamond paste on nylon pad
5	6 micron diamond paste on napped cloth
6	1/4 micron diamond paste on napped cloth

The coupons were ultrasonically cleaned in isopropanol between each step.

Table 4

XPS Curve Fitting Parameters

Oxidation State	Species	B. E. (eV)	HWHM (eV)	Gausian/ Lorentzian	Tail Hight	Exp. Slope	Tail Mix
			Cr 2p$_{3/2}$				
Cr	Metal	574.1	0.7	0.65	0.001	0.07	0.5
Cr^{4+}	CrO$_2$	575.2	0.85	0.85	0.001	0.07	0.5
Cr^{3+}	Cr$_2$O$_3$	576.3	1.2	0.5	0.001	-	0.5
Cr^{3+}	CrOOH	577.0	1.1	0.5	0.001	-	0.5
Cr^{6+}	Cr(OH)$_3$	577.1	1.1	0.5	0.001	-	0.5
Cr^{6+}	CrO$_3$	578.3	0.7	0.5	0.001	-	0.5
Cr^{6+}	CrO$_4^{2-}$	579.3	0.7	0.5	0.001	-	0.5
			Cr 2p$_{1/2}$				
Cr	Metal	583.3	1.0	0.56	0.001	0.06	0.5
Cr^{4+}	CrO$_2$	584.7	1.0	0.55	0.001	0.08	0.5
Cr^{3+}	Cr$_2$O$_3$	586.0	1.3	0.5	0.001	-	0.5
Cr^{3+}	CrOOH	586.7	1.2	0.5	0.001	-	0.5
Cr^{6+}	Cr(OH)$_3$	586.8	1.2	0.5	0.001	-	0.5
Cr^{6+}	CrO$_3$	587.5	0.9	0.5	0.001	-	0.5
Cr^{6+}	CrO$_4^{2-}$	588.5	0.9	0.5	0.001	-	0.5
			Fe 2p$_{3/2}$				
Fe	Metal	706.8	0.9	0.5	0.001	0.075	0.5
Fe	FeS$_2$	707.2	0.7	0.65	0.001	-	0.5
Fe	Fe$_{1-x}$S	708.0	1.2	0.5	0.001	-	0.5
Fe^{2+}	FeO	709.0	1.1	0.5	0.001	-	0.5
Fe^{3+}	Fe$_2$O$_3$	710.9	1.3	0.5	0.001	-	0.5
Fe	FeS	711.8	1.2	0.65	0.001	-	0.5
			Ni 2p$_{3/2}$				
Ni	Metal	852.3	0.8	0.6	0.001	0.07	0.5
Ni^{2+}	NiO	854.5	0.9	0.5	0.001	-	0.5
Ni^{2+}	Ni(OH)$_2$	856.6	1.3	0.5	0.001	-	0.5

Oxidation State	Species	B. E. (eV)	HWHM (eV)	Gausian/ Lorentzian	Tail Hight	Exp. Slope	Tail Mix
			O 1s				
O^{2-}	Oxide	529.9	1.0	0.5	0.001	-	0.5
O^{2-}	OH⁻	531.4	1.1	0.5	0.001	-	0.5
O^{2-}	H_2O	532.7	1.1	0.5	0.001	-	0.5
			C 1s				
C	Adventitous	284.6	0.75	0.7	0.001	-	0.5
C	$R-CH_2-OH$	285.7	0.75	0.7	0.001	-	0.5
C	R-COOH	288.0	0.8	0.5	0.001	-	0.5
			Al 2p				
Al^{3+}	Al_2O_3	74.3	1.0	0.6	0.001	-	0.5
Al^{3+}	AlOOH	75.2	1.1	0.5	0.001	-	0.5
Al^{3+}	Al(OH)	75.6	1.0	0.5	0.001	-	0.5
			Cu2p$_{3/2}$				
Cu	Metal	932.4	0.70	0.8	0.001	0.10	0.5
Cu^{1+}	Cu2O	932.2	0.90	0.7	0.001	0.15	0.5
Cu^{2+}	CuO	933.2	1.15	0.3	0.001	0.08	0.5

XPS Curve Fitting parameters

B.E. is binding energy in eV.
HWHM is the Half Width at Half Maximum in eV.

Table 5

Acid	Fe in ppb/ml	Fe MDL	Cr < in ppb/ml	Ni < in ppb/ml
lactic	4.9	1.9	5	7.5
Oxalic	6.8	0.7	1.9	2.8
Citric	3.0	1.5	4.0	6.0
Deionized Water	0	1.5	4.0	6.0

Concentrations of stainless steel type 304 metal component elements (Fe, Ni and Cr) found in 1 mM organic acid solutions after 5 minute exposure.

- MDL is the Minimum Detection Limit which is the lowest detectable limit of the specific element in ppb divided by the number of milliliters of solution.

Table 6

UV-Vis adsorption peak positions

Organic Acid	Lactic	Oxalic	Citric
		306	
	318		
	326		325
Corresponding			358
adsorption peaks	421		
in nanometers		430	
(nm)			465
			623
			633
	637		
	641		641
	655	655	655
		961	

100 mls of 1M concentrations of each of the organic acids (lactic, citric and oxalic) was added to separate 250 ml Erlenmeyer flasks. 5 g of Fe_3O_4.

Table 7

Number of cells per milliliter in the innoculated SRB media

304 stainless steel "as polished"	1.61×10^9 cells/ml
304 stainless steel "as heat treated"	2.16×10^9 cells/ml
Al6x stainless steel "as polished"	1.65×10^9 cells/ml
Al6x stainless steel "as heat treated"	1.24×10^9 cells/ml
AA 2024-T3 "as polished"	2.21×10^9 cells/ml
JPC	1.47×10^9 cells/ml
Control	0 cells/ml

The control was a solution sample randomly taken from uninoculated Postgate media C which contained an Al6x stainless steel coupon.

Table 8

BIOFILM FORMATION IN TUBING
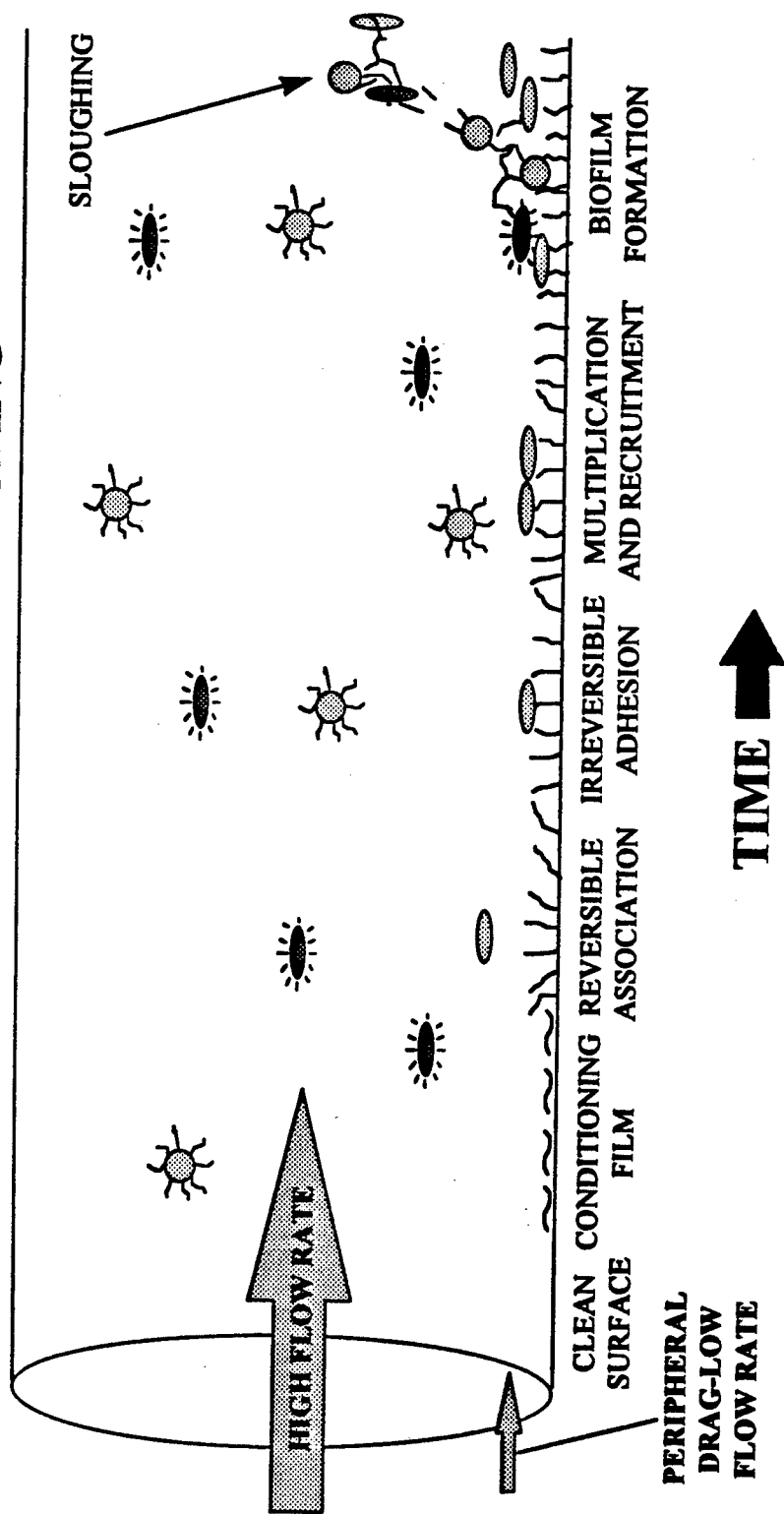
Figure 1[1]
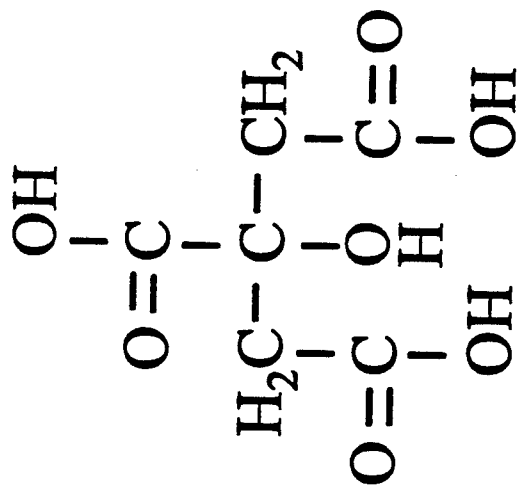
(a) Citric Acid
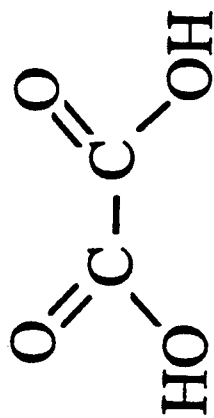
(b) Oxalic Acid
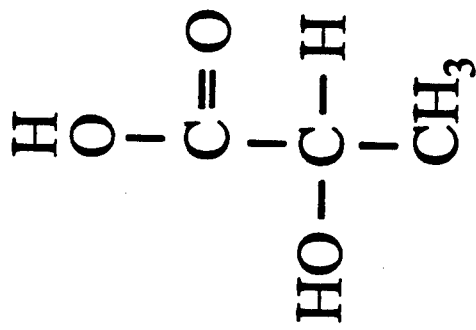
(c) Lactic Acid

Figure 2
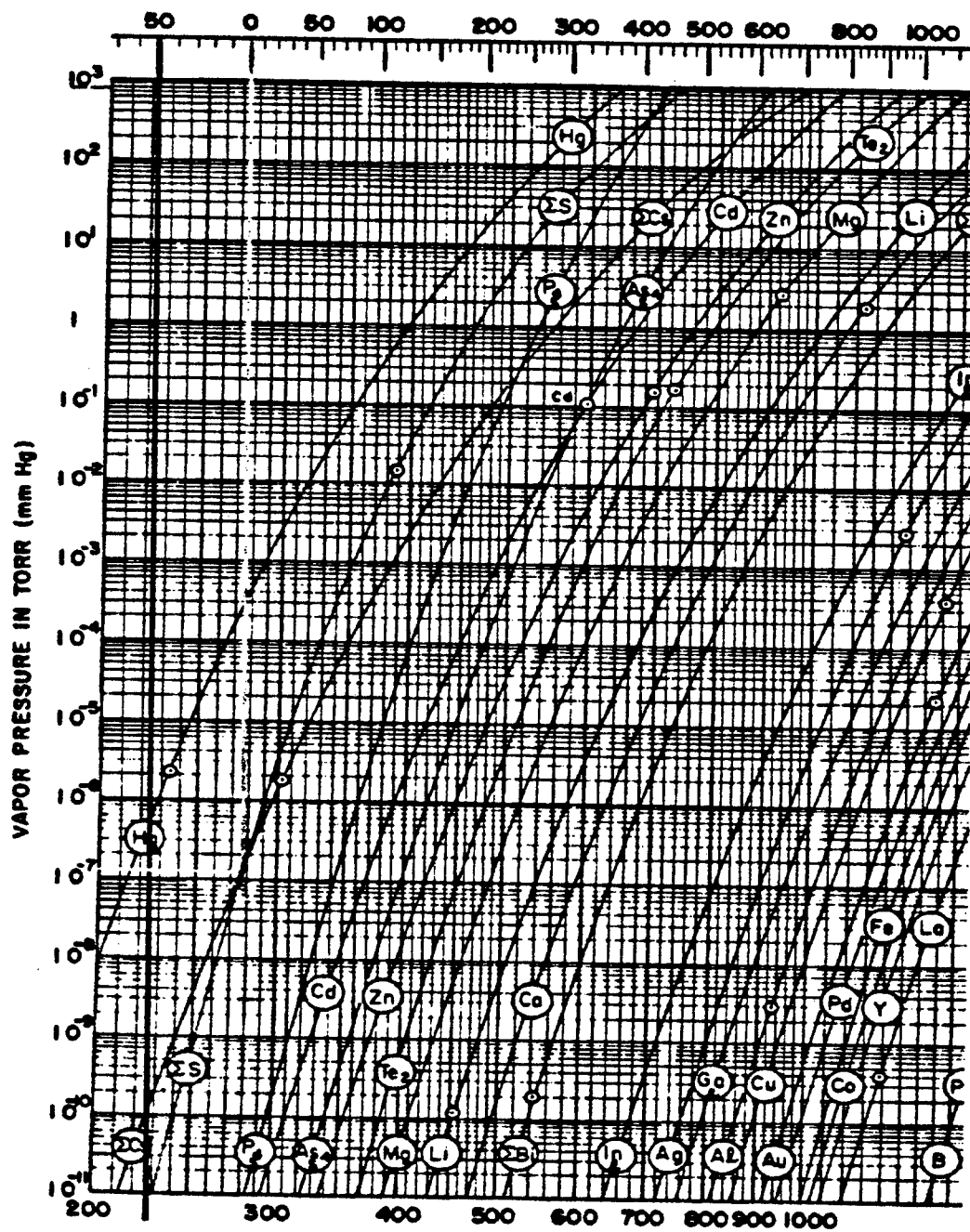
Vapor Pressure vs. Temperature in Degrees C (top axis) or K (lower axis)

Figure 3

a) XPS Spectra   b) XANES Spectra
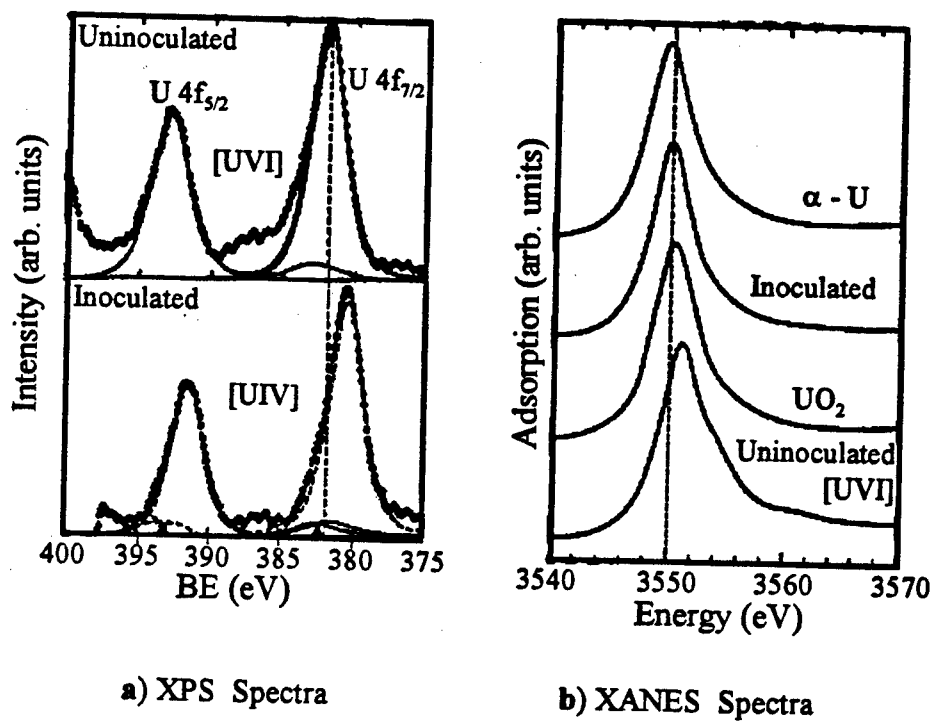
Comparison of XPS spectra and XANES spectra for Uranium from uninoculated

clostridia sp media and from inoculated *clostridia sp* media.[30]

Figure 4

S2p XPS Spectra
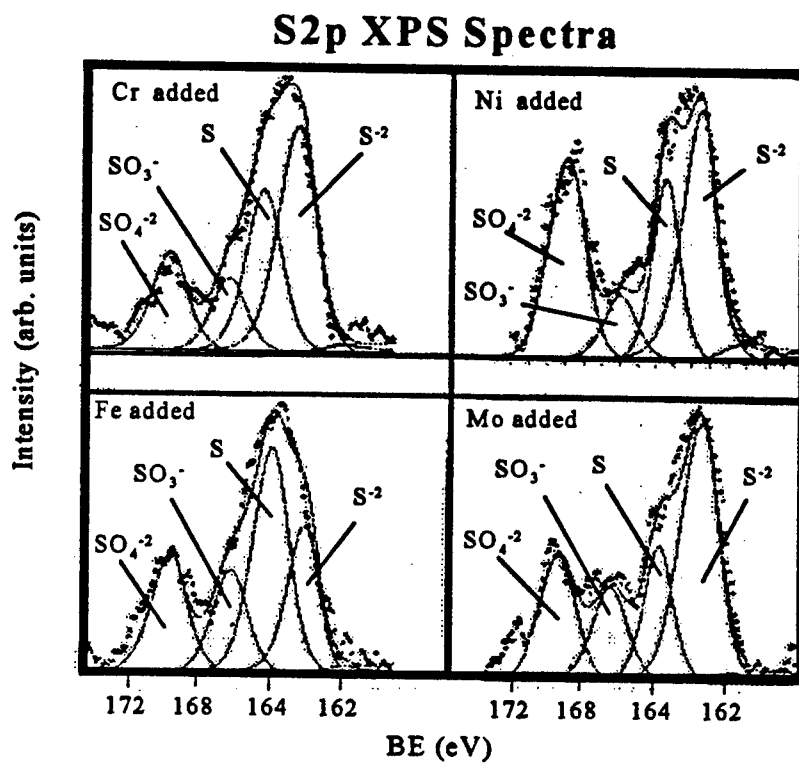
S2p Spectra for biomass of Desulfovibrio sp. following addition of Fe $^{+3}$, Cr $^{+3}$,

Ni $^{+2}$ and Mo $^{6+}$ additions.[31]

Figure 5

Generally Accepted Sulfate Reduction Cycle

$$SO_4^{2-} \big) \xrightarrow[\text{outside cell}]{\text{enters cell}} SO_4^{2-} + ATP \rightleftharpoons APS + PP$$

APS reductase

$$SO_3^{2-} + AMP$$

bisulfide reductase

$$S_3O_6^{2-}$$

thiosulfate reductase

$$S^{2-} \big) \xleftarrow[\text{outside cell}]{} S_2O_3^{2-} \leftarrow$$
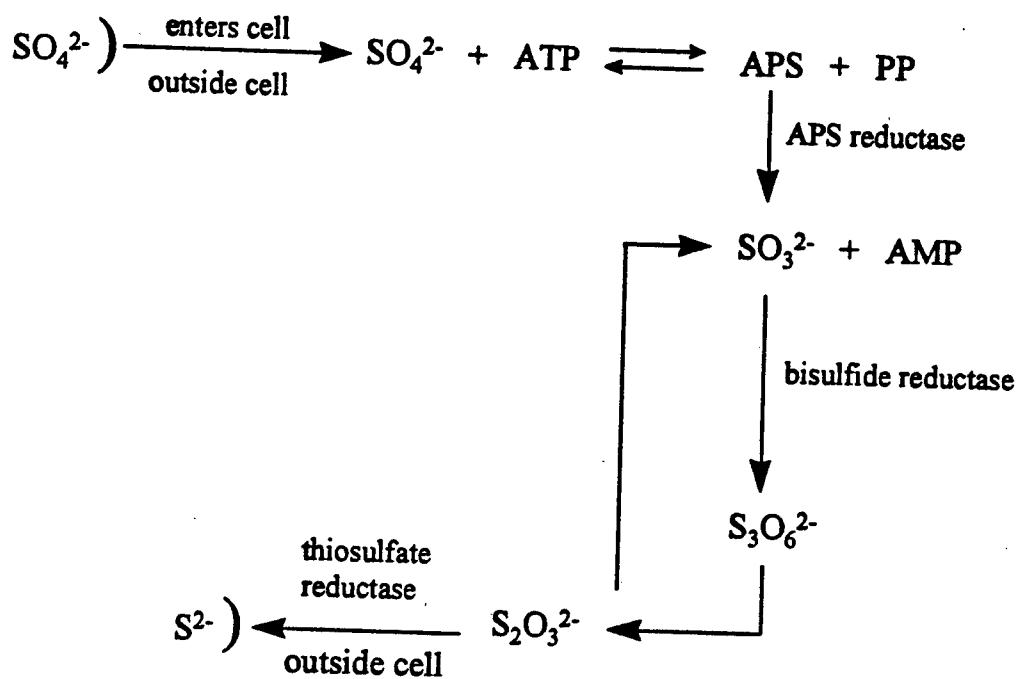
PP - pyrophosphate   **AMP - adenosine 5'-monophosphate**

ATP - adenosine 5'-triphosphate

Figure 6
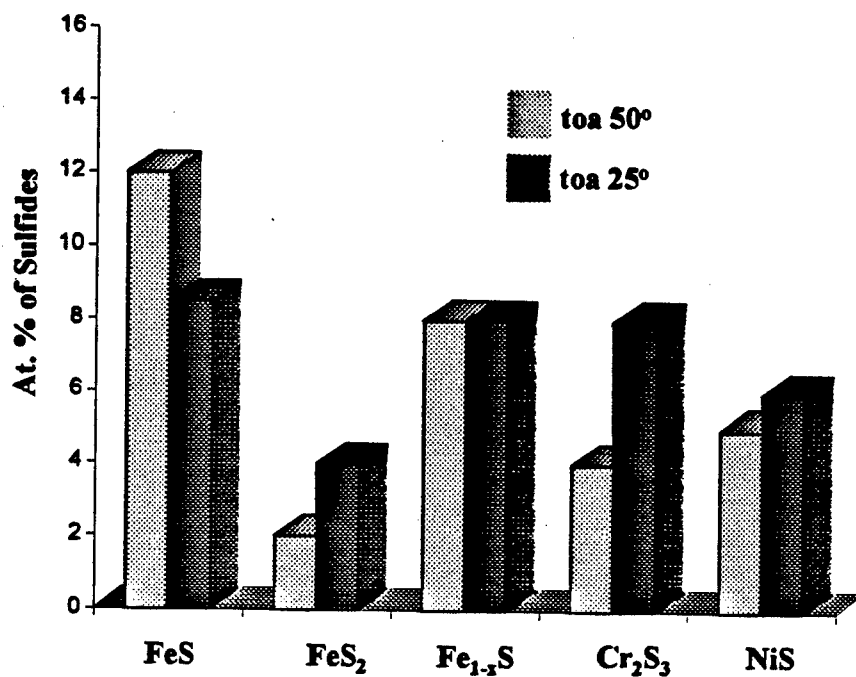
Relative proportions of sulfides on 304 ss as % of total metal spectra. Acquired

performing ARXPS at toa's of 50° and 20°.

Figure 7[34]
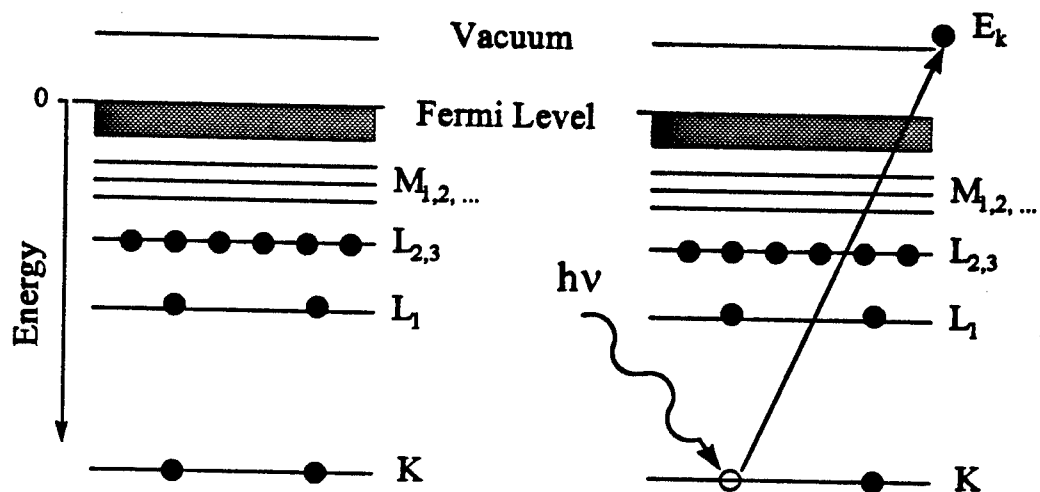
Schematic of photoelectron excitation hv is the energy in the incident x-ray and E_k

is the kinetic energy of the emitted electron

- The kinetic energy of the emitted electron (E_k).

- The incident X-ray energy (hv).

- The binding energy of the emitted electron (E_b).

- the work function of the sample and the spectrometer (ϕ).

Figure 8

Wide scan of as polished stainless steel type 304 toa 50°
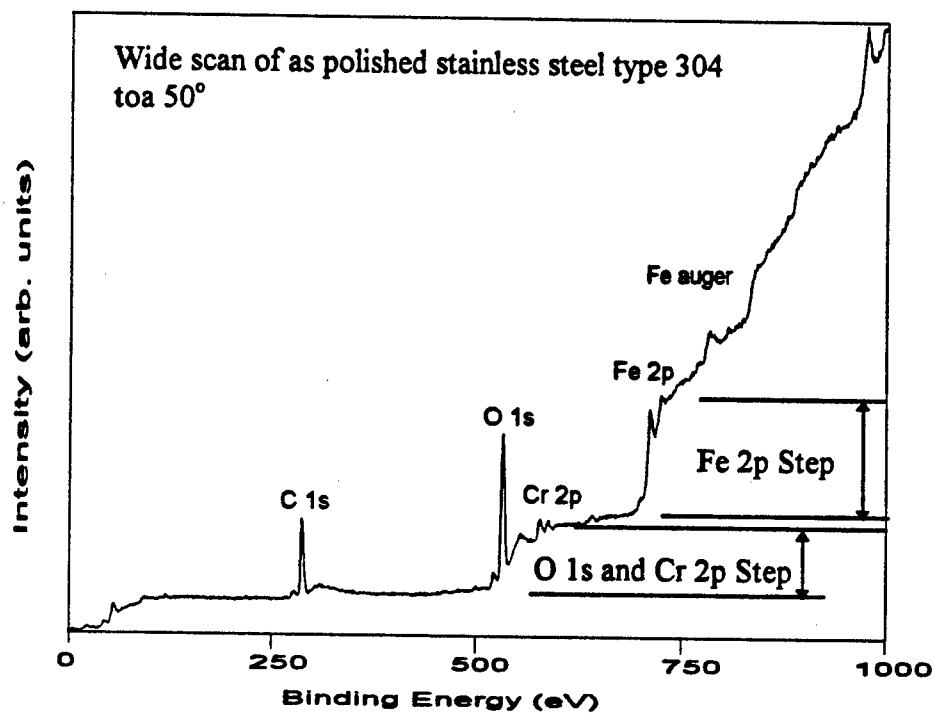
Typical 1000 eV range wide scan of a stainless steel 304 coupon. The Fe and Cr

comprise most of the bulk therefore they are the largest steps.

Figure 9
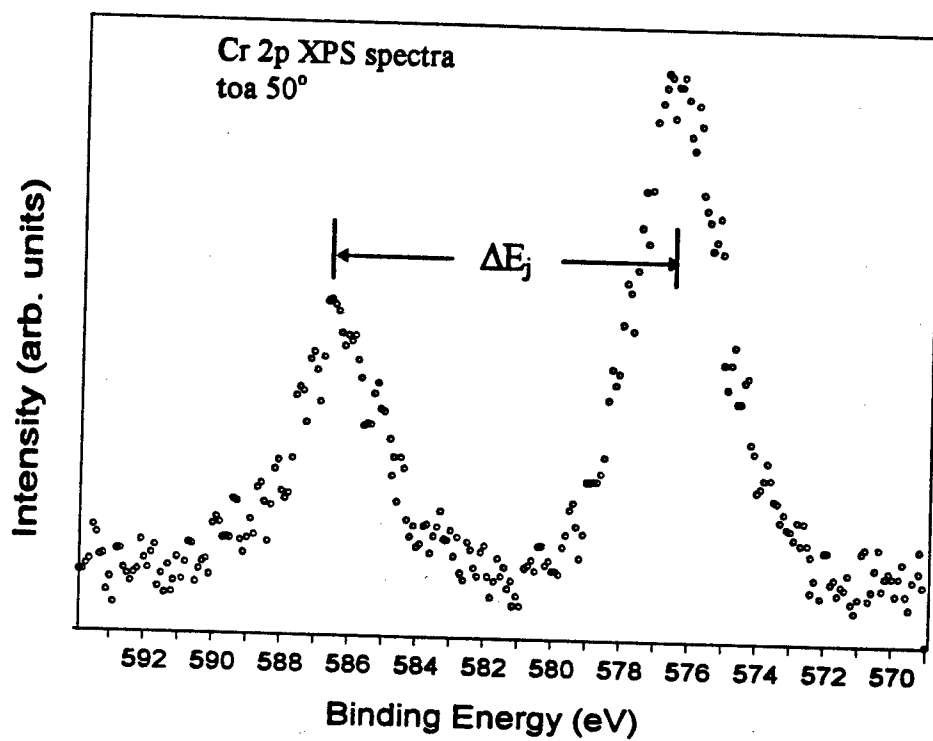
Narrow or high resolution scan of Cr 2p spectra illustrating the spin orbital

splitting which is seen in chlorine and elements of higher atomic number.

Figure 10
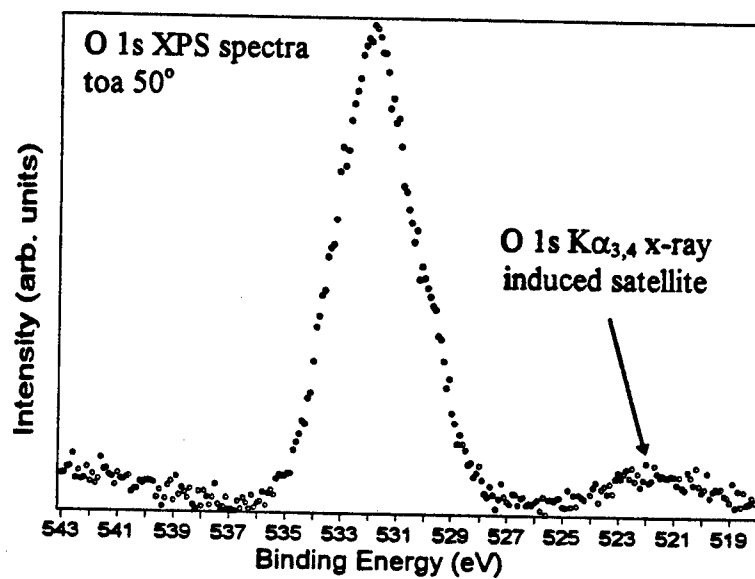
Narrow region scan of O 1s XPS spectra illustrating an x-ray induced satellite.

Figure 11
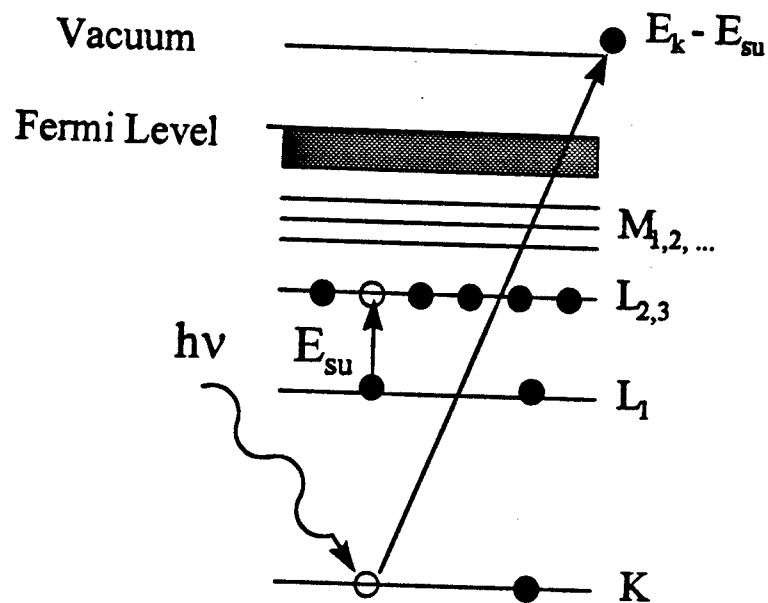
Schematic diagram of process of shake-up satellite electron emission.

- The shake up energy is E_{su}

Figure 12
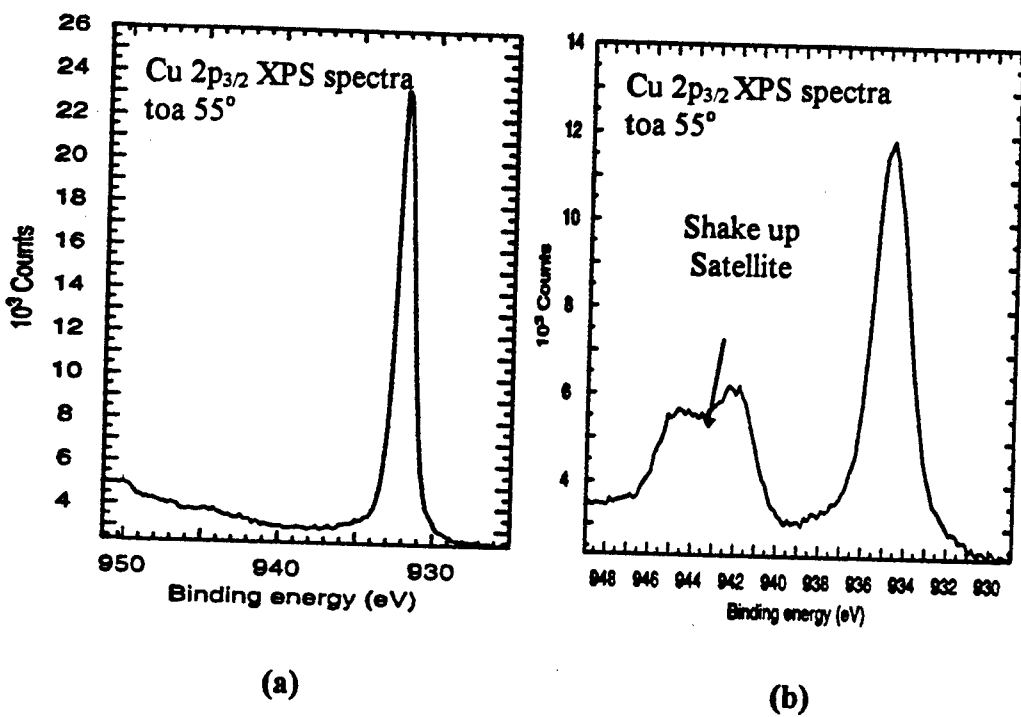
(a) Cu 2p$_{3/2}$ XPS spectra[35] collected from CuCl sample

(b) Cu 2p$_{3/2}$ XPS spectra[36] collected from CuCl$_2$ sample

Figure 13
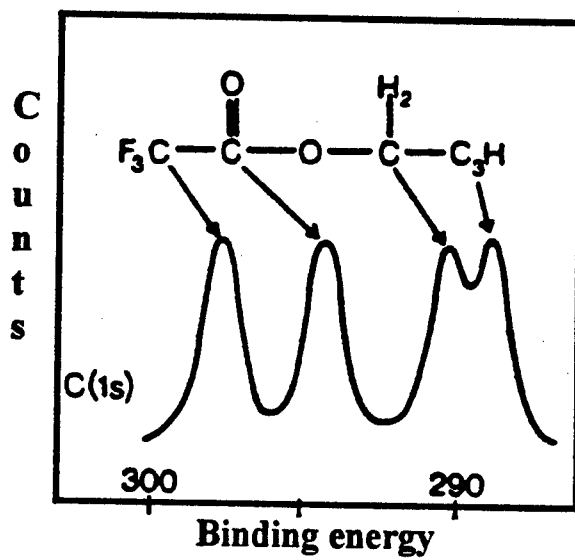
Relative chemical shifts for C 1s XPS spectra[39] for ethyl trifloroacetate.

Figure 14

Analyzer
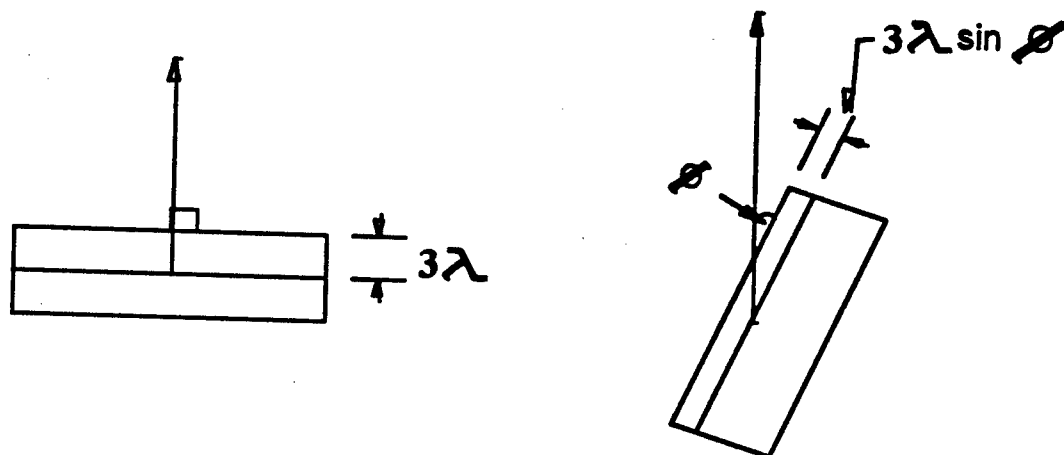
Illustration of the effect of varying the take off angle of photoelectrons assumes

the analyzer is at the top of the page.

- The mean Free path of electrons through the material (λ)

- The take off angle (toa) or emission angle (ϕ)

Angular Resolved X-ray Photoelectron Spectroscopy (ARXPS)

Figure 15
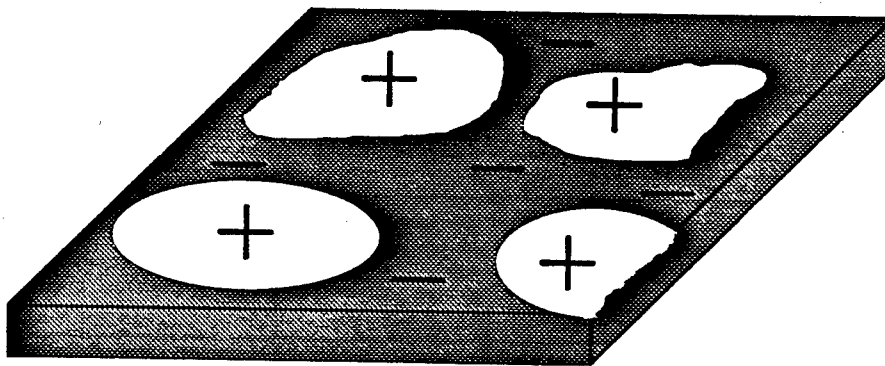
Representation of metal surface during corrosion. The shaded areas represent the cathodic areas and the white areas are the anodic areas of the sample surface.

Figure 16

$$\text{Oxidation Reaction} \quad M \longrightarrow M^{+n} + ne^-$$

$$\text{Reduction Reaction} \quad X + n'e^- \longrightarrow X^{-n'}$$
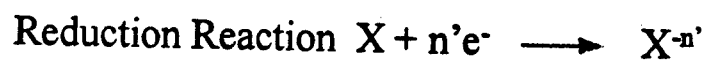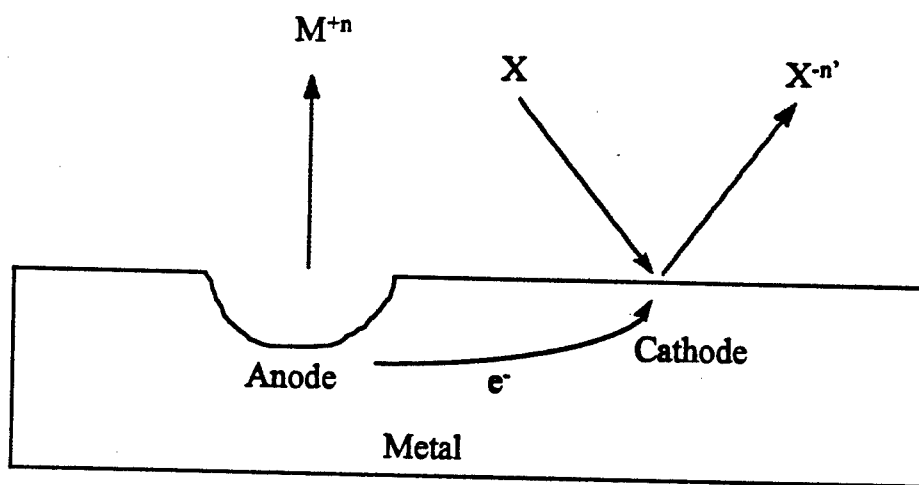
This is a schematic including the general oxidation and reduction reactions for an actively corroding surface.

Figure 17
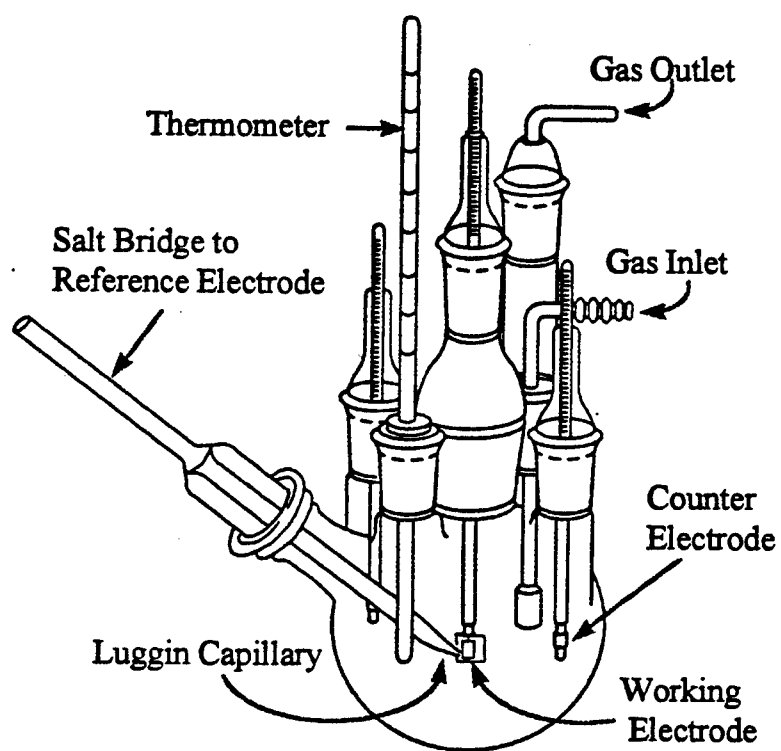
Schematic diagram of common polarization cell.[40]

Figure 18
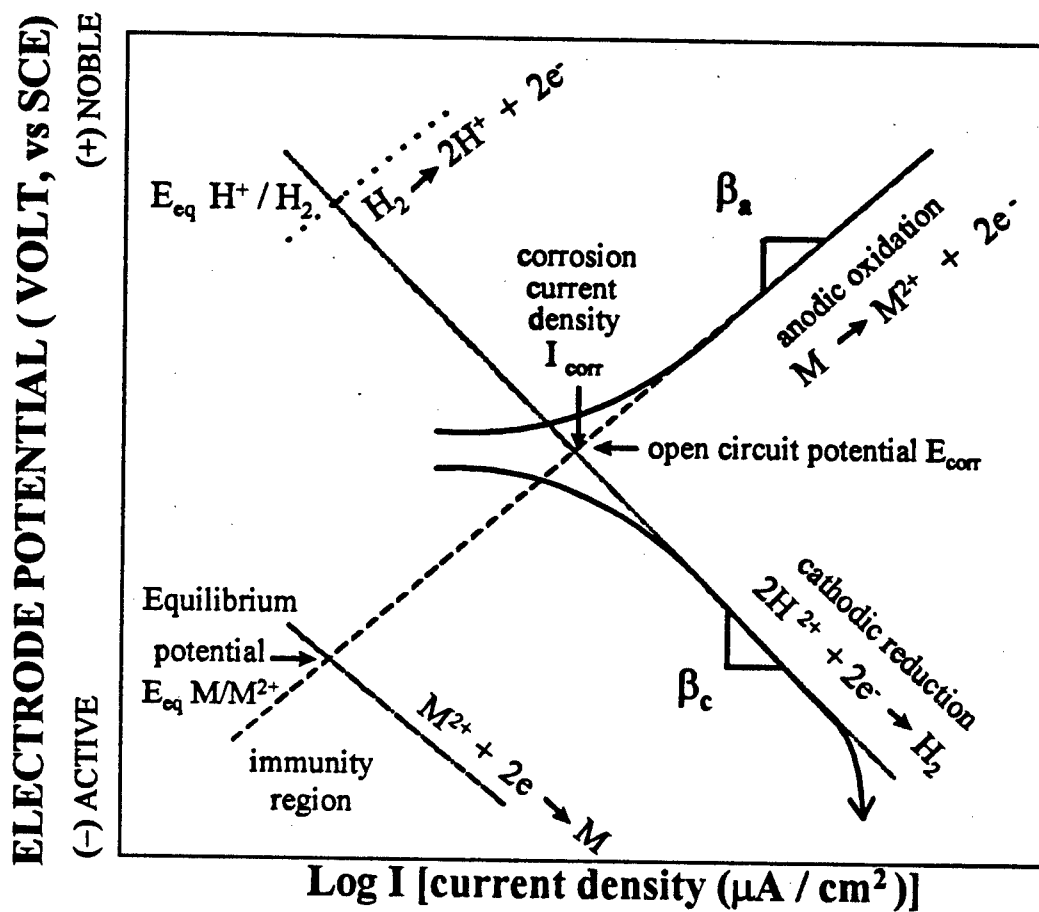
Diagram of Polarization half cell reactions and potential, current relations.

Figure 19
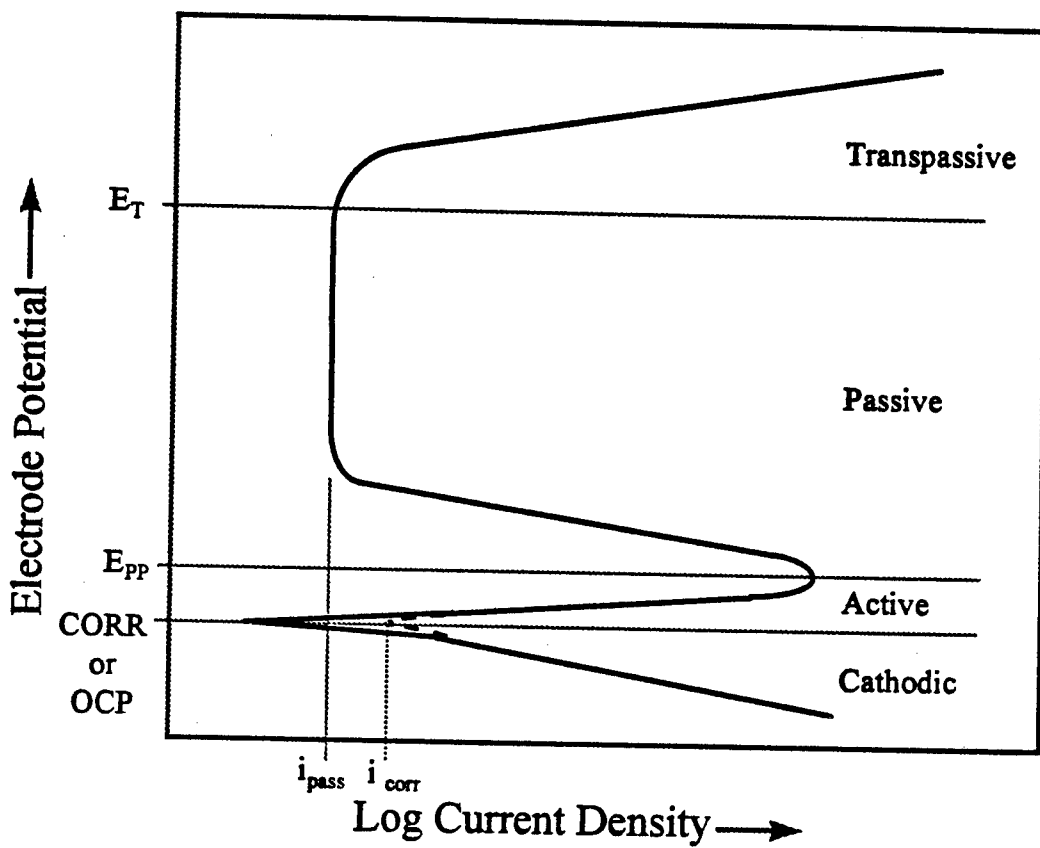
Schematic of active-passive polarization behavior

Figure 20
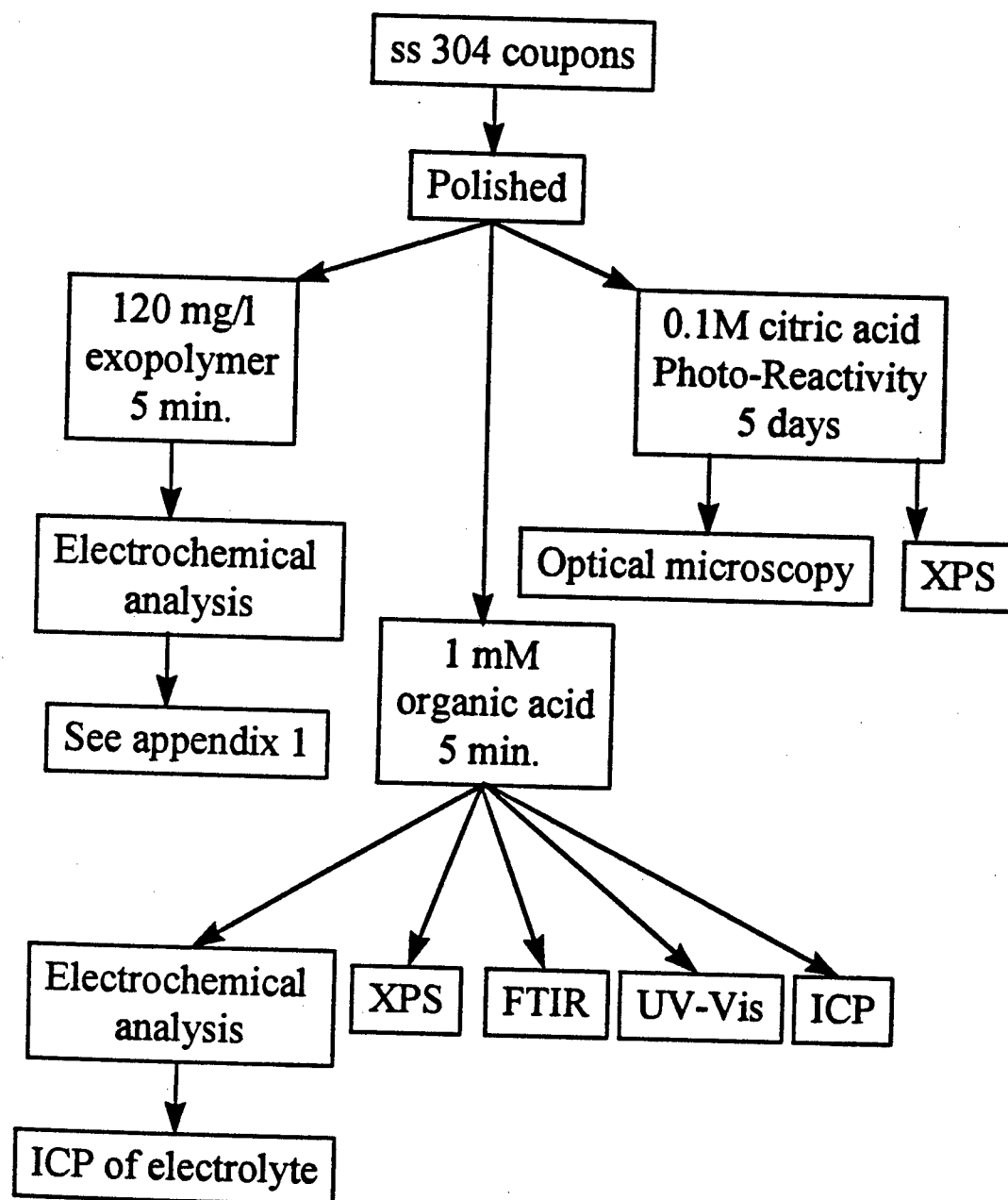
Flow chart of conditioning film research.

Figure 21

Electrochemical Sample Mount
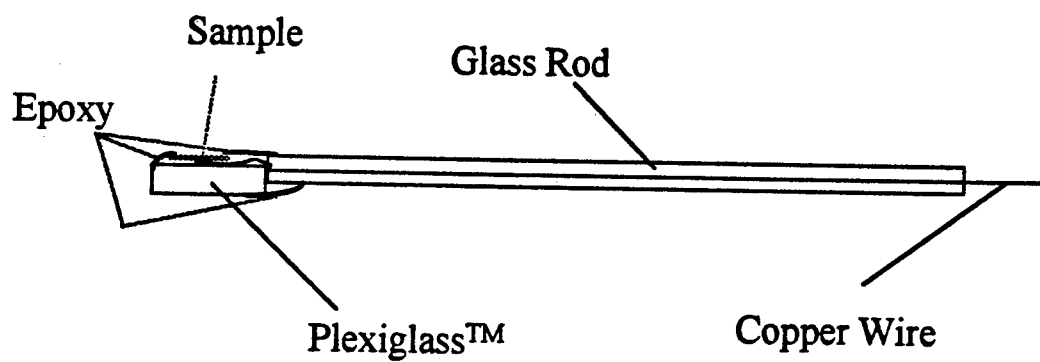
Schematic of the electrochemical analysis probe used for all the electrochemistry

in this research.

Figure 22

Inductively Coupled Plasma Atomic Emission Spectroscopy (ICP-AES).

Sample Introduction

Sample

Liquid or Solid

Nebulizer or Vaporization source

Plasma

Excitation

Emitted radiation

Dispersion (spectrometer)

Prism
Diffraction grating

Detection

Photoplate
Photomultiplier tube
Photo-diode array

Data processing

Computer

results

Figure 23

FT-IR
Microspectrometer

X-ray Ring

VUV Ring

Bright IR

Synchotron Light Source

Sample
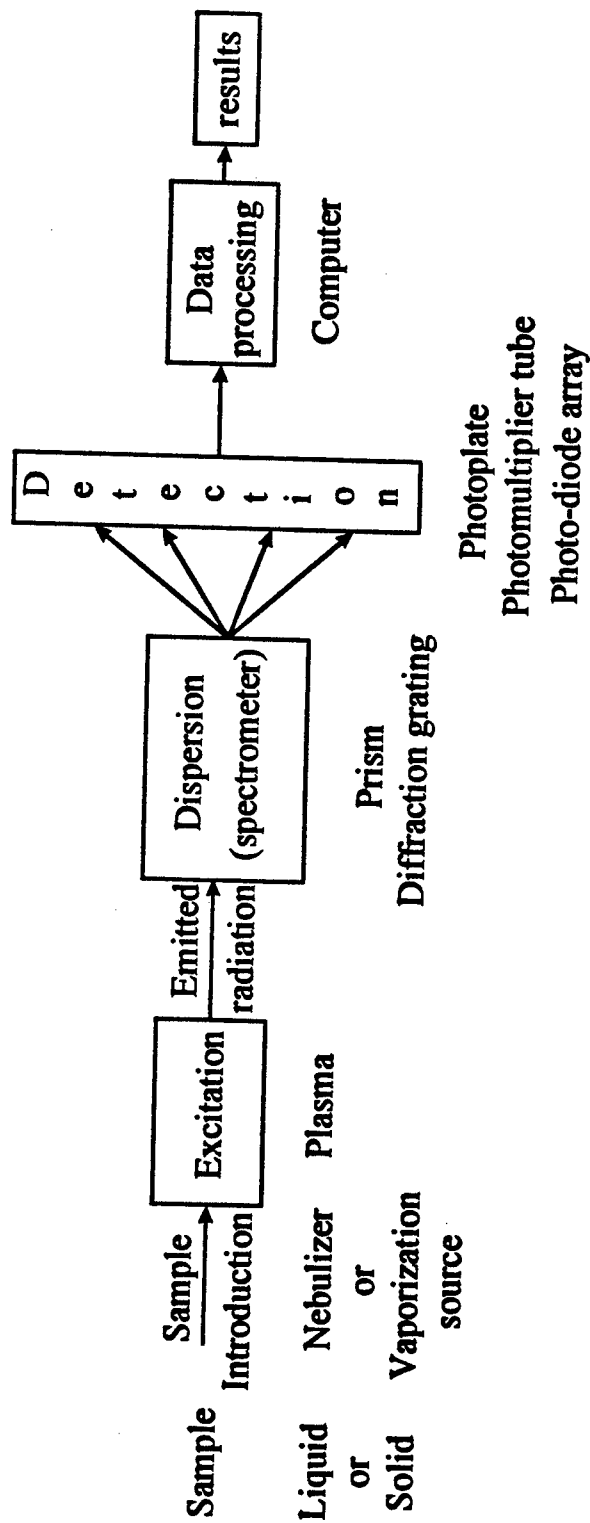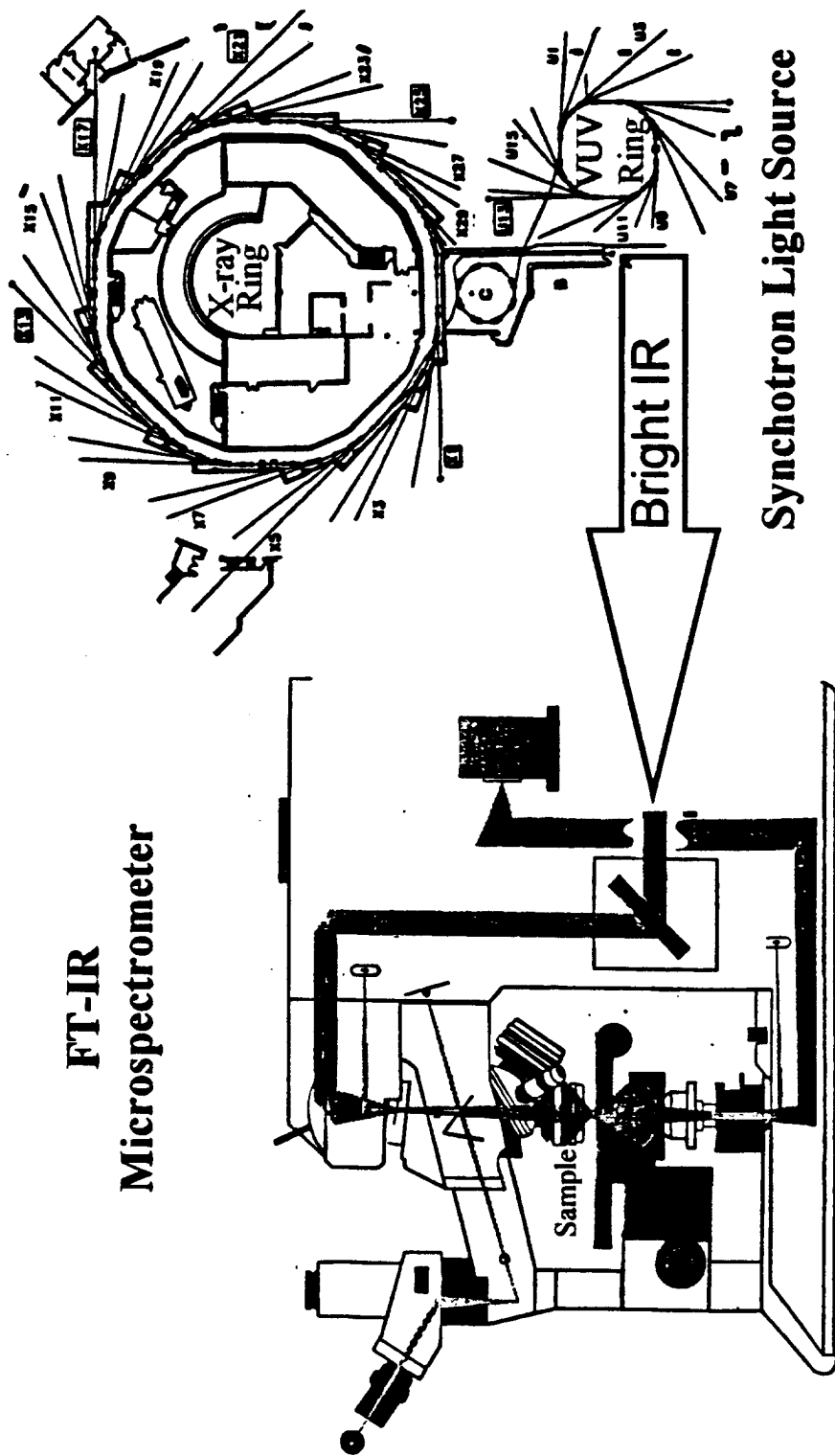
Schematic of the Bright IR Synchotron Light Scource and FT-IRM

Figure24

Tungsten lamp

Deuterium lamp

Source lens

Light filter

Source lens

Cuvette

Source lens

Slit

Photodiode array

Grating
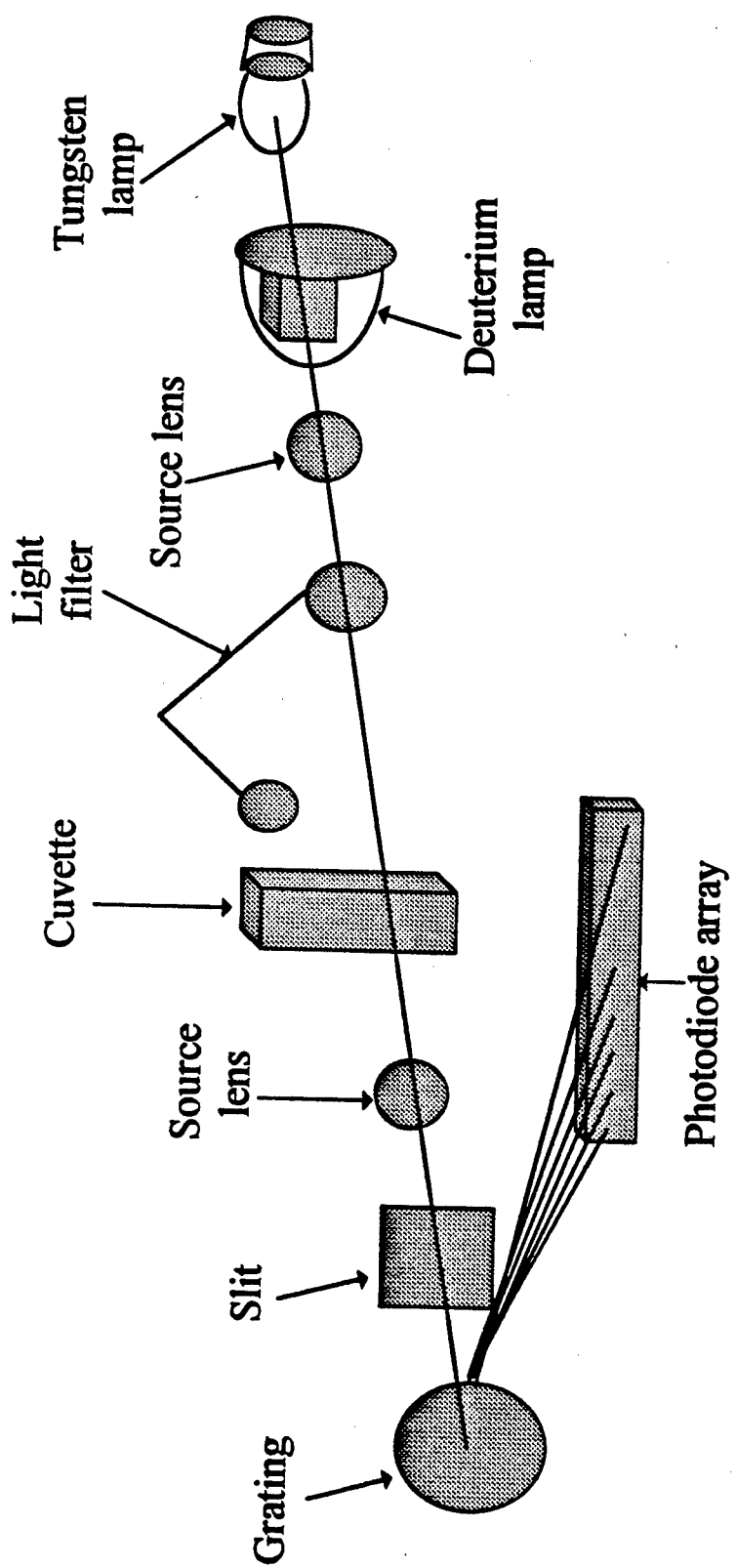
Arrangement of the optics of a UV-Vis spectrophotometer

Figure 25

```
            ┌─────────┐
            │  Media  │
            └─────────┘
                 │
                 ▼
           ┌────────────┐
           │ 10 ml Vol. │
           └────────────┘
                 │
                 ▼
           ┌────────────┐
           │ Autoclave  │
           └────────────┘
                 │
                 ▼
    ┌────────────────────────────────┐
    │ Immersion of coupons in media  │
    └────────────────────────────────┘
         │                    │
         ▼                    ▼
  ┌──────────────┐      ┌───────────┐
  │ Inoculation  │      │  Control  │
  └──────────────┘      └───────────┘
         │                    │
         ▼                    ▼
    ┌────────────────────────────────┐
    │ Incubation for 5 days, at 28° C │
    └────────────────────────────────┘
                 │
                 ▼
```

In glove bag,
• take samples for cell counts
•filter solution for ICP
•recover coupons for XPS

| XPS | ICP | Cell counts |
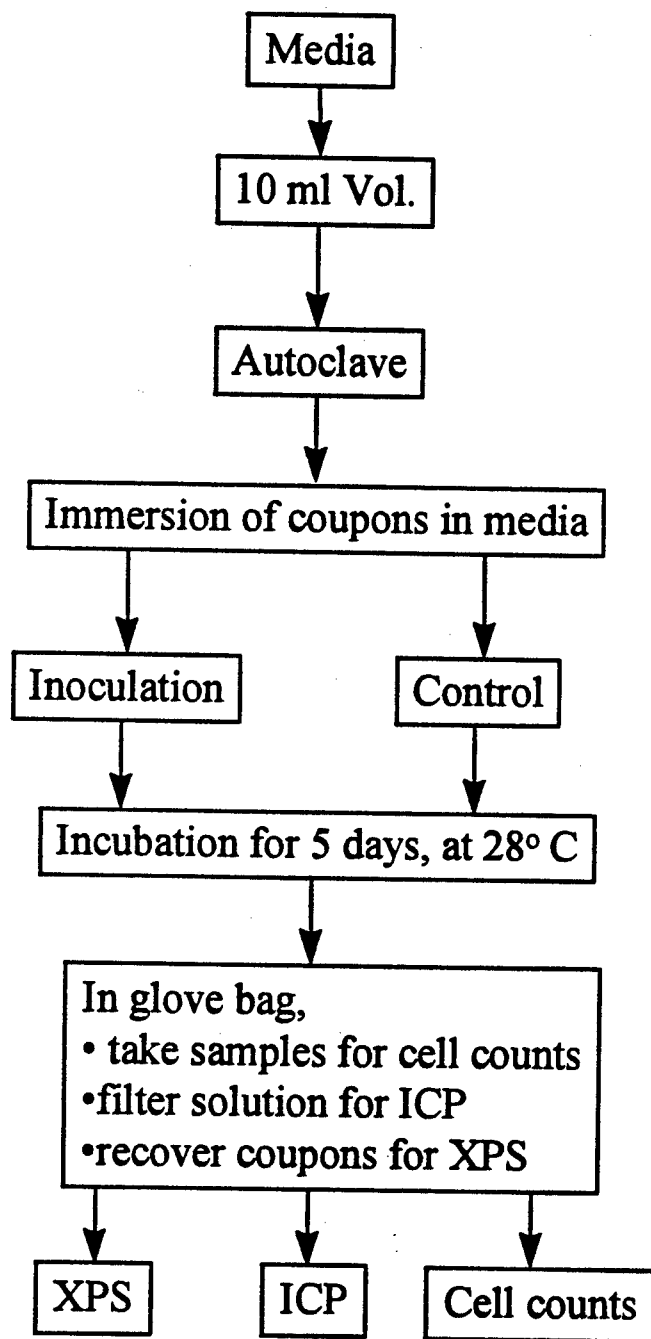
Flow Chart of SRB research.

Figure 26

Stainless Steel type 304 coupons
1cm x 1.5 cm x 1 mm

Tygon™ Band

Ground glass disks
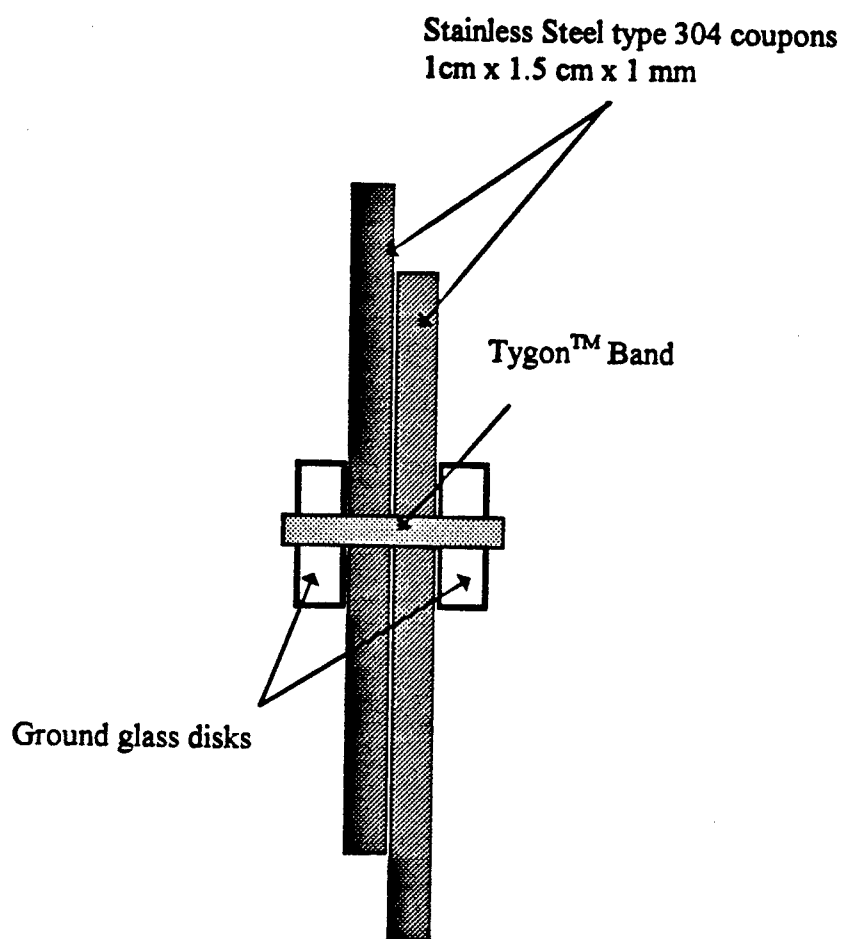
Illustration of stainless steel 304 crevice arrangement for exposure to sulfate
reducing bacteria

Figure 27

Potentiodynamic Polarization Plots of untreated Stainless Steel type 304 and Stainless Steel type 304 after exposure to lactic acid performed in 0.1 M HCl
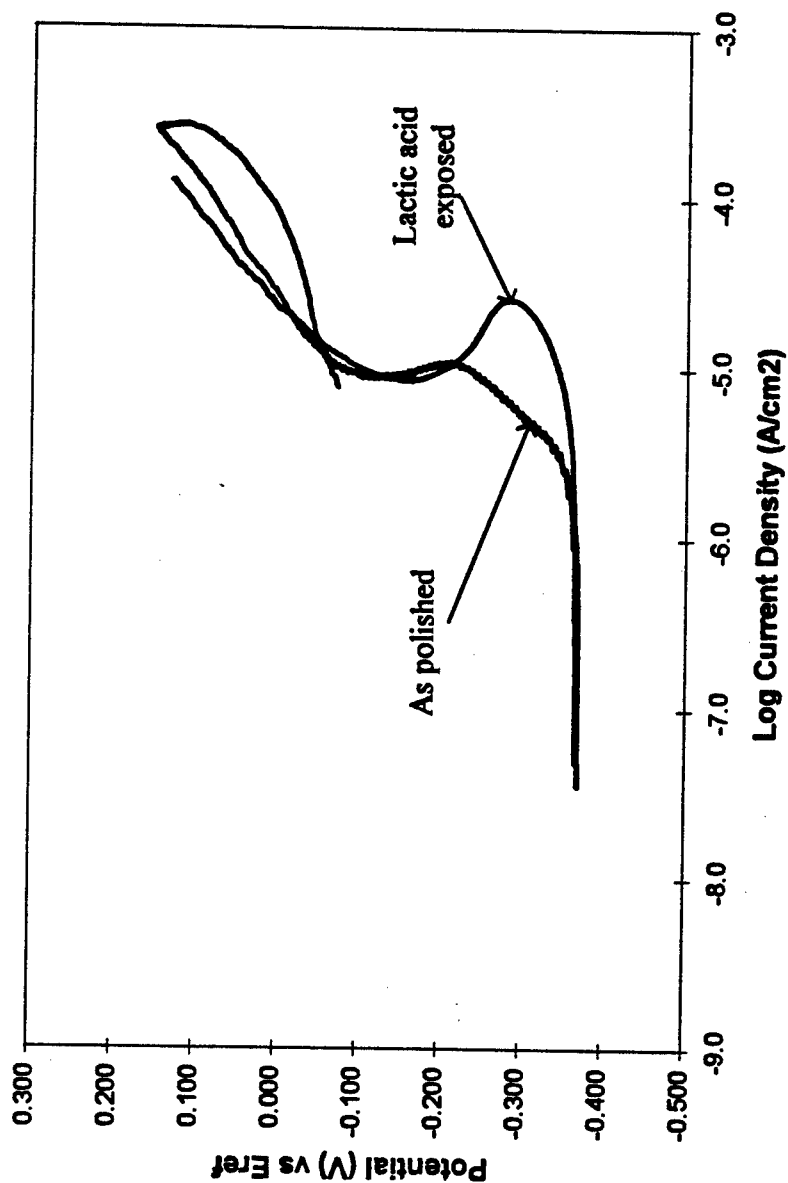
Eref is SCE, the scan rate was 1 mV/sec and there was no cathodic pretreatment of the samples.

Figure 28

Potentiocyclic Polarization Plots of untreated Stainless Steel type 304 and Stainless Steel type 304 after exposure to oxalic acid performed in 0.1 M HCl
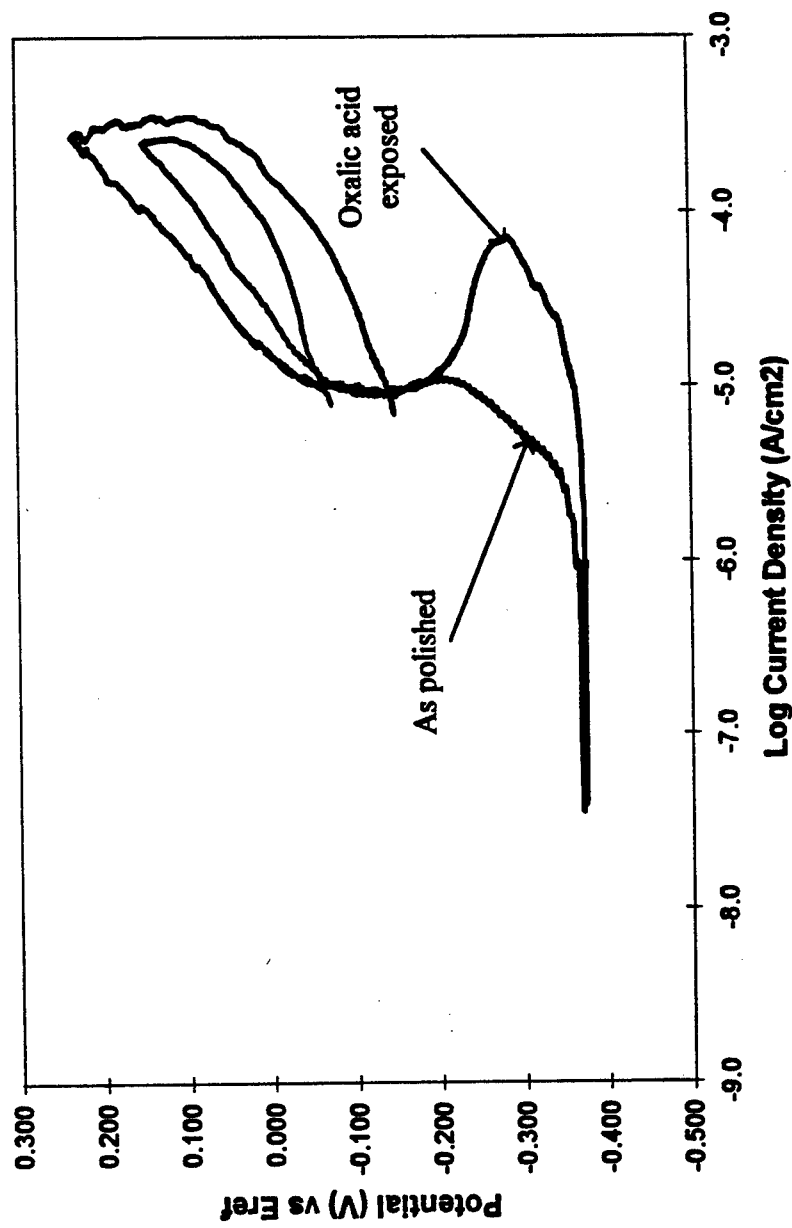
Eref is SCE, the scan rate was 1 mV/sec and there was no cathodic pretreatment of the samples.

Figure 29

Potentiocyclic Polarization Plots of untreated Stainless Steel type 304 and Stainless Steel type 304 after exposure to citric acid performed in 0.1 M HCI
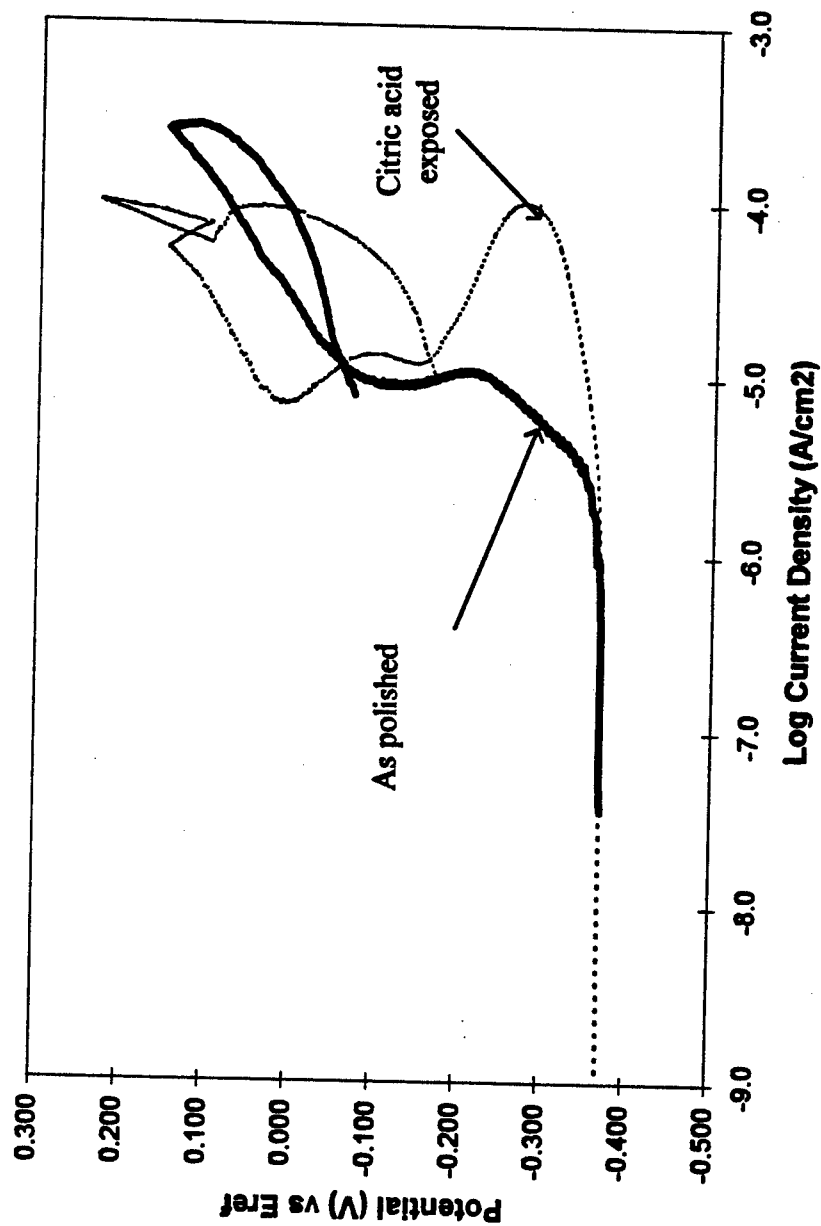
Eref is SCE, the scan rate was 1 mV/sec and there was no cathodic pretreatment of the samples.

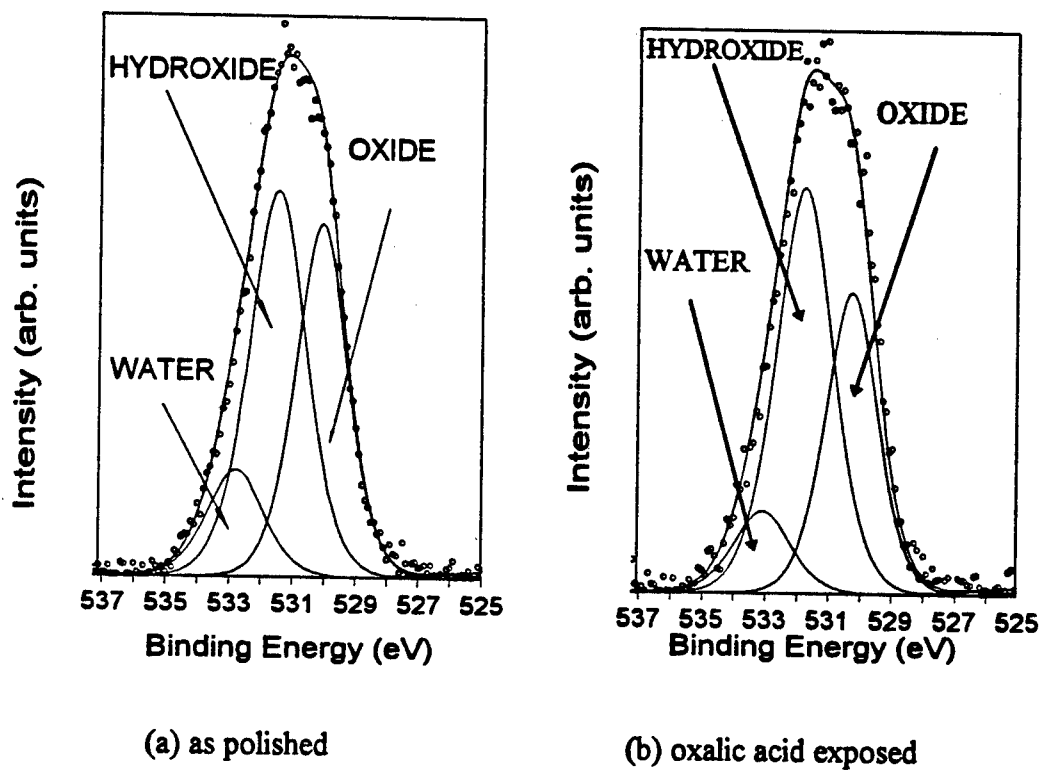Figure 30

Fe 2p$_{3/2}$ XPS Spectra
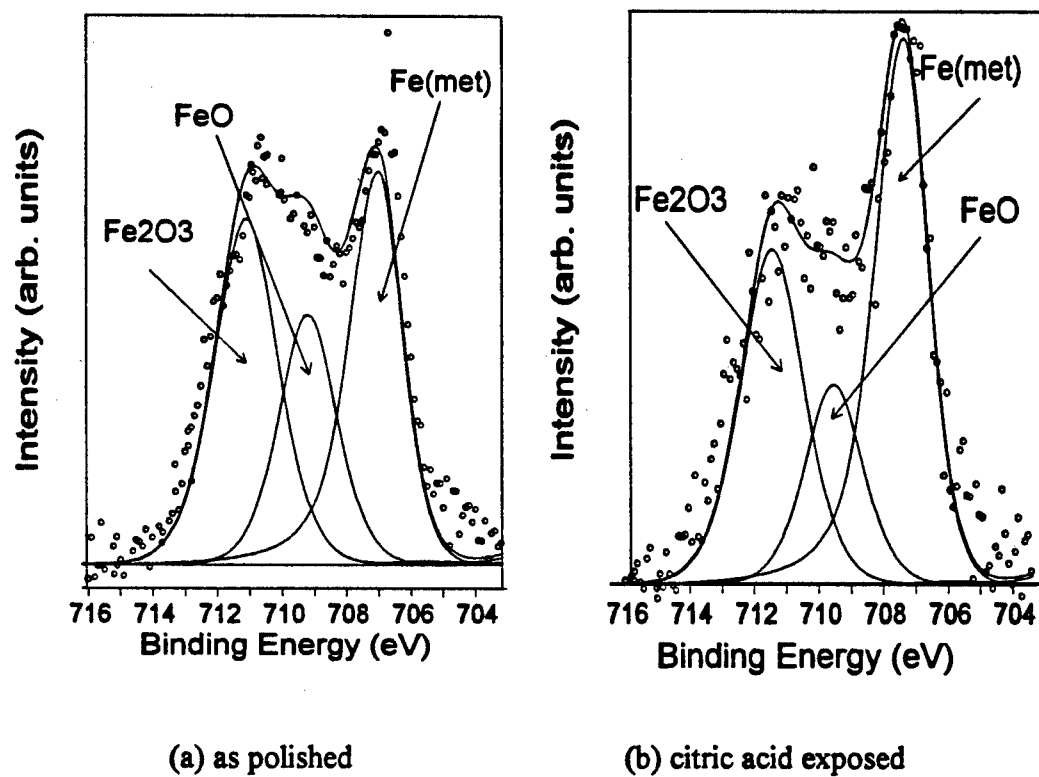
(a) as polished

(b) citric acid exposed

Fe 2p$_{2/3}$ XPS spectra toa 50° of austenitic stainless steel type 304 before and after

exposure to 1 mM citric acid solution.

Figure 31

Fe 2p$_{3/2}$ XPS Spectra
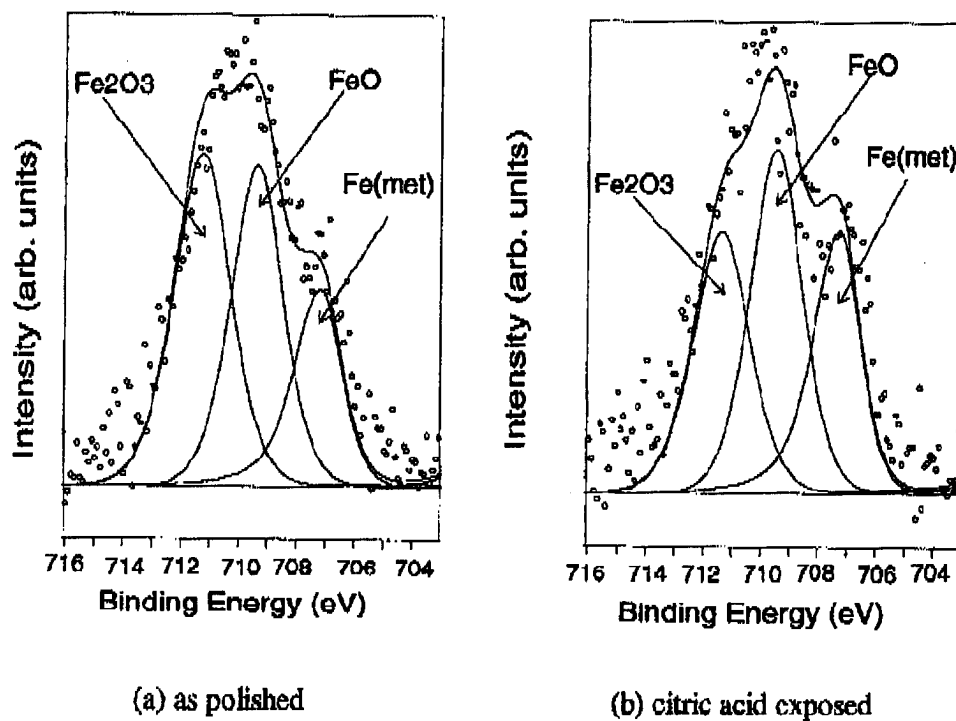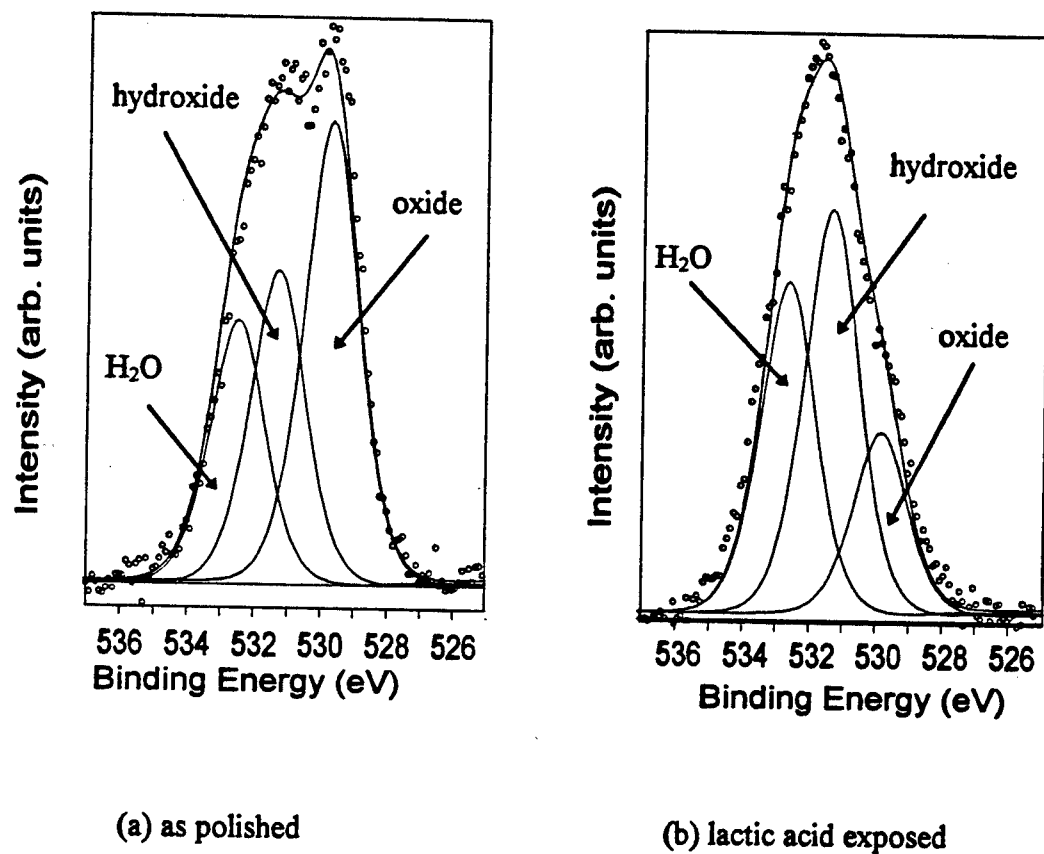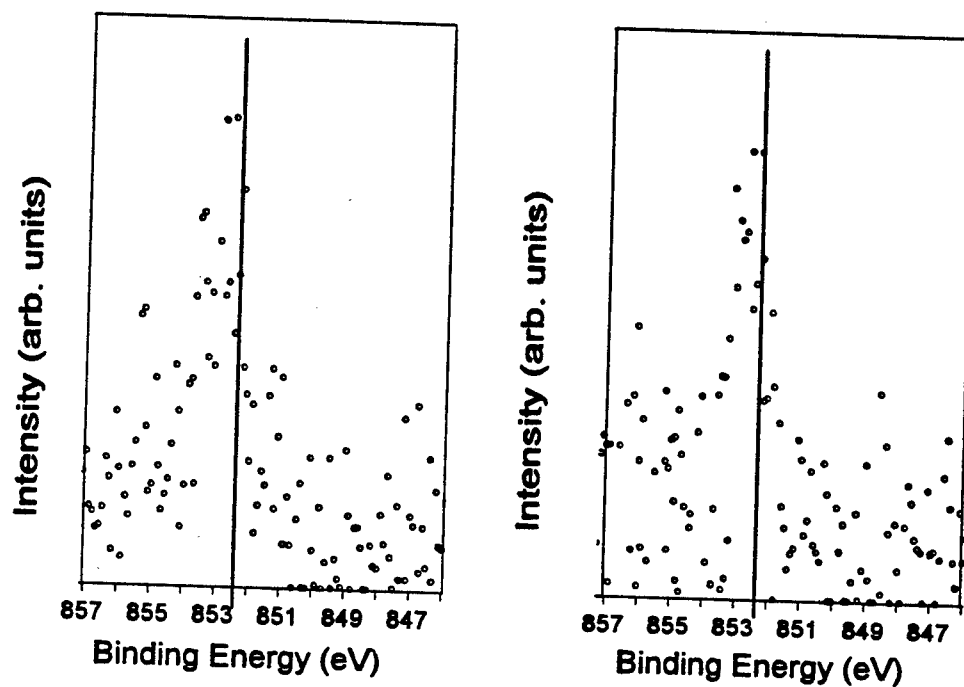

(a) as polished

(b) citric acid exposed

Fe 2p$_{3/2}$ XPS spectra toa 20° of austenitic stainless steel type 304 before and after

exposure to 1 mM citric acid solution.
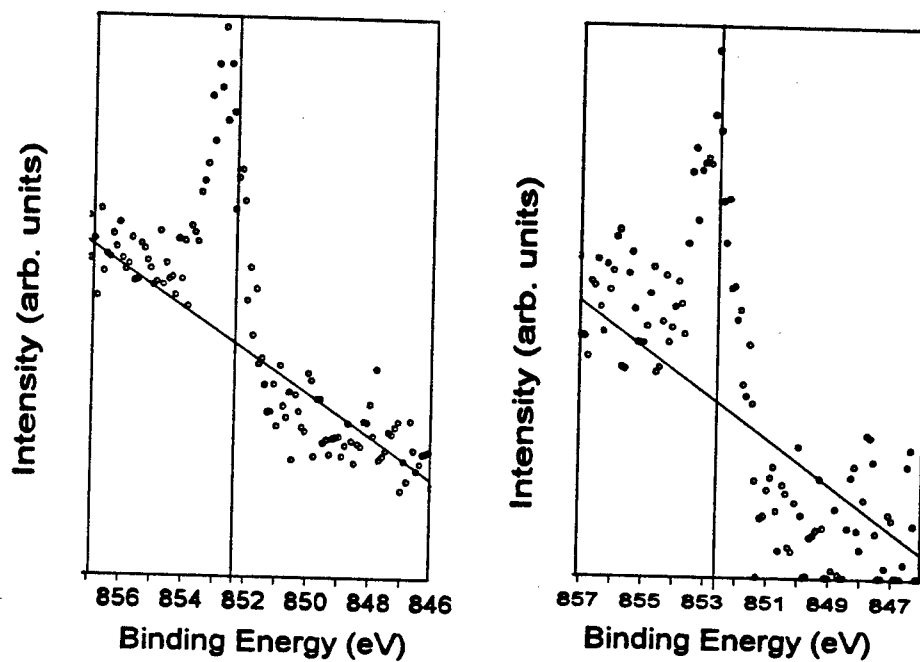
Figure 32

Fe 2p₃/₂ XPS Spectra
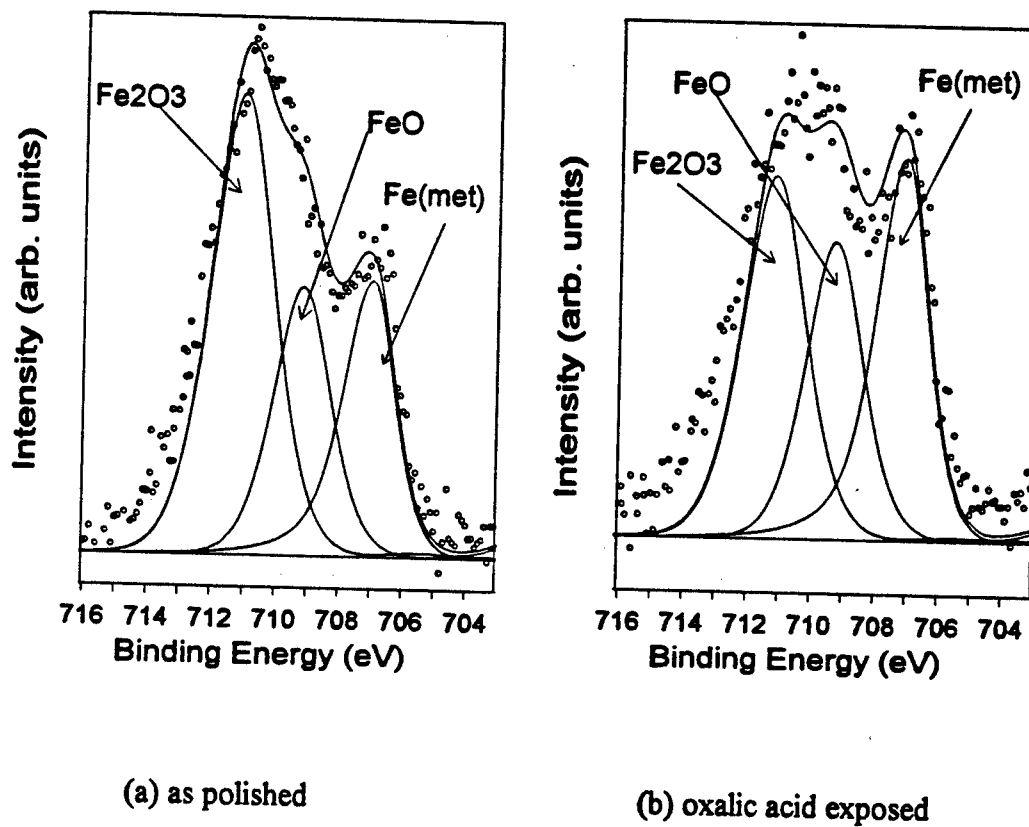
(a) as polished

(b) oxalic acid exposed

Fe 2p₂/₃ XPS spectra toa 50° of austenitic stainless steel type 304 before and after exposure to 1 mM oxalic acid solution.

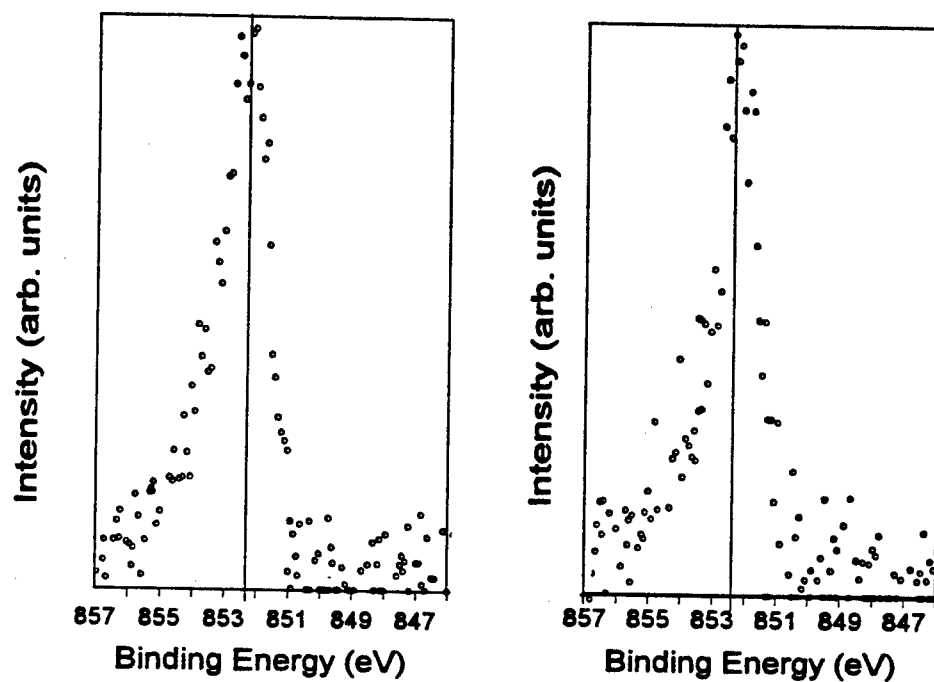Figure 33

Fe 2p$_{3/2}$ XPS Spectra
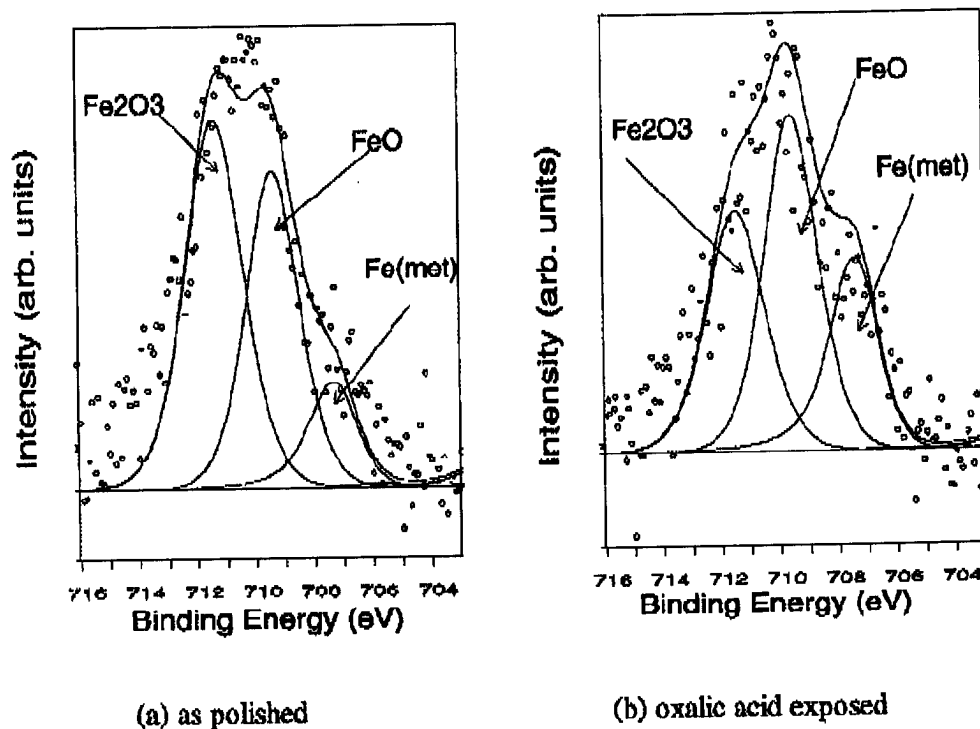
(a) as polished

(b) oxalic acid exposed

Fe 2p$_{3/2}$ XPS spectra toa 20° of austenitic stainless steel type 304 before and after

exposure to 1 mM oxalic acid solution.

Figure 34

Fe 2p₃/₂ XPS Spectra
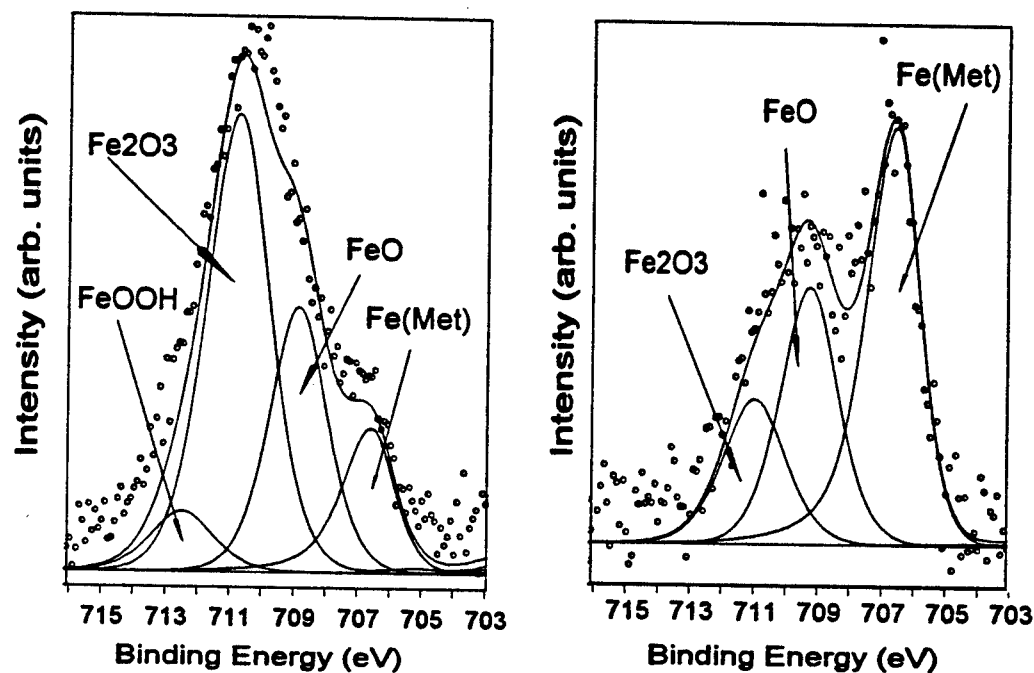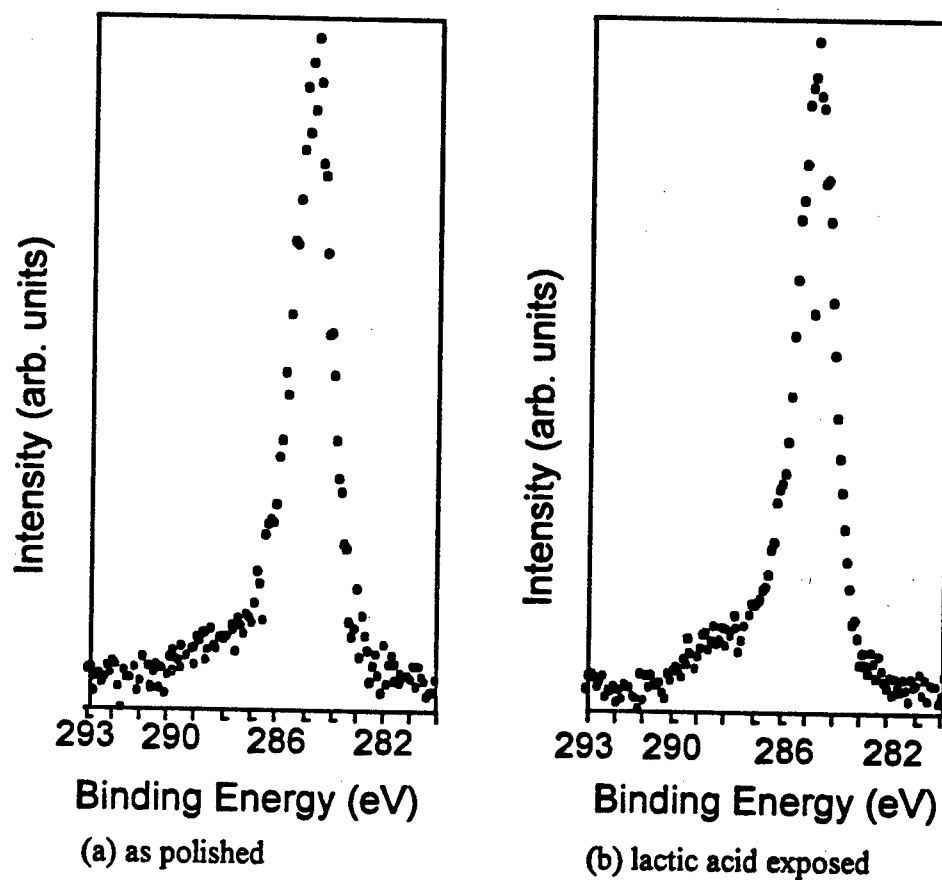

(a) as polished   (b) lactic acid exposed

Fe 2p₂/₃ XPS spectra toa 50° of austenitic stainless steel type 304 before and after

exposure to 1 mM lactic acid solution.

Figure 35

Fe 2p$_{3/2}$ XPS Spectra
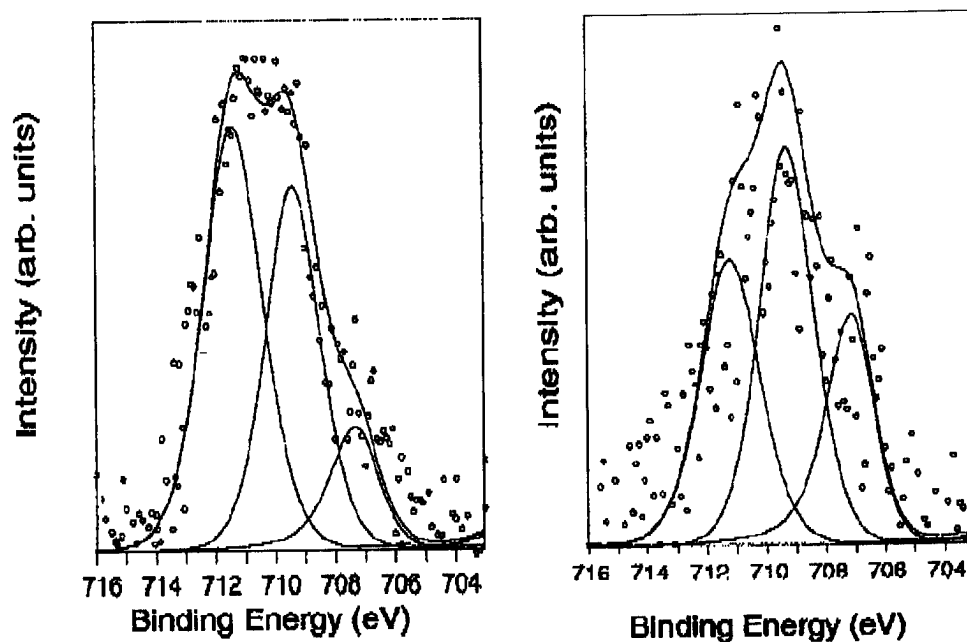
(a) as polished　　　　　　　　　　(b) lactic acid exposed

Fe 2p$_{3/2}$ XPS spectra toa 20° of austenitic stainless steel type 304 before and after

exposure to 1 Mm lactic acid solution.

Figure 36
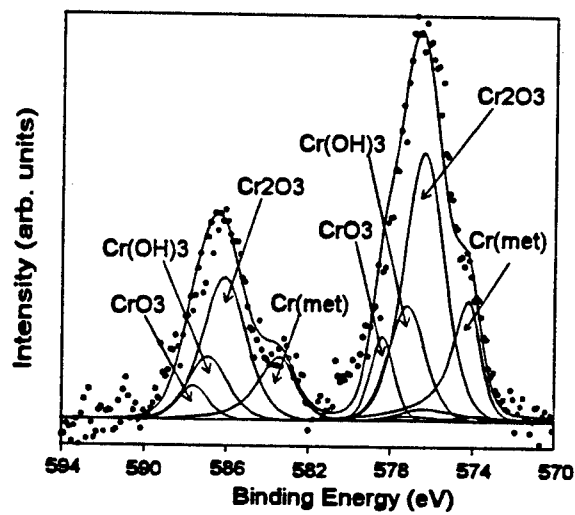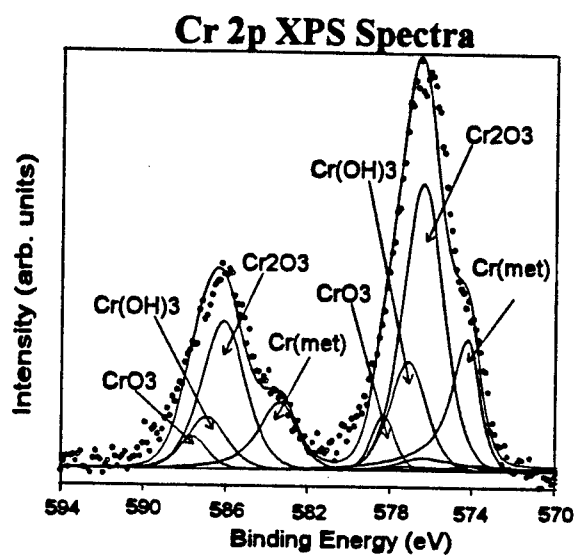
Cr 2p XPS Spectra

(a) as polished

(b) citric acid exposed

Cr 2p XPS spectra toa 50° of austenitic stainless steel type 304 before and after exposure to 1 mM citric acid solution.
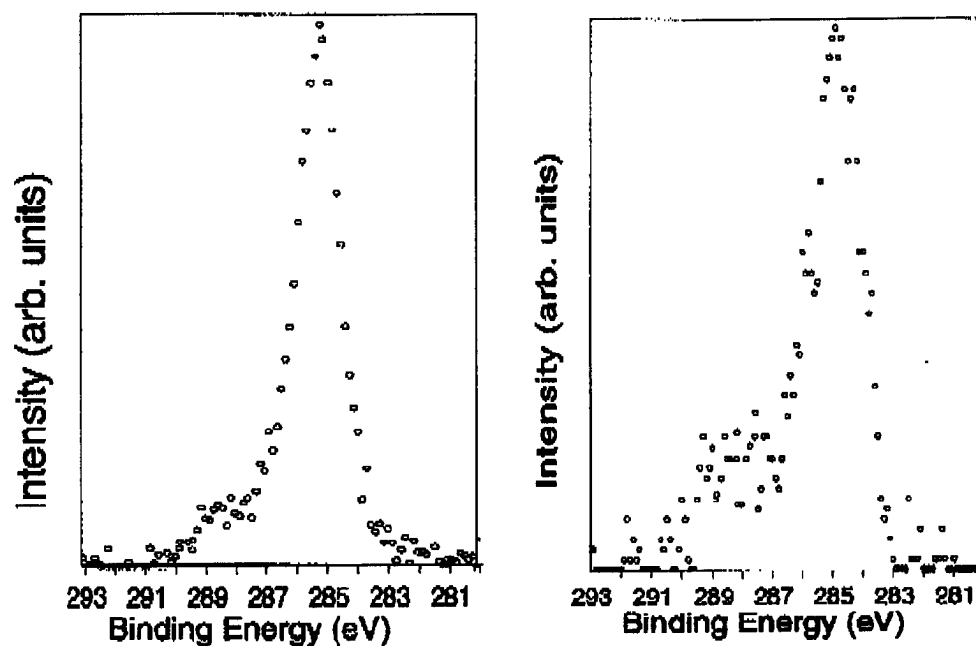
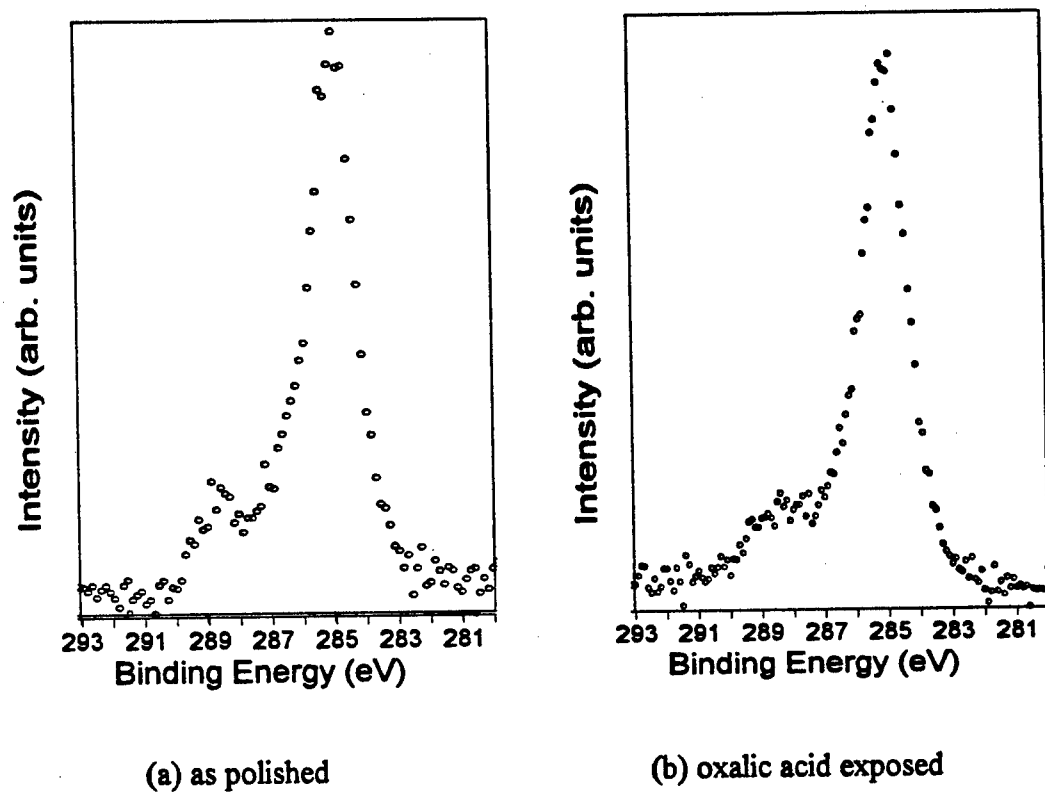**Figure 37**

Cr 2p XPS Spectra

(a) as polished

(b) citric acid exposed
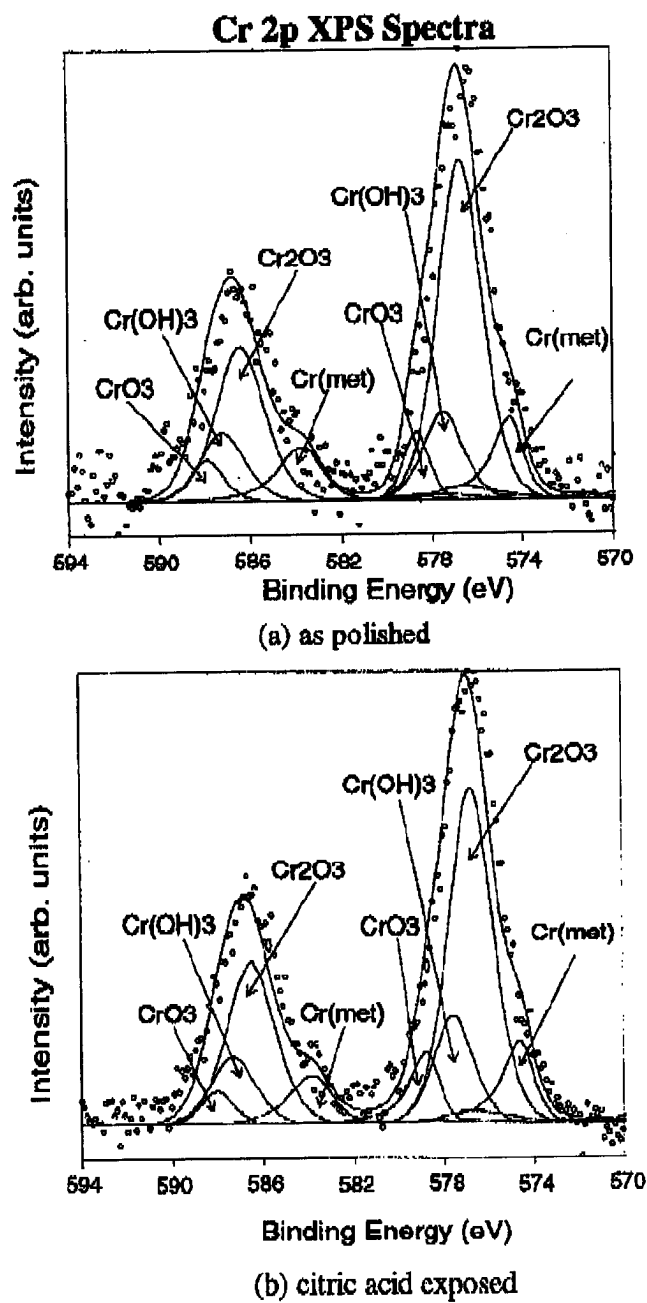
Cr 2p XPS spectra toa 20° of austenitic stainless steel type 304 before and after exposure to 1 mM citric acid solution.

Figure 38

Cr 2p XPS Spectra

(a) as polished

(b) oxalic acid exposed

Cr 2p XPS spectra toa 50° of austenitic stainless steel type 304 before and after exposure to 1 mM oxalic acid solution.

Figure 39

(a) as polished
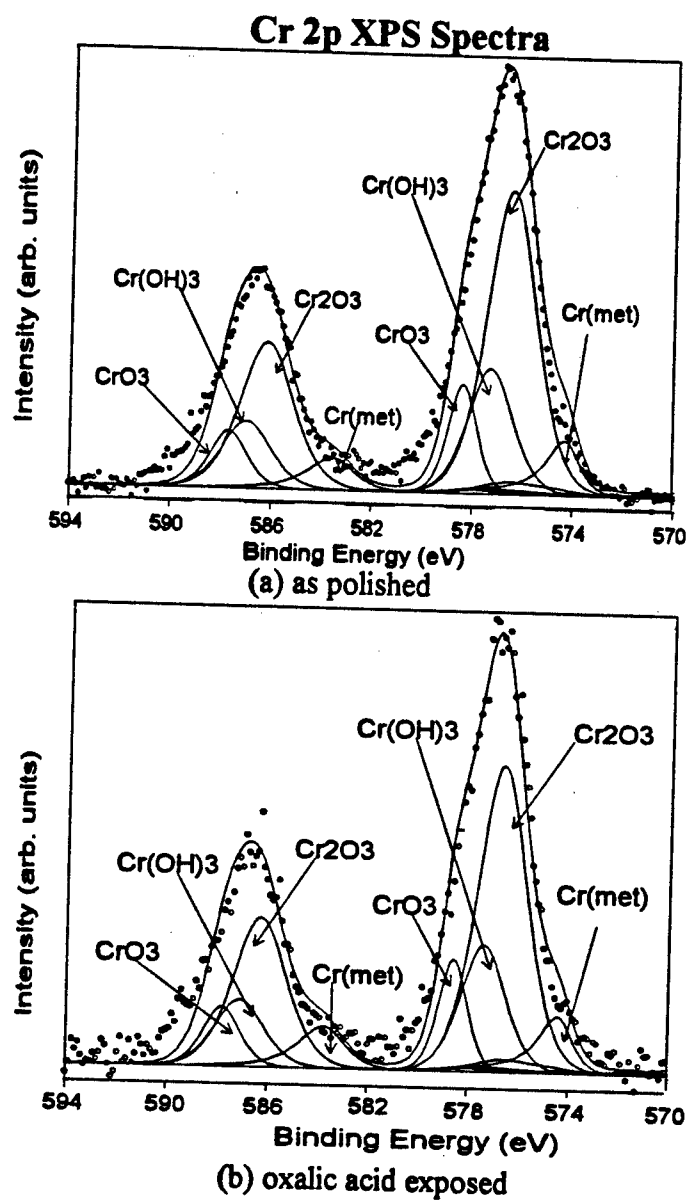
(b) oxalic acid exposed
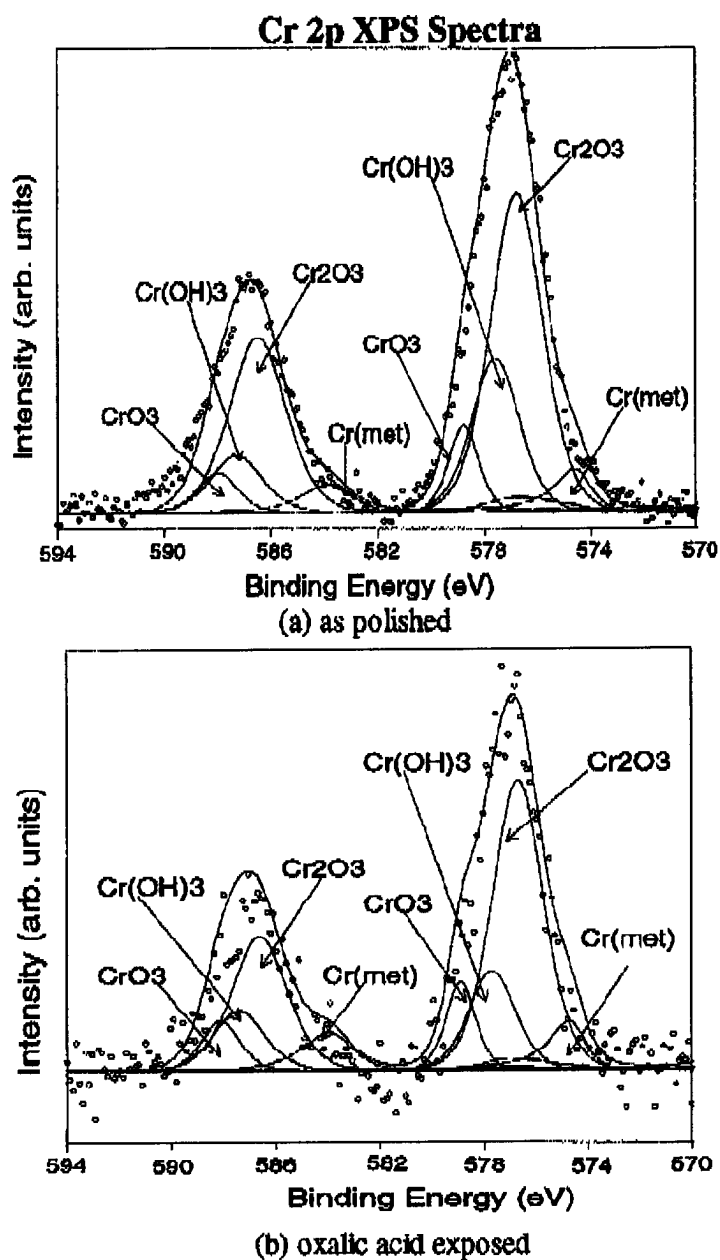
Cr 2p XPS spectra toa 20° of austenitic stainless steel type 304 before and after exposure to 1 mM oxalic acid solution.

Figure 40

Cr 2p XPS Spectra

(a) as polished

(b) lactic acid exposed
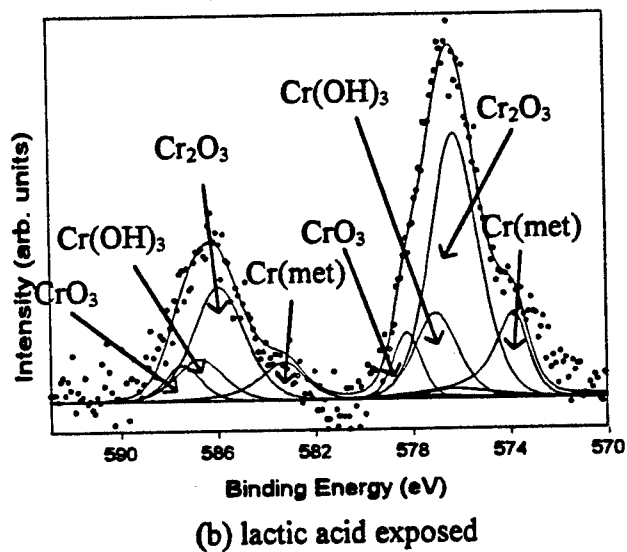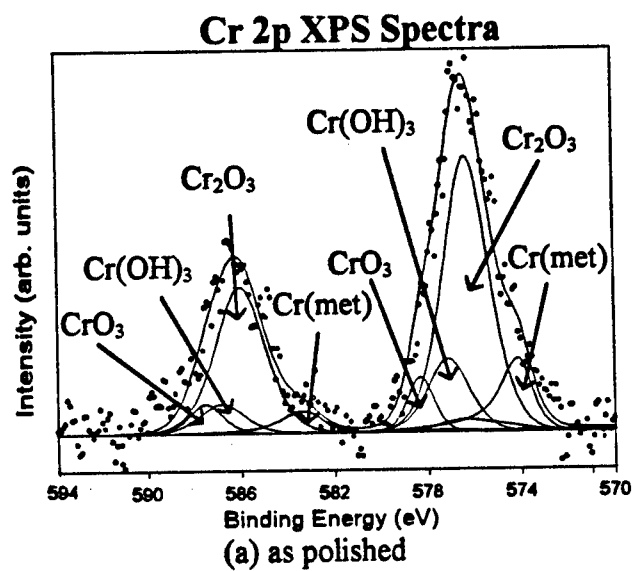
Cr 2p XPS spectra toa 50° of austenitic stainless steel type 304 before and after exposure to 1 mM lactic acid solution.
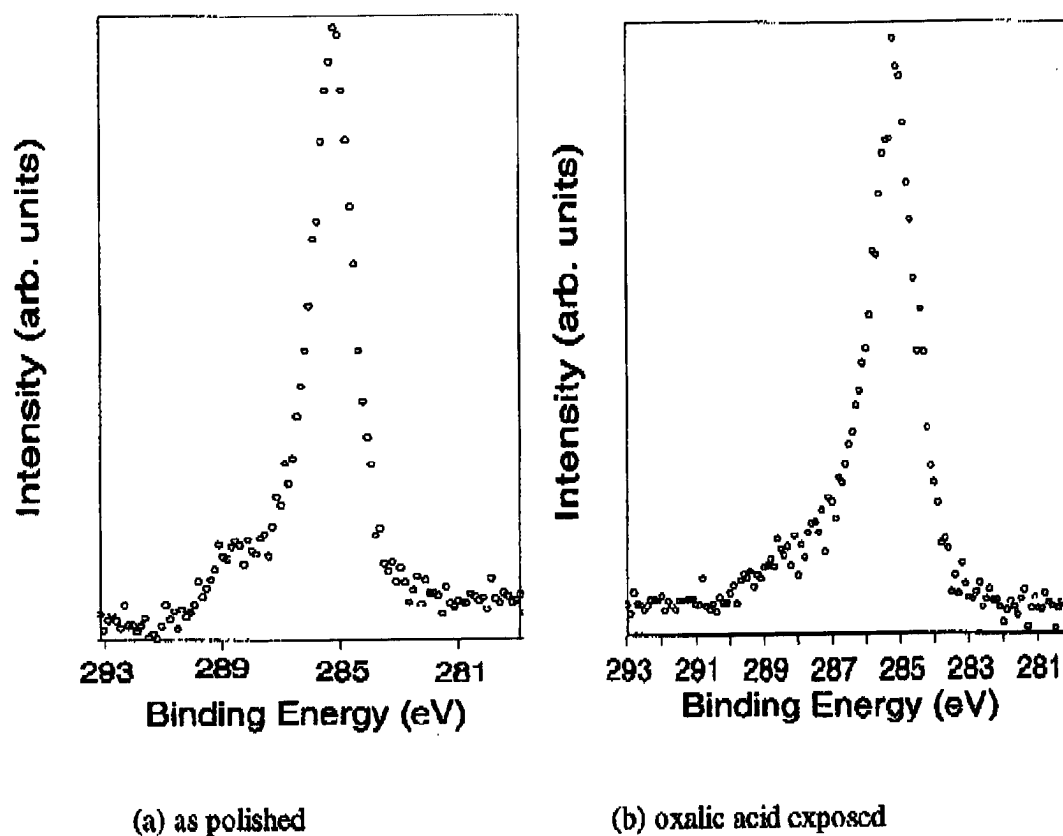
Figure 41

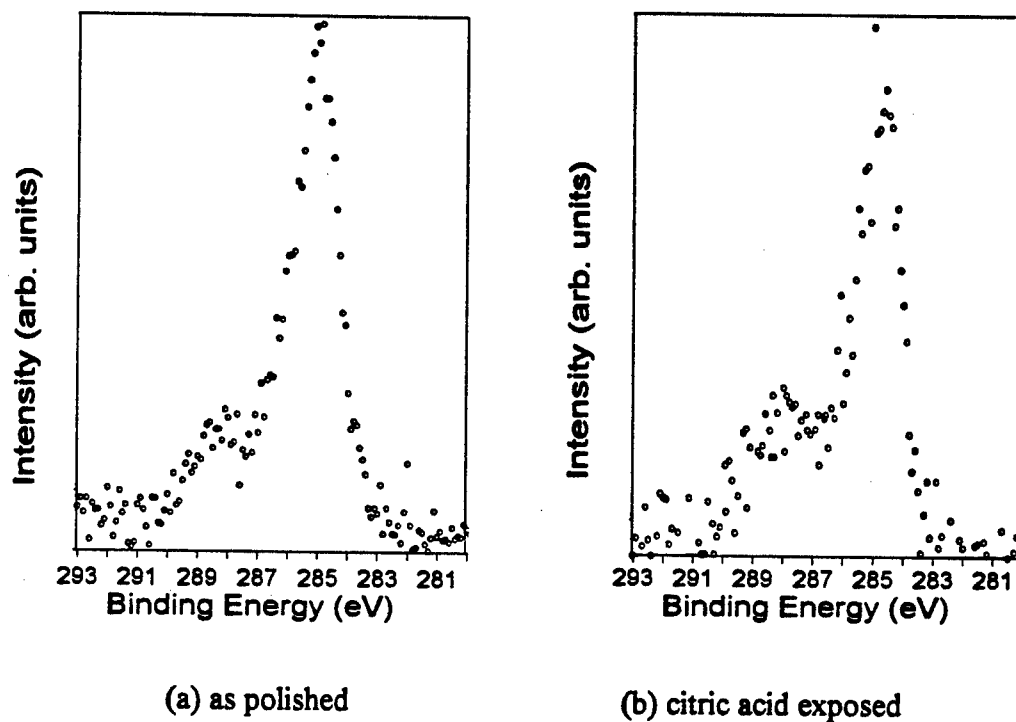# Cr 2p XPS Spectra

(a) as polished

(b) lactic acid exposed
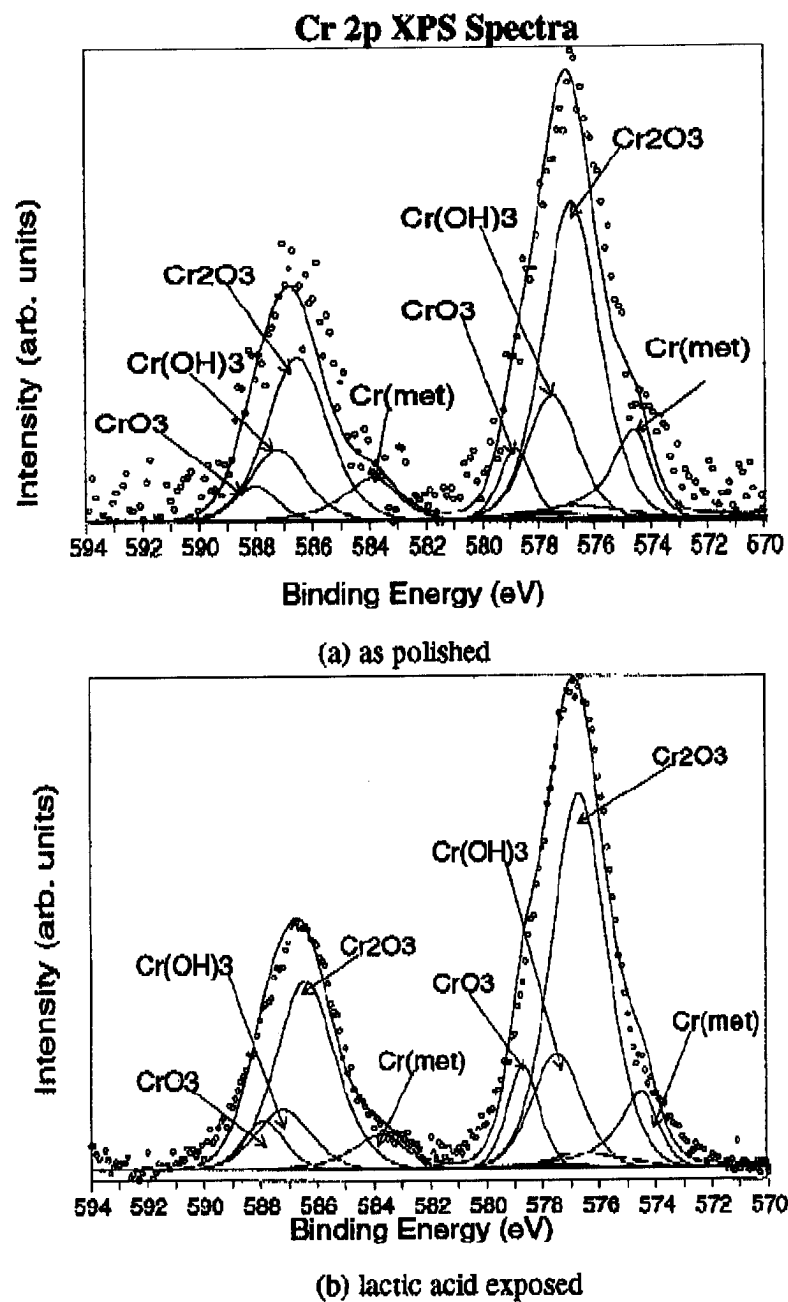
Cr 2p XPS spectra toa 20° of austenitic stainless steel type 304 before and after
exposure to 1 mM lactic acid solution.

Figure 42

O 1s XPS Spectra
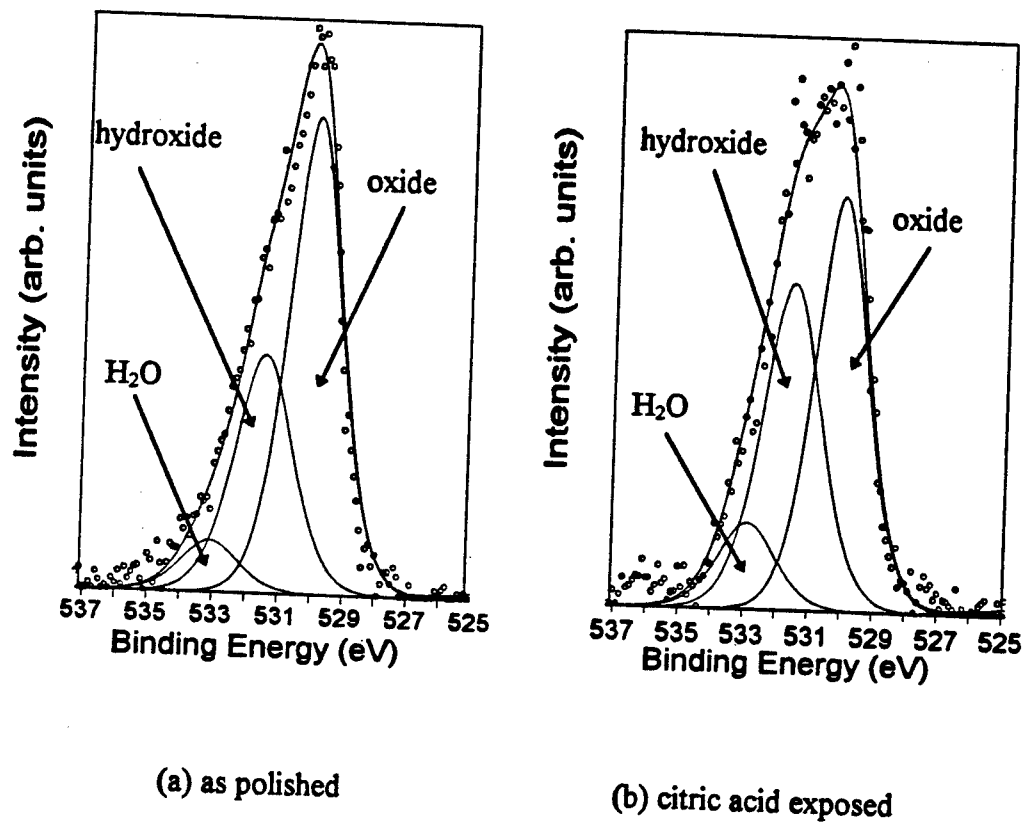
(a) as polished

(b) citric acid exposed
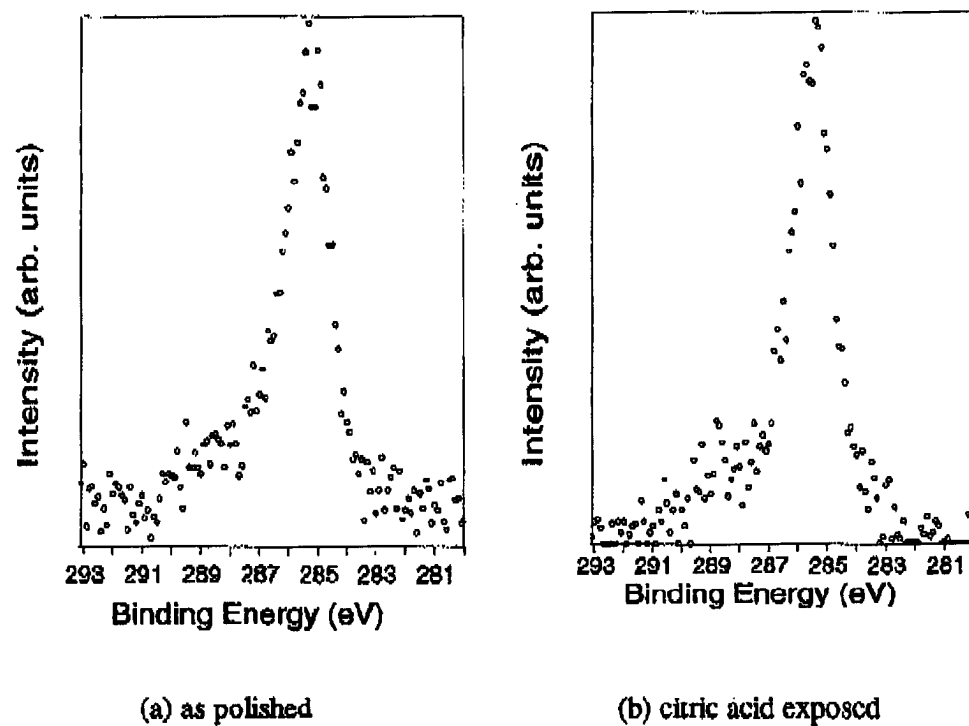
O 1s XPS spectra toa 50° of austenitic stainless steel type 304 before and after

exposure to 1 mM citric acid solution.

Figure 43

O 1s XPS Spectra

(a) as polished   (b) oxalic acid exposed

O 1s XPS spectra toa 50° of austenitic stainless steel type 304 before and after

exposure to 1 mM oxalic acid solution.

Figure 44

O 1s XPS Spectra

(a) as polished   (b) lactic acid exposed

O 1s XPS spectra toa 50° of austenitic stainless steel type 304 before and after

exposure to 1 mM lactic acid solution.

Figure 45

# Ni 2p₃/₂ XPS Spectra

a) as polished

(b)lactic acid exposed

Ni 2p 3/2 XPS spectra toa 50° of austenitic stainless steel type 304 before and after

exposure to 1 mM lactic acid solution.

Figure 46

Ni 2p$_{3/2}$ XPS Spectra

a) as polished

(b)oxalic acid exposed

Ni 2p$_{3/2}$ XPS spectra toa 50° of austenitic stainless steel type 304 before and after

exposure to 1 mM oxalic acid solution.

Figure 47

Ni 2p$_{3/2}$ XPS Spectra

(a) as polished   (b)citric acid exposed

Ni 2p$_{3/2}$ XPS spectra toa 50° of austenitic stainless steel type 304 before and after

exposure to 1 mM citric acid solution.

Figure 48

C 1s XPS Spectra

(a) as polished

(b) lactic acid exposed

C 1s XPS spectra toa 50° of austenitic stainless steel type 304 before and after

exposure to 1 mM lactic acid solution.

Figure 49

C 1s XPS Spectra

(a) as polished   (b)lactic acid exposed

C 1s XPS spectra toa 20° of austenitic stainless steel type 304 before and after

exposure to 1 mM lactic acid solution.

Figure 50

C 1s XPS Spectra

| (a) as polished | (b) oxalic acid exposed |

C 1s XPS spectra toa 50° of austenitic stainless steel type 304 before and after

exposure to 1 mM oxalic acid solution.

Figure 51

C 1s XPS Spectra

(a) as polished

(b) oxalic acid exposed

C 1s XPS spectra toa 20° of austenitic stainless steel type 304 before and after

exposure to 1 mM oxalic acid solution.

Figure 52

C 1s XPS Spectra

(a) as polished   (b) citric acid exposed

C 1s XPS spectra toa 50° of austenitic stainless steel type 304 before and after

exposure to 1 mM citric acid solution.

Figure 53

C 1s XPS Spectra

(a) as polished   (b) citric acid exposed

C 1s XPS spectra toa 20° of austenitic stainless steel type 304 before and after exposure to 1 mM citric acid solution.

Figure 54

FT-IR Spectra
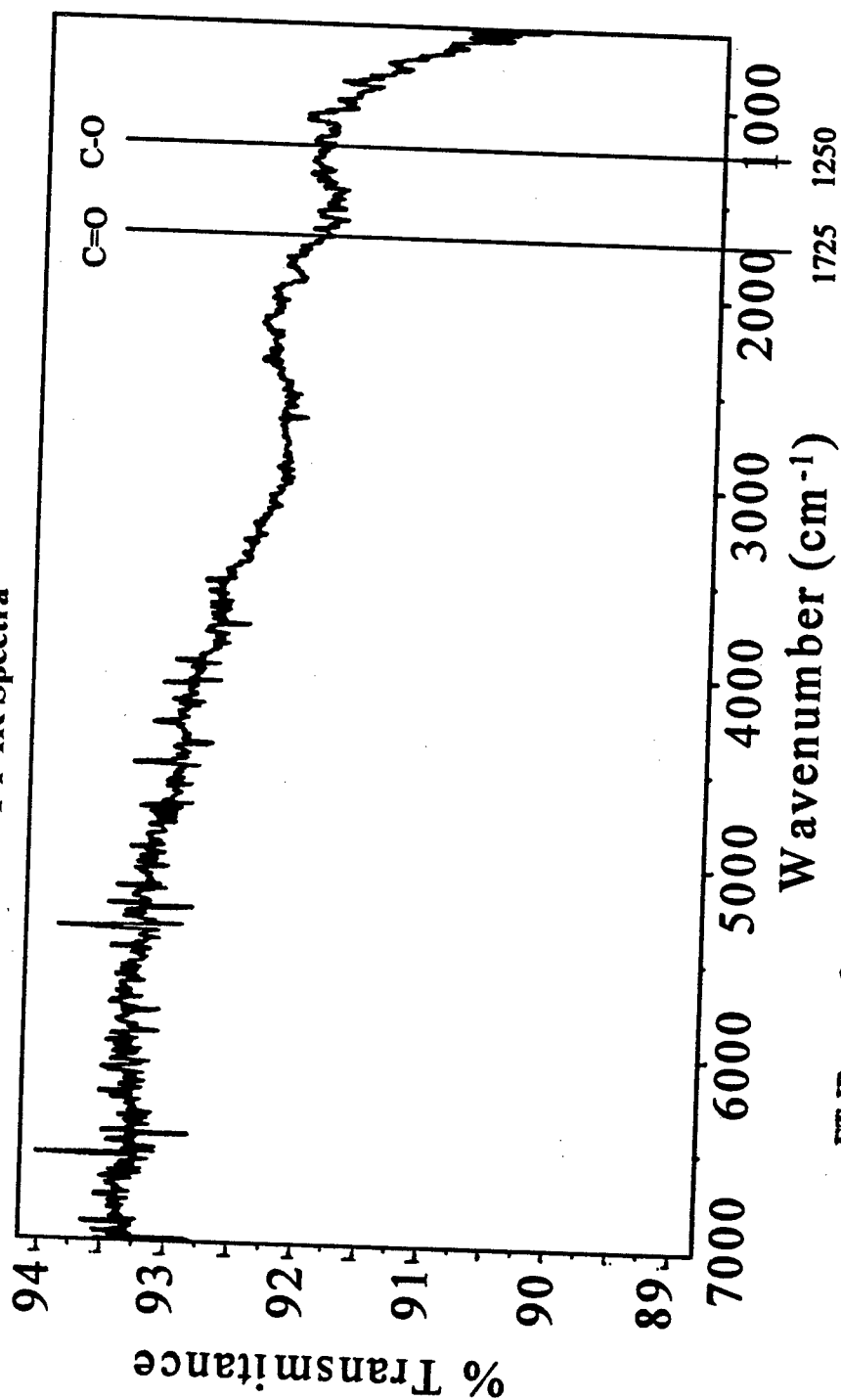
FT-IR scan of a 1mM citric acid exposed stainless steel 304 surface

Figure 55.

C 1s XPS Spectra
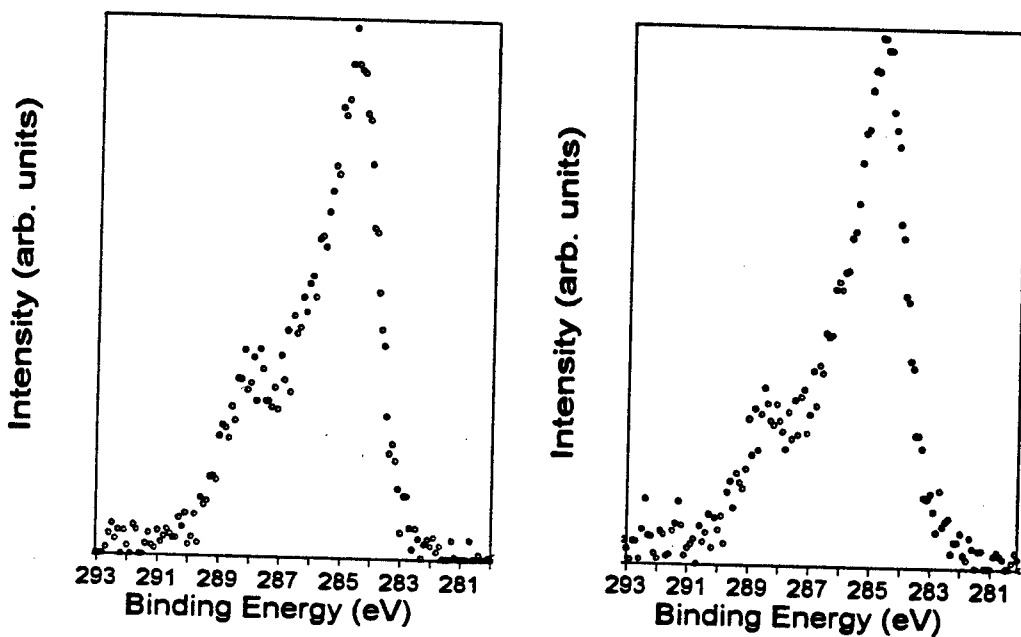
(a) 5 day 0.1M citric acid exposure in dark.

(b) 5 day 0.1M citric acid exposure in light.

C 1s XPS spectra toa 50° of austenitic stainless steel type 304 after exposure to 0.1 M citric acid for 5 days in light and dark environments.
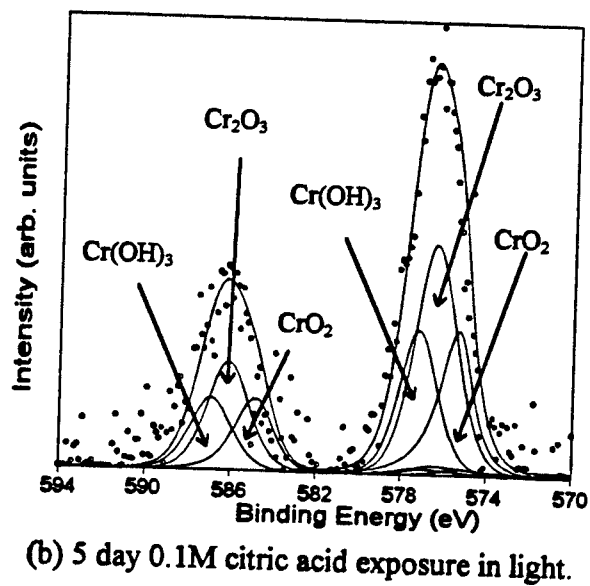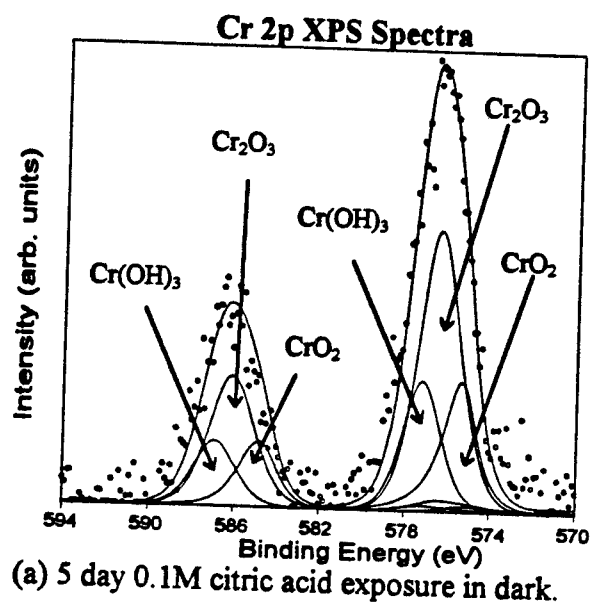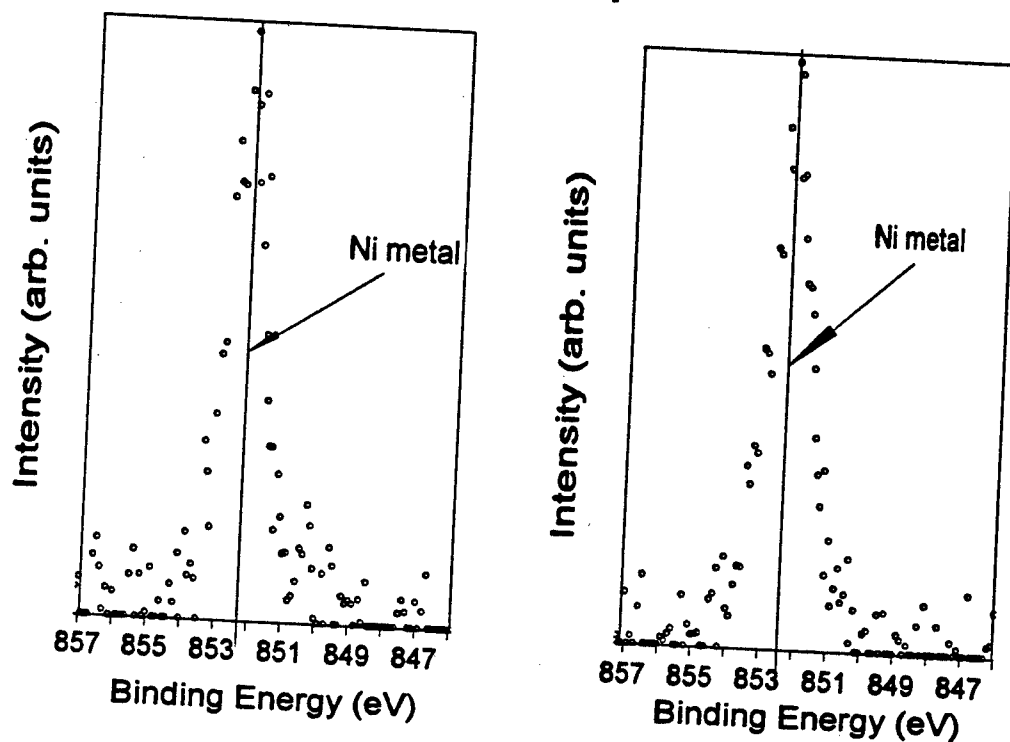
Figure 56

C 1s XPS Spectra
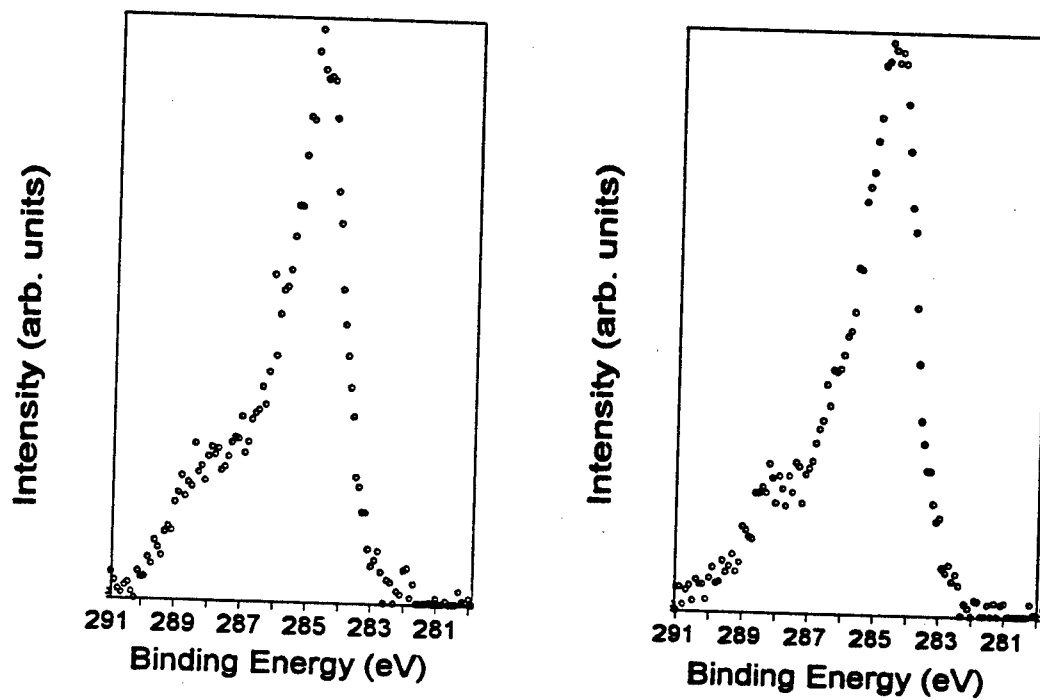
(a) 5 day 0.1M citric acid exposure in dark.

(b) 5 day 0.1M citric acid exposure in light.

C 1s XPS spectra toa 20° of austenitic stainless steel type 304 after exposure to 0.1 M citric acid for 5 days in light and dark environments.
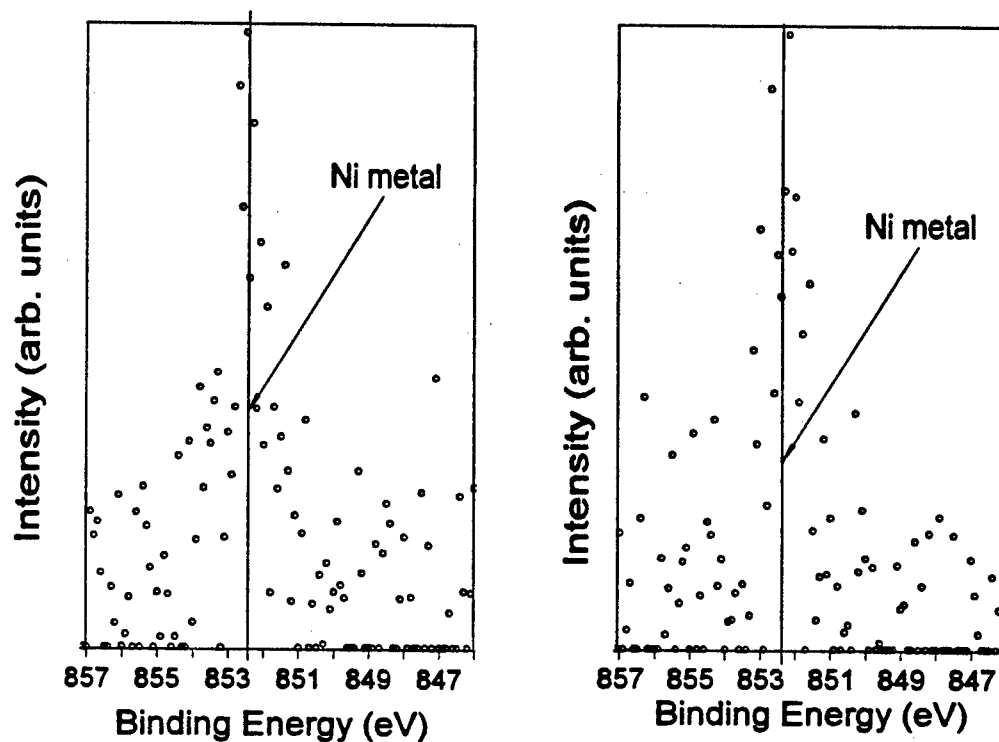
Figure 57

Fe 2p$_{3/2}$ XPS Spectra
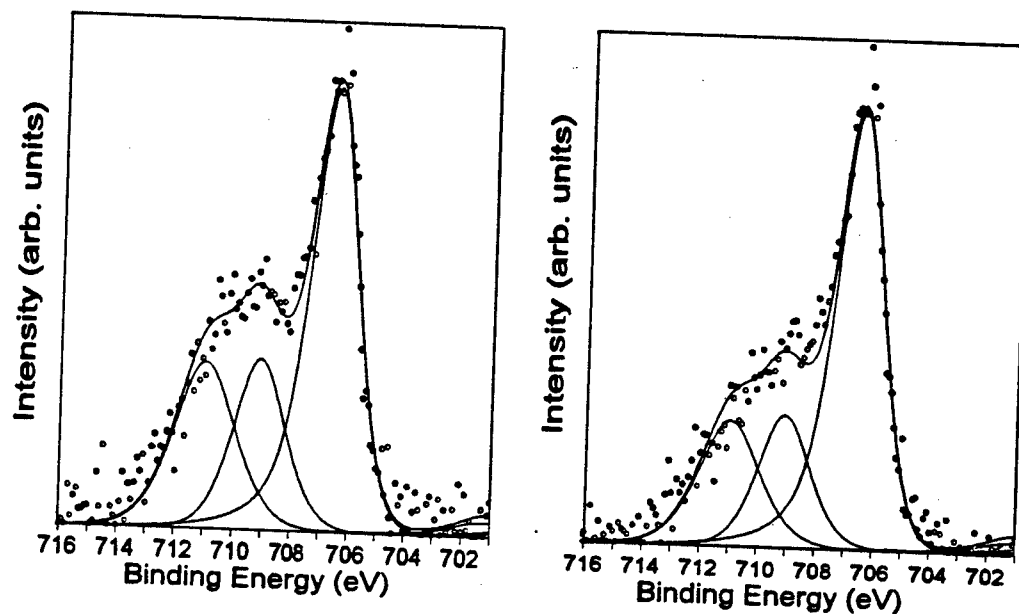
(a) 5 day 0.1M citric acid exposure in

dark

(b) 5 day 0.1M citric acid exposure in

light

Fe 2p$_{3/2}$ XPS spectra toa 50° of austenitic stainless steel type 304 after exposure to

0.1 M citric acid for 5 days in light and dark environments

Figure 58

Fe 2p₃/₂ XPS Spectra
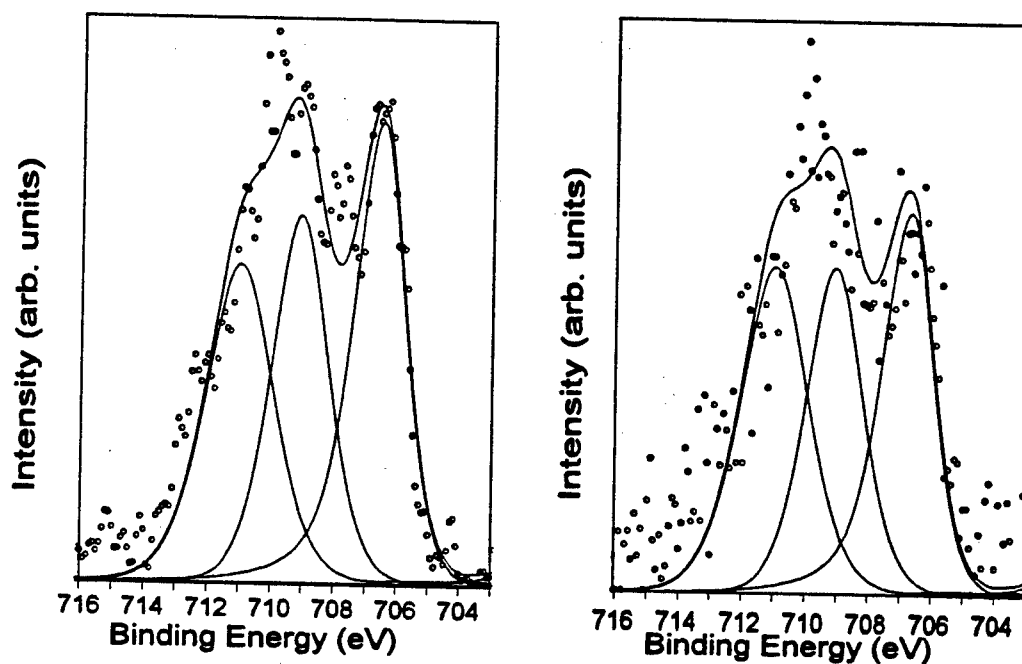
(a) 5 day 0.1M citric acid exposure in dark

(b) 5 day 0.1M citric acid exposure in light

Fe 2p₃/₂ XPS spectra toa 20° of austenitic stainless steel type 304 after exposure to

0.1 M citric acid for 5 days in light and dark environments.

Figure 59
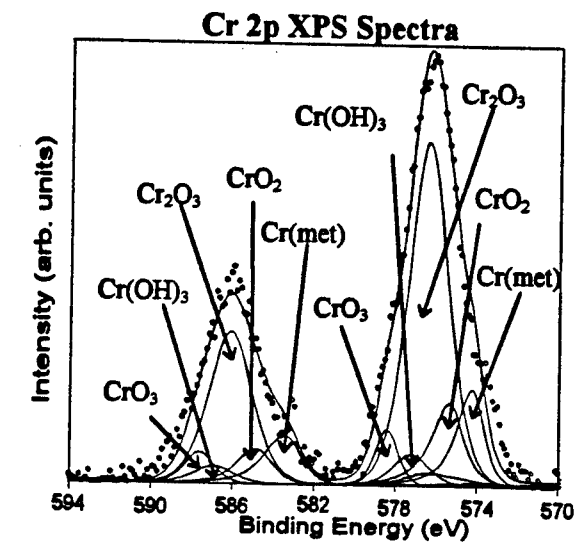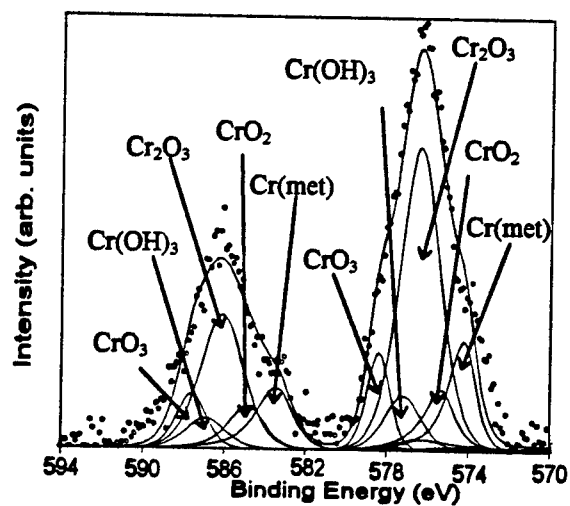
Cr 2p XPS Spectra

(a) 5 day 0.1M citric acid exposure in dark

(b) 5 day 0.1M citric acid exposure in light

Cr 2p XPS spectra toa 50° of austenitic stainless steel type 304 after exposure to

0.1 M citric acid for 5 days in light and dark environments.

Figure 60

Cr 2p XPS Spectra

(a) 5 day 0.1M citric acid exposure in dark.

(b) 5 day 0.1M citric acid exposure in light.

Cr 2p XPS spectra toa 20° of austenitic stainless steel type 304 after exposure to

0.1 M citric acid for 5 days in light and dark environments.

Figure 61

Ni 2p$_{3/2}$ XPS Spectra

(a) 5 day 0.1M citric acid exposure in dark.

(b) 5 day 0.1M citric acid exposure in light.

Ni 2p$_{3/2}$ XPS spectra toa 50° of austenitic stainless steel type 304 after exposure to

0.1 M citric acid for 5 days in light and dark environments.

Figure 62

Ni 2p3/2 XPS Spectra

(a) 5 day 0.1M citric acid exposure in dark.

(b) 5 day 0.1M citric acid exposure in light.

Ni 2p3/2 XPS spectra toa 20° of austenitic stainless steel type 304 after exposure to

0.1 M citric acid for 5 days in light and dark environments.

Figure 63

Optical micrograph 10x magnification of iron sulfide nodules on "as heat treated" 304 stainless steel surface
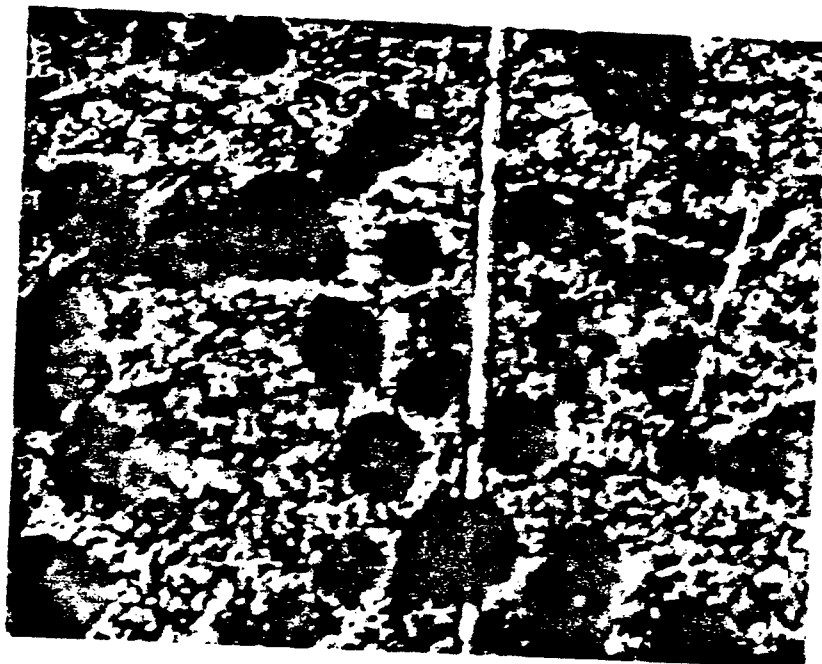
Figure 64

Survey XPS spectra of "as heat treated" stainless steel 304 after exposure to
desulfovibrio desulfuricans **for 5 days in Postgate growth media C**
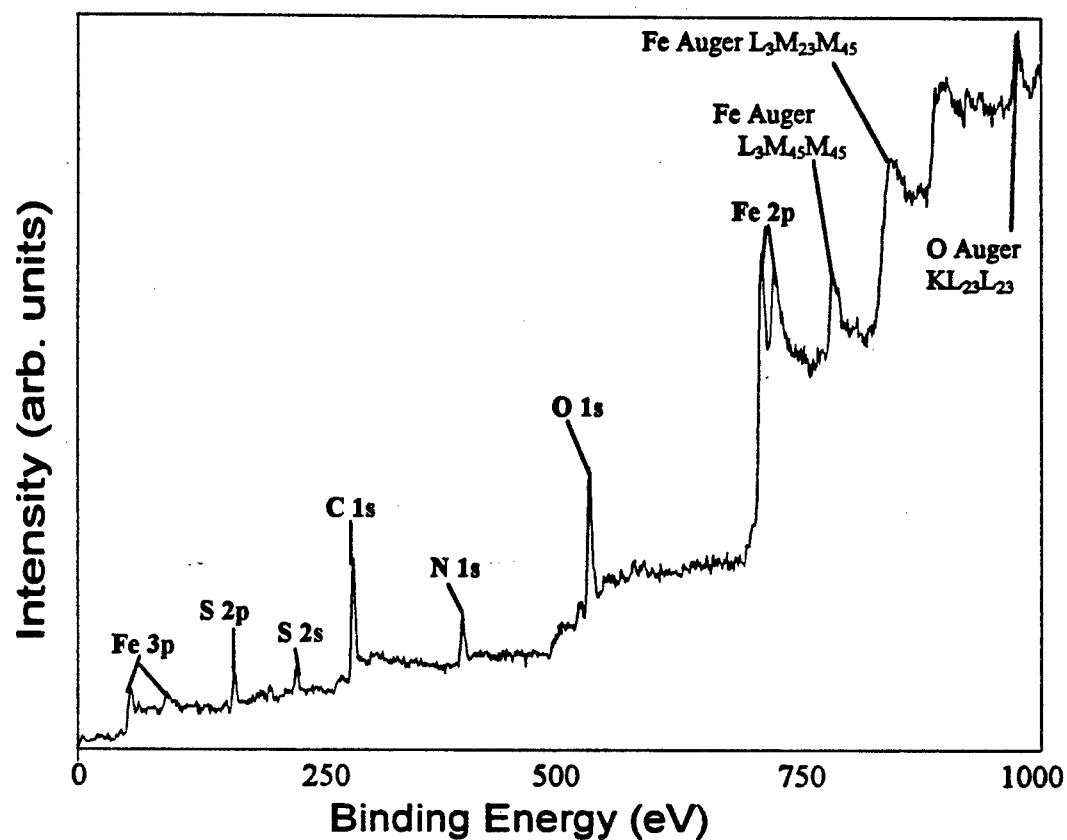
Figure 65

Fe 2p₃/₂ XPS Spectra
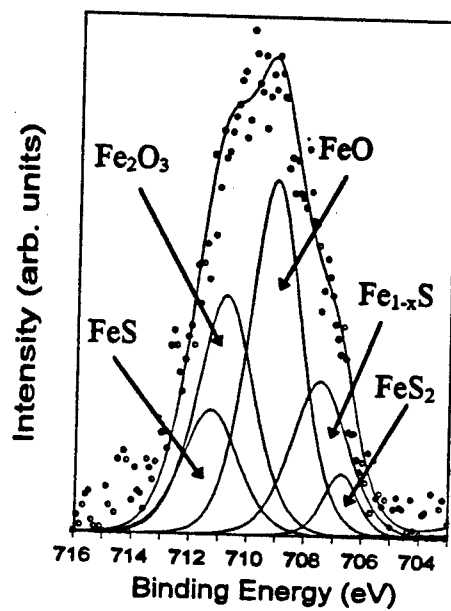
Fe 2p₃/₂ spectra from an "as heat treated" 304 stainless steel coupon after exposure to SRB's for 5 days.
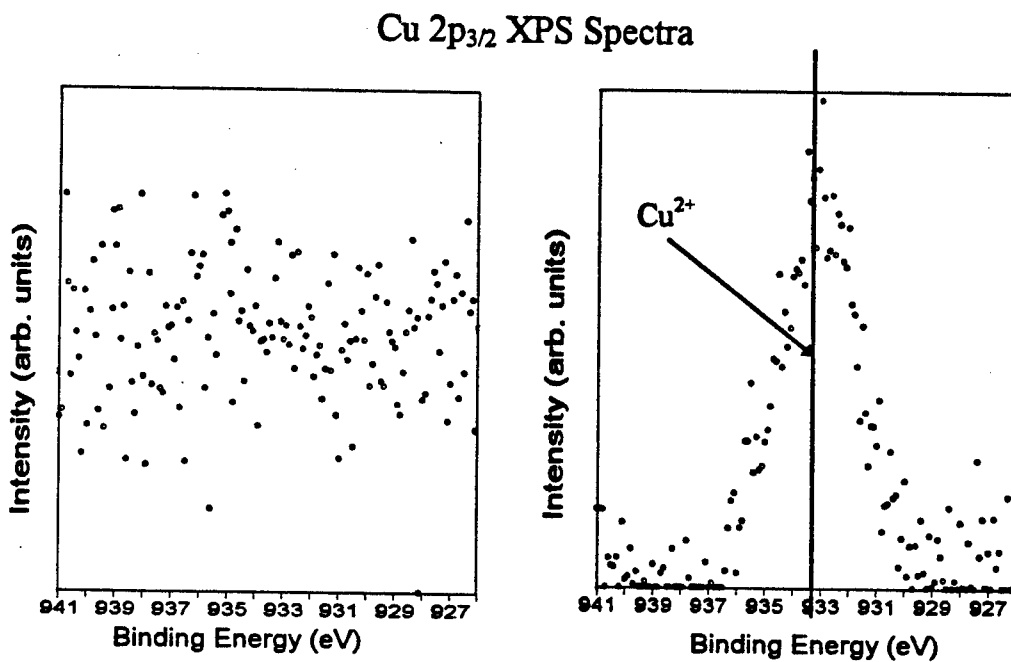
Figure 66

AA 2042-T3 exposed to *Desulfovibrio desulfuricans* and uninoculated growth media for 5 days
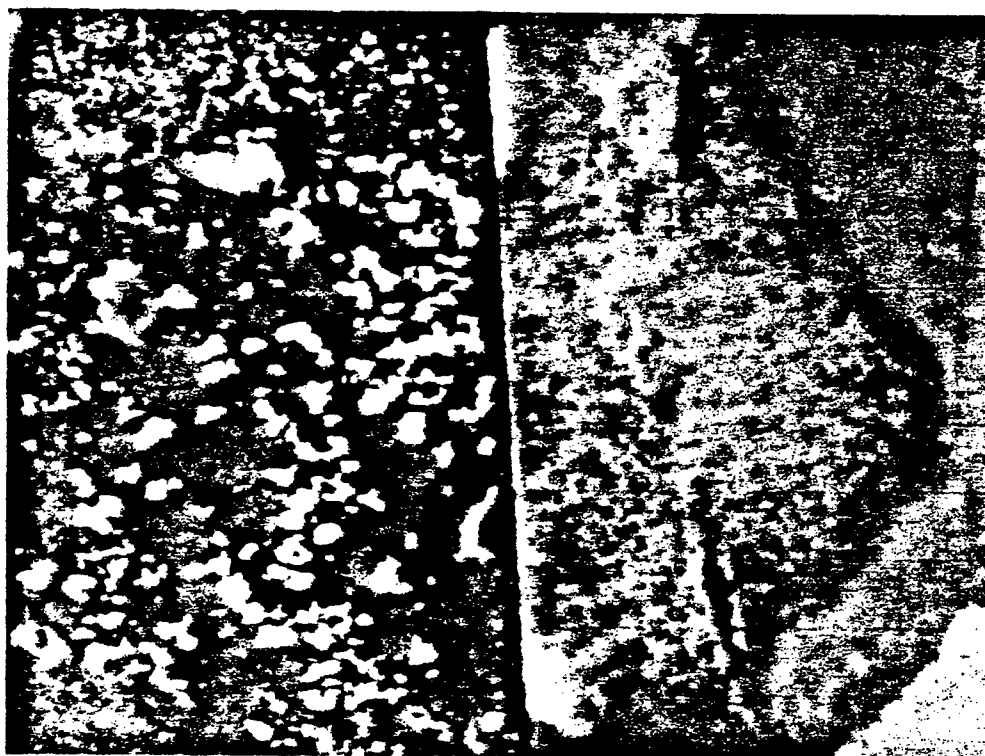
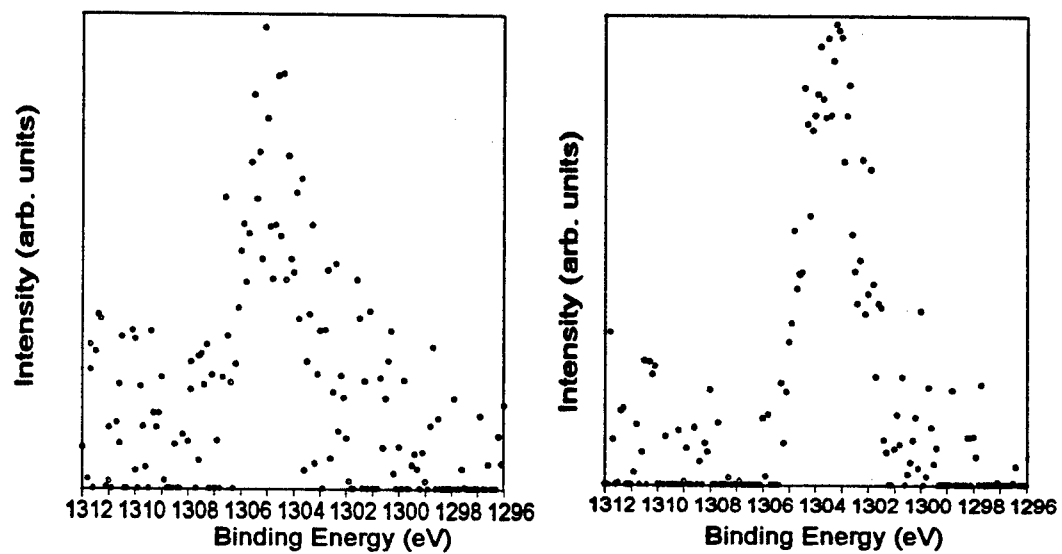Exposed to Postgate media C only   Exposed to SRB inoculated Postgate media

Figure 67

Cu 2p$_{3/2}$ XPS Spectra

Cu 2p$_{3/2}$ XPS spectra of AA 2024-T3 after 5 day exposure to SRB inoculated
media and uninoculated media toa 50°

Figure 68

Mg 2s XPS Spectra
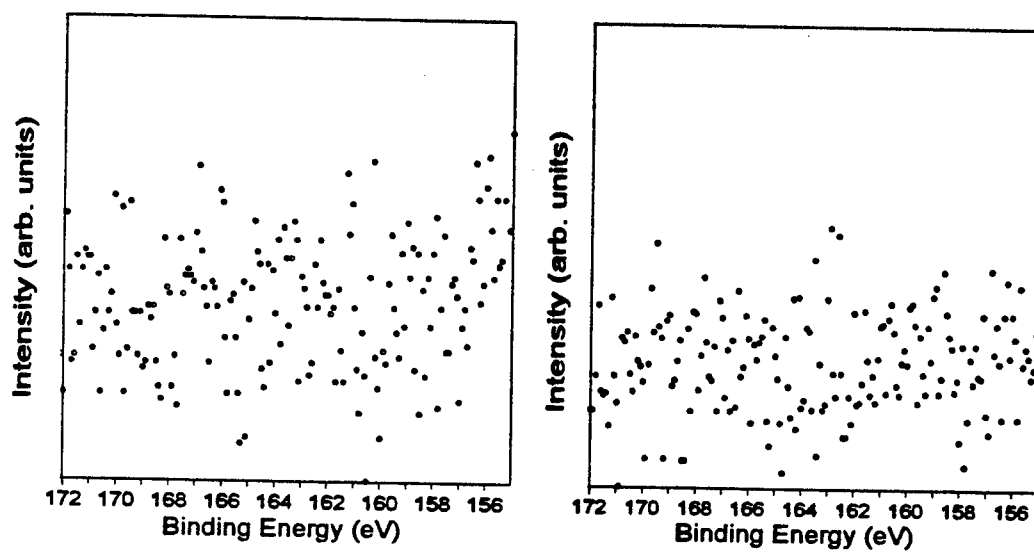

Mg 2s XPS spectra of AA 2024-T3 after 5 day exposure to SRB inoculated media
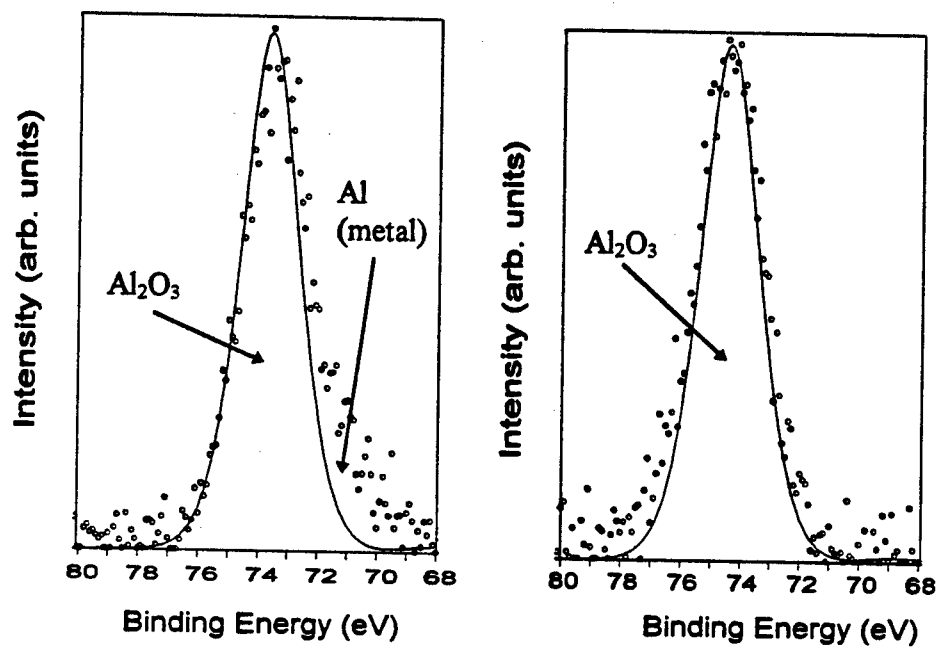and uninoculated media toa 50°

Figure 69

S 2p XPS Spectra

S 2p XPS spectra of AA 2024-T3 after 5 day exposure to SRB inoculated media and uninoculated media toa 50°.
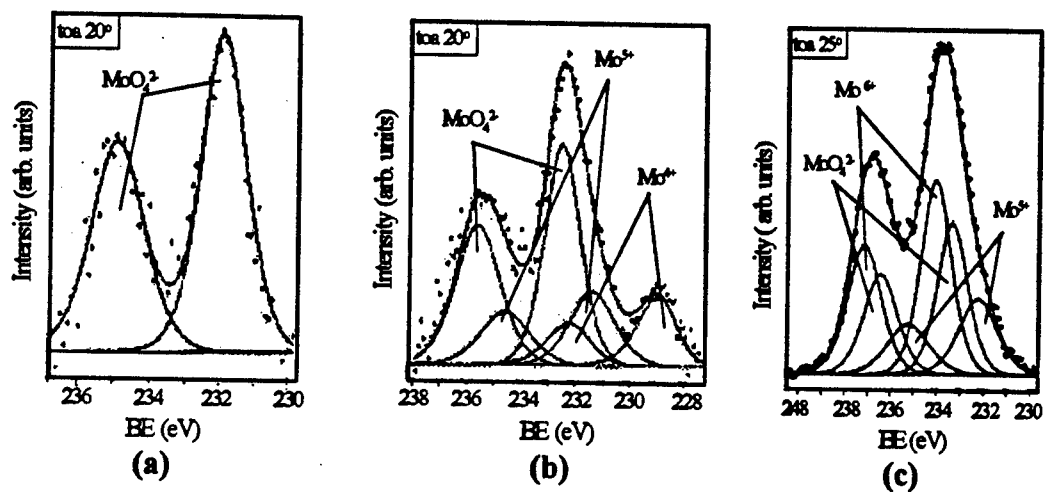
Figure 70

Al 2p XPS Spectra

Al 2p XPS spectra of AA 2024-T3 after 5 day exposure to SRB inoculated media and uninoculated media toa 50°
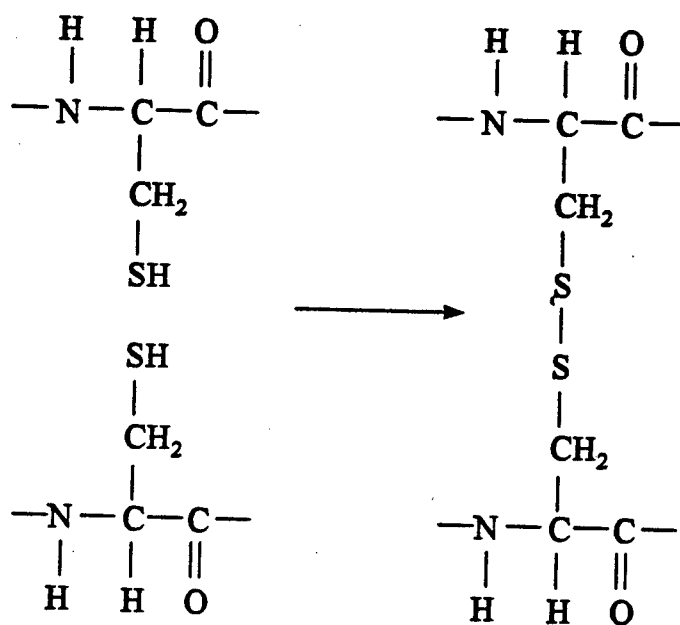
Figure 71

Mo3d spectra

a) Following molybdate addition to solution of protein containing exopolymer

b) Molybdate adsorbed onto 304 ss.

c) Following exposure of b) to protein containing exopolymer

Figure 72

Cysteine oxidation to Cystine

Figure 73